UNIVERSITÀ DEGLI STUDI DI PALERMO

DIPARTIMENTO DI SCIENZE DELLA TERRA E DEL MARE

In Collaboration with

UNIVERSITAT DE BARCELONA

DEPARTAMENT DE DINÀMICA DE LA TERRA I DE L'OCEÀ

XXXIII ciclo

Dottorato di Ricerca in Scienze della Terra e del Mare

WATER MASSES EXCHANGE THROUGH THE STRAIT OF SICILY DURING THE LAST DEGLACIAL PERIOD AND THE HOLOCENE

Sergio Trias Navarro

2022

Tutor: Dr. Antonio Caruso

Co- Tutor: Prof. Isabel Cacho

El Mar

Antes que el sueño (o el terror) tejiera
mitologías y cosmogonías,
antes que el tiempo se acuñara en días,
el mar, el siempre mar, ya estaba y era

¿Quién es el mar? ¿Quién es aquel violento
y antiguo ser que roe los pilares
de la tierra y es uno y muchos mares
y abismo y resplandor y azar y viento?

Quien lo mira lo ve por vez primera,
siempre. Con el asombro que las cosas
elementales dejan, las hermosas
tardes, la luna, el fuego de una hoguera.

¿Quién es el mar, quién soy? Lo sabré el día
ulterior que sucede a la agonía.
“

De “El otro, el mismo” (Jorge Luis Borges).

AGRADECIMENTOS

Este capítulo de la tesis es quizás el que más ganas tenía de escribir y a su vez el que más inquietud me generaba. Hay tanta gente a la que debo agradecer tanto, que en cierta manera va a ser difícil poder expresarlo con palabras. Mientras escribo estas líneas me vienen cantidad de recuerdos compartidos con tantos de vosotros, partícipes de una u otra manera de esta aventura. Como dijo el filósofo chino Lao Tse, "Un viaje de mil leguas comienza con un primer paso", y si hoy me encuentro a las puertas de publicar esta tesis es, primero de todo, gracias a mi familia. A mis hermanos Javi y Loida con los que he disfrutado de innumerables buenos momentos y también de innumerables y deliciosas peleas para combatir el aburrimiento. A mis abuelas/os, tías/os y primas/os con las que tanto he compartido y tantos recuerdos atesoro. Pero especialmente gracias a mi madre y a mi padre, por su apoyo incondicional. Siempre. Y puedo asegurar que no ha sido tarea fácil. Por aguantar estoicamente todas mis travesuras desde que aprendí a ponerme en pie y por empujarme cuando más lo necesitaba. Por supuesto, mil millones de gracias a mi pareja Mariella, que siempre ha estado allí y me ha ayudado en los momentos difíciles del camino. Que me ha apoyado en todo momento, capeando los temporales que surgían y a la que debo un viaje a Hawái. Todas las presentaciones que he practicado con ella haciendo de público, me hacen pensar que prácticamente podría defender ella este trabajo. Decir que se ha vuelto experta en foraminíferos sería decir poco.

Querría hacer mención especial a mi codirectora de tesis Isabel Cacho, que siempre me ha hecho el camino un poco más fácil. Muchas gracias por haberme dado la oportunidad de desarrollar el doctorado y haber depositado tu confianza en mí. Merced de su calidad como científica y su enorme contribución en este trabajo, debo sobreponer su calidad humana. Gracias por tu actitud tan positiva y constructiva en todo momento. Ha sido una experiencia estupenda y hemos demostrado que controlar la hora no es la mejor virtud de ambos y que un desayuno más largo de lo previsto te puede hacer llegar tarde a una conferencia. Gracias también a mi director de tesis Antonio Caruso por su acogida en la ciudad de Palermo y por su ayuda en momentos de dificultad.

Además, querría agradecer a todos aquellos profesores e investigadores que he conocido en la universidad de Palermo, el haber podido compartir tantas inquietudes, algunas científicas y otras no, a lo largo de los tres años que he vivido allí. Muy especialmente a Athina Tzevahirtzian, mi compañera de despacho, pero mucho más que eso, con la cual hasta he compartido una pandemia mundial en una ciudad extranjera. Por tu compañía, risas, consejos, alegría, locuras, también alguna que otra bronca y tantas noches de "vamos a tomar una". Sólo por conocer gente como tú, ha valido la pena hacer el doctorado. A mi gran amigo Filippo, un gran amante de la cerveza artesana, que me ha acompañado a lo largo de estos años en Palermo y con el que siempre he podido contar.

Y por supuesto, muchísimas gracias a todo el personal docente, investigador y amigos de la Universidad de Barcelona. A María de la Fuente, con la que tantas horas de "Bootcamp" he compartido antes de empezar la jornada laboral y que tanto esfuerzo ha dedicado a la lectura de los diversos capítulos de la tesis, enriqueciéndola sobremanera. Muchas gracias por todas las horas invertidas y tu lectura crítica. Y sobretodo por compartir tantos días de playa, vóley, terracitas al sol y risas, muchas risas. A Maria Jaume, que compartía la misma pasión que nosotros por hacer "Bootcamp" a las 8 de la mañana, por el vóley, por las risas y por ir a la Leo. Que tuvo que ausentarse temporalmente de la universidad y aunque construí un muñeco a su imagen y semejanza para tenerla cerca, no acaba de ser lo mismo.

A Leopoldo Pena, por su inestimable contribución en la adquisición de los datos publicados. Tanto con el tratamiento de muestras en el laboratorio, como en llevar a cabo los diferentes análisis. Pero, además, por su gran contribución en el apartado escrito, su lectura crítica y comentarios que han hecho posible la consecución de este trabajo. Y no podría dejar de agradecer a Ester Garcia su gran ayuda, paciencia y compañía en el laboratorio de la sala blanca. A Eduardo Paredes, que se encargó de llevar a cabo gran parte de los análisis en los que se fundamenta esta tesis y que tantas historias de alienígenas y de videntes místicos me ha contado. Muchas gracias.

Y qué decir de Albert Català, que ha estado conmigo en todos los análisis de elementos traza, el que me enseñó los protocolos de limpieza y a realizar los cálculos de los errores. Cómo nos

divertimos. Y la de risas y vermuts que nos hemos hecho juntos. Tampoco me puedo olvidar de Judit Torner, a la que conozco de una vida y que siempre será mi Water-Cop. Recuerdo que cuando éramos más jóvenes nos encontrábamos en todas las fiestas populares. Empezamos juntos la universidad y aquí seguimos, quien lo hubiera dicho. Gracias a Jaime Frigola que ha participado en todos los capítulos de la tesis. También a Fabrizio Lirer por sus sugerencias.

Tampoco podría despedirme sin mencionar a mi compañera de despacho Andrea, que me ha acompañado cada día, lloviera o hiciera sol, porque nevar en Barcelona, pues poco. Gracias por tener siempre bonitas palabras. También a Monserrat Guart, por su apoyo en el laboratorio, pero sobre todo por tener siempre una sonrisa. A Mar Selvaggi, Pau Abelló y Sara Campderrós con los que emprendí un viaje oceanográfico allende los mares y del que regresamos con la mochila cargada de momentos inolvidables. Cuanto reímos, cantamos, bebimos alguna que otra cerveza y porqué no decirlo, a ratos, también trabajamos. A Raúl Redondo y Cinzia Atzei con los que he compartido tantos vermuts interminables, cenas y noches de "tranquis" y con los que he reido hasta quedarme afónico. Gracias por compartir una parte de este camino tan incierto que recorremos y que nadie sabe donde nos llevará, aunque yendo con vosotros dos posiblemente será a un bar. Y por supuesto, imposible no agradecer a mi inseparable amigo Marc Rivas, con el que he viajado a tantos lugares y con el que incluso he sobrevivido al ataque de un elefante, el estar siempre ahí. Hay tantas cosas que podría decir, de todo lo que hemos vivido juntos que no cabrían en mil y una páginas, así que simplemente mil y una gracias. A todas las personas que he conocido por el camino y a las que me dejo de nombrar, gracias. Y a todas mis amigas y amigos con los que comparto alegrías y tristezas, días de lluvia y días de sol, canciones y tiramisú. Con esto me despido, sabiendo que esta tesis es un poco de todas. Muchísimas gracias.

This work was founded by the project TIMED (683237) of the European Research Council (Consolidator Grants). I thank the doctoral school in Earth and Sea Sciences from University of Palermo which supported the research. I also thank ISMAR-CNR (Napoli) for core NDT-6-2016 which it was recovered by the NEXTDATA expedition on board R/V CNR-Urania in 2016.

The cure for boredom is curiosity.

There is no cure for curiosity.

Dorothy Parker

CONTENTS

1 ABSTRACT

The main goal of this thesis is to explore the inter-basin connection between the eastern and the western Mediterranean (E- and W-Med, respectively) during the last deglacial and Holocene periods (last 15 kyr). The thesis is based on the study of a sediment core recovered at the west flank of Sicily channel (W-Sicily), strategically located under the current path of the surface Atlantic waters and directly below the present-day hydrographic boundary layer between the Eastern Mediterranean Sourced Water (EMSW) and the Western Mediterranean Deep Water (WMDW). This key location allows to explore past changes in both surface and deep water exchange between the E and the W-Med. In this thesis, a combination of several analytical tools are presented to provide information of different oceanographic variables: (i) Physical and chemmical sea water properites have been inferred trough the analysis of microfossil assemblages, stable isotopes and trace elements in both planktic and benthic foraminifera; (ii) Dynamics of sediment supply have been based on grain-size, elemental geochemical composition and sediment rate analysis; (iii) Changes in the export rates of EMSW have been studied through the analysis of $^{143}Nd/^{144}Nd$ isotope ratios (εNd) in planktic foraminifera coatings, a novel quantitative tracer of water mass provenance.

One of the most outstanding results of this thesis has been the identification of an intensified EMSW flow at W-Sicily during the Younger Dryas (YD, 12.95-11.65 kyr BP). In this thesis is presented by the first time, solid evidence of a previous hypothesised enhanced YD deep-water interconnection between the E-and the W-Med. This situation is here atributted to the combined effect of; 1) the weakening of the W-Med deep-water convection associated with the simultaneous formation of the Organic Rich Layer (ORL) and 2) enhanced convection in the Aegean and Levantine basins favoured by the prevailing YD cold and arid conditions. It is also here proposed that this enhanced western flow of EMSW, ceased the stagnation at ~900m in the Alboran Sea that had initiated with the last ORL. At the same time, probably to balance the high outflow of the EMSW through the Strait of Sicily, the data here generated is consistent with an increased flow of Modified Atlantic Water (MAW) entering into the E-Med.

The new produced εNd data also allows to quantify by the first time a substantial weakening in the westward flow of EMSW (16% ± 6) during the last sapropel interval (S1, from 10.5 to 7 kyr BP). This limited exit of EMSW through the Strait of Sicily might have ended in lesser MAW flowing towards the E-Med, resulting in a reduced influence of this surface water at the studied area, as is reflected in the planktonic foraminifera assemblage. As a consequence, the predominant climatic conditions that prevailed in central-southern Europe during the S1 interval played an essential role, conditioning the surface hydrology and promoting intense seasonality at the W-Sicily, characterized by intense winter mixing and stratified warm summers. The characterization of deep water properties allows, by the first time, to propose that these climatic conditions led to the formation of a western sourced anomalous high salinity intermediate-water during the last phase of the S1 (S1b, from ~8.2 to ~7 kyr BP), likely produced in the Tyrrhenian Sea area. The reactivation of the interconnection between the E- and W-Med took place about 1 kyr before the absolute end of the S1 (6.1 kyr cal. BP), suggesting the end of the eastern basin stagnant conditions at intermediate depths, while the re-ventilation of the deep basin would have taken longer.

2 INTRODUCTION

One of the most important challenges of climate research is to improve our understanding about the mechanisms which are involved in the natural climate variability. In such context, the analysis of past climate is essential to understand the climate system dynamics, processes and feedbacks that can determineclimate evolution at both short and long term. Climate system oscillations are mainly controlled by a coupled interaction between the atmosphere and the ocean. The ocean is a key element of the global heat redistribution from tropic to polar regions, which at the same time act as a reservoir for carbon, heat, and water vapor (Bigg et al., 2003; Delworth & Zeng, 2016; Trenberth & Caron, 2001). In the Northern Hemisphere, changes in the Atlantic Meridional Overturning Circulation (AMOC) are closely linked with climate instabilities (McManus et al., 2004; Trenberth & Caron, 2001; Walker, 1995). The AMOC consists of relatively warm and salty surface-water layer which flow northward losing buoyancy and sinking at higher latitudes of the North Atlantic Ocean to return southward at depth (Fig. 1) (Boyle & Keigwin, 1987; Kuhlbrodt et al., 2007).

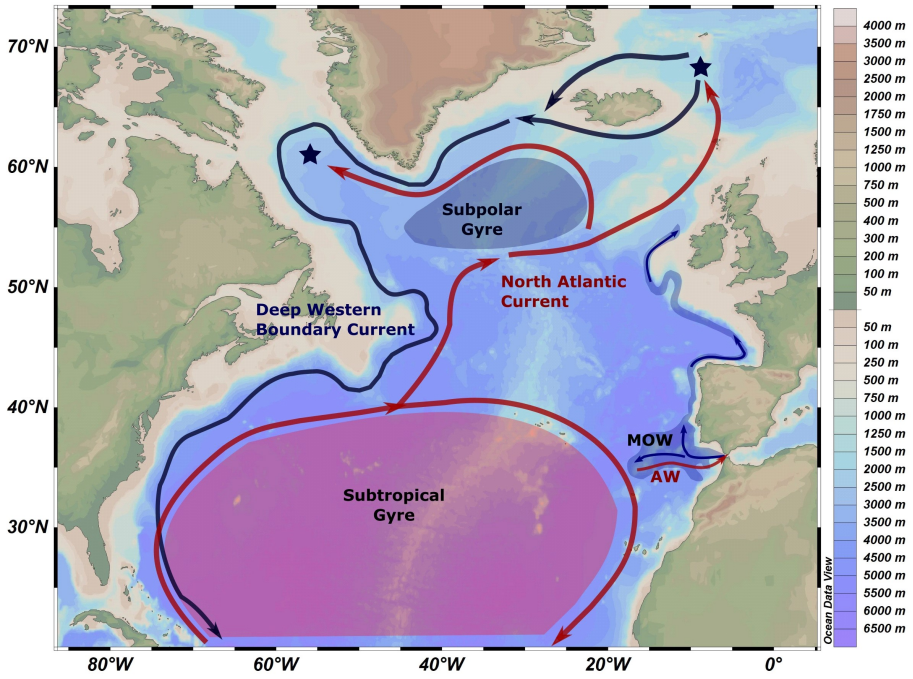

Fig. 1. Schematic present-day North Atlantic circulation. Red and blue arrows represent surface and deep currents respectively. Blue stars represent deep-water convection areas. Abreviations; MOW, Modified Atlantic water; AW, Atlantic Water.

Therefore, the AMOC represents a net northward transport of heat from lower to higher latitudes in the Atlantic Ocean. Several studies demonstrate that past changes in the AMOC induced severe climatic shifts around Europe, which probably had a global scale impact (de Abreu et al., 2005; Lynch-Stieglitz et al., 2007; McManus et al., 2004; Walker, 1995). Moreover, climate changes driven by past fluctuations of the AMOC have been reflected in the Mediterranean Sea circulation, as several authors have previously argued (Cacho et al., 2000, 2002; Frigola et al., 2008). The Mediterranean Sea and Atlantic Ocean behave as a closely coupled system connected through the Strait of Gibraltar, where surface Atlantic waters enter into the Mediterranean Sea and Mediterranean waters exit to the Atlantic Ocean at depth (Millot, 1987, 1999; Skliris, 2014). Consequently, changes in the outflowing Mediterranean waters properties should drive changes in the AMOC, that could trigger changes in the climate system (Bahr et al., 2015; Swingedouw et al., 2019). As the most climate models predict, the AMOC could change in the coming decades turning weaker (Frajka-Williams et al., 2019; Kaufman et al., 2009; Liu et al., 2020; Weijer et al., 2020). In this context, the study of the paleoclimatic data from the Mediterranean Sea, could provide new light to better understand its future impact over the AMOC and thus climate system evolution.

2.1 Climate and geography of the Mediterranean Sea

The Mediterranean is a semi-enclosed Sea formed by two sub-basins, the eastern Mediterranean (E-Med) and the western Mediterranean (W-Med), connected through the Strait of Sicily. It is surrounded by north Europe on the north, north Africa on the south and west Asia on the east and is connected to the Atlantic Ocean through the Strait of Gibraltar (Fig. 3). The Mediterranean Sea stretches 3060 km in longitude and 1600 km in latitude, occupying an area about 2.5 million km^2 (excluding the Black Sea). It reach more than 4 km depth in the deepest zones of the basin with an average depth of ~1500 m (Lionello, 2012; Rohling et al., 2009).

The Mediterranean Sea is an excellent sensor of climate oscillations that allow us to explore the paleoclimatic evolution of the northern hemisphere in a reduced spatial scale. Due to its small volume in comparison with the oceans and its limited communication with the Atlantic ocean,

climatic oscillations are detected at once and amplified in the paleoceanographic sedimentary records (Cacho et al., 2002; Rohling et al., 2009; Sbaffi et al., 2001).

The climate of the Mediterranean region is characterized by mild and wet winters and warm and dry summers, as the result of the interaction between the subtropical high pressure belt and the temperate mid-latitude westerlies (Kutiel & Maheras, 1998; Lionello, 2012; Lolis et al., 2002; Rohling et al., 2009). During summer, high-pressure conditions dominate all over the Mediterranean basin causing drought, while during winter the influence of the temperate westerlies prevails, spreading southward from the central Europe and bringing Atlantic depressions (Lolis et al., 2002; Maheras et al., 1999; Saaroni & Edelson, 2003).

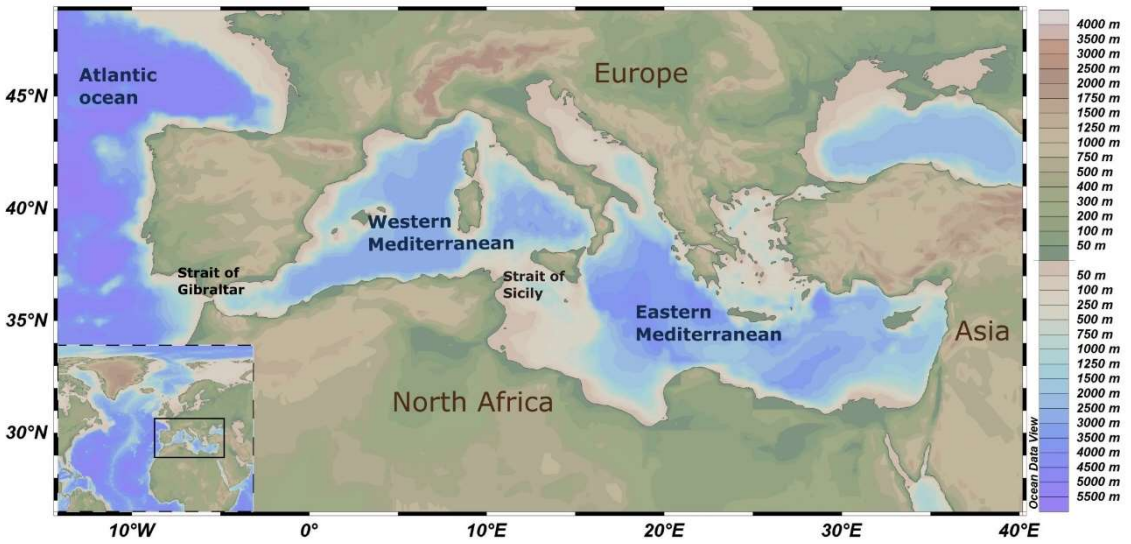

Fig. 2. Schematic map of the Mediterranean Sea and the sorrounded bordelands. Basic map obtained from Ocean Data View.

2.2 Oceanography of the Mediterranean Sea

Mediterranean Termohaline Circulation (Med-THC) is controlled by the intensity of the mid-latitude westerlies, the inflowing Atlantic waters and the Mediterranean hydrological balance mostly controlled by the climate of the tropical regions which modulate the rainfall regime (Cacho et al., 2001; Cacho, Grimalt, et al., 1999; Combourieu Nebout et al., 2002; Rohling et al., 1998; F. J. Sierro et al., 2005; Skliris, 2014). The Med-THC is fuelled by three deep-water convection

cells, located at the Gulf of Lions, Adriatic Sea and Aegean Sea, and one intermediate-water convection cell located at Levantine Sea (Fig. 3).

The negative balance between evaporation and precipitation across the Mediterranean Sea promote an anti-estuarine circulation where surface Atlantic Waters (AW) enter into the Mediterranean Sea through the Strait of Gibraltar and the underlying Mediterranean waters (i.e. Mediterranean Outflow Waters, MOW) exit to the Atlantic Ocean (Fig. 3) (Pinardi & Masetti, 2000). The AW turn saltier by evaporation and mixing with the underlying Mediterranean waters along its eastward path, forming the Modified Atlantic waters (MAW) (La Violette, 1986; Millot, 1999). The MAW flows in the upper layer (0-200 m) along the North African coast as the so-called Algerian current and eventually enter into the E-Med through the Strait of Sicily (Millot, 1987; Pinardi & Masetti, 2000). Over the Cyprus-Rhodes area, in the Levantine Sea, MAW forms intermediate waters (Levantine Intermediate Water, LIW) by winter convection (Lascaratos et al., 1993; Millot, 1987, 1999; Pinardi & Masetti, 2000). The LIW flows westwards spreading through all the Mediterranean basin between ~150 and ~700 m (Malanotte-Rizzoli et al., 1999; Pinardi & Masetti, 2000).

In the Adriatic Sea, the mixing between cold surface Adriatic waters and LIW produces the Adriatic Deep Water (ADW), which widespreads into the deep E-Med basin through the Strait of Otranto contributing to the Eastern Mediterranean Deep Water (EMDW) (Gacic et al., 2001; Mantziafou & Lascaratos, 2008; POEM group, 1992). Moreover, the Cretan Deep Water (CDW) produced in the Aegean Sea area also contribute to the EMDW. Nowadays ADW is the main component of the EMDW, but during the 1990 decade for exemple, the Aegean Sea area became the main source of EMDW formation, a situation called Eastern Mediterranean Transition (EMT) (Lascaratos et al., 1993; Malanotte-Rizzoli et al., 1999; Mantziafou & Lascaratos, 2008).

EMDW enters into the W-Med togheter with LIW through the Strait of Sicily and heads northwards, pass the Corsica channel and flow westwards to reach the Gulf of Lions where forms Western Mediterranean Deep Water (WMDW) (Pinardi & Masetti, 2000). During winter, north-westerlies winds coming from the Rhone Valley cause cooling and evaporation of surface MAW,

which turn denser, sinking and mixing with the underlying LIW to form the WMDW (Millot, 1987; Rohling et al., 2009). The WMDW spreads into the Balearic Sea and the south Tyrrhenian Sea underlaying the LIW and reaching ~3000 m depth (Millot, 1999). When the WMDW reaches the Alboran Sea, flows westwards along the Moroccan coast and together with LIW and EMDW eventually exit into the northern Atlantic Ocean as MOW, completing the cycle of the Med-THC (Millot, 1999, 2009; Pinardi & Masetti, 2000).

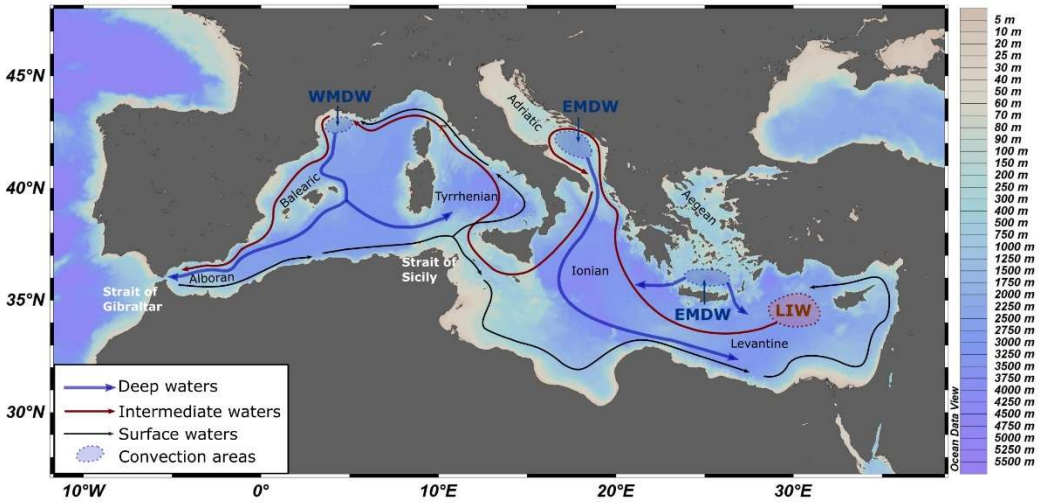

Fig. 3. Schematic map of the Med-THC. Black arrows represent the general surface circulation, red arrrows the LIW and blue arrows the deep-water circulation.

2.3 Paleoceanography of the Mediterranean Sea

Several paleoclimatic and paleoceanographic studies have demonstrated that the Med-THC is highly sensitive to past climate oscillations at different timescales (Cacho et al., 2000, 2001; Cisneros et al., 2016; Frigola et al., 2007; Rohling et al., 2002, 2009, 2015; Sierro et al., 2005; Zielhofer et al., 2017). For example, during the last deglacial period, sea level rise has been proposed as the main driver of deep water convection weakening in the Western Mediterranean Sea (W-Med), that led to the formation of the Last Organic Rich layer in the deep basin (ORL: 15-8.9 kyr BP) (Cacho et al., 2002; Pérez-Asensio et al., 2020; Rogerson et al., 2008). ORLs have been deposited in the Alboran Sea during the last 3 Myr and consist in dark sediment layers with organic carbon higer than 0.8% (Murat, 1999). In the Eastern Mediterranean sea it has been well documented a major hydrological perturbation related to an increase in the north African rivers

system runoff, as a result of intensified African Monsoon over north Africa during the African Humid Period (AHP; from ~15 to 6 kyr BP, Shanahan et al., 2015). Many evidences indicate that enhanced fresh-water flow towards the E-Med caused an important surface water stratification, which ended in the collapse of the E-Med deep/intermediate convection, that resulted in the deposition of an organic-rich sediment layer, the so-called last sapropel or S1 (De Lange et al., 2008; Grant et al., 2016; Lourens et al., 1992; Mercone et al., 2001; Rohling, 1994; Rossignol-Strick, 1985; Toucanne et al., 2015).

Sapropels have been defined for the first time by Kidd et al. (1978) as sediments with carbon organic concentrations (C_{org}) higher than 2%, although other studies proposed C_{org}>1% to consider sapropel sediments (Murat & Got, 2000). However, the original C_{org} of sapropel deposits can be removed by post-depositional oxidation and therefore, may not represent the entirely event (De Lange et al., 2008; Thomson et al., 1995). In such context, biogenic Ba (barite) is an useful proxy to identify sapropel layers since is hardly removed once deposited and reflects the original C_{org} signal (De Lange et al., 2008; Rohling et al., 2015; Wu et al., 2016). Sapropel events occurred in both E-Med and W-Med since the late Miocene, during times of precession minima characterized by maximum summer insolation on the northern hemisphere. This situation resulted in intensified African monsoon precipitation, promoting stronger runoff of north African river systems into the Mediterranean Sea (DeMenocal et al., 2000; Hilgen, 1991; Lourens et al., 1996; Nijenhuis & De Lange, 2000; Rohling et al., 2015; Rohling & De Rijk, 1999; Rossignol-Strick, 1985; Scrivner et al., 2004; F. J. Sierro et al., 1999; Wehausen & Brumsack, 1998). The rapid influx of fresh-water from north African rivers resulted in strong surface ocean stratification in parallel with an increased export productivity, that led to the establishment of deep-basin anoxic conditions which resulted in the formation of sapropel layers in the sedimentary record (De Lange et al., 2008; Lourens et al., 1992; Rohling, 1994; Rohling et al., 2015; Rossignol-Strick, 1985; Schmiedl et al., 2010; Scrivner et al., 2004).

2.4 Objectives

The main goal of this research is to identify potential variations in the surface and deep-water exchange between the eastern and western Mediterranean sub-basins (E-Med and W-Med) during the last deglacial period and the Holocone (last 15 kyr). These changes should reflect oscillations in the outflow of the the eastern originated water masses, i.e. LIW and EMDW, into the W-Med through the Strait of Sicily. Since both LIW and EMDW, toghether with WMDW, contribute to the exit of MOW through the Strait of Gibraltar to the Atlantic ocean (Fig. 4), changes in the contribution of both eastern water-massses into the W-Med, necessarily would altered the MOW composition that ultimately contributes to the AMOC (Bahr et al., 2015; Millot, 2009; Pinardi & Masetti, 2000; van Dijk et al., 2018).

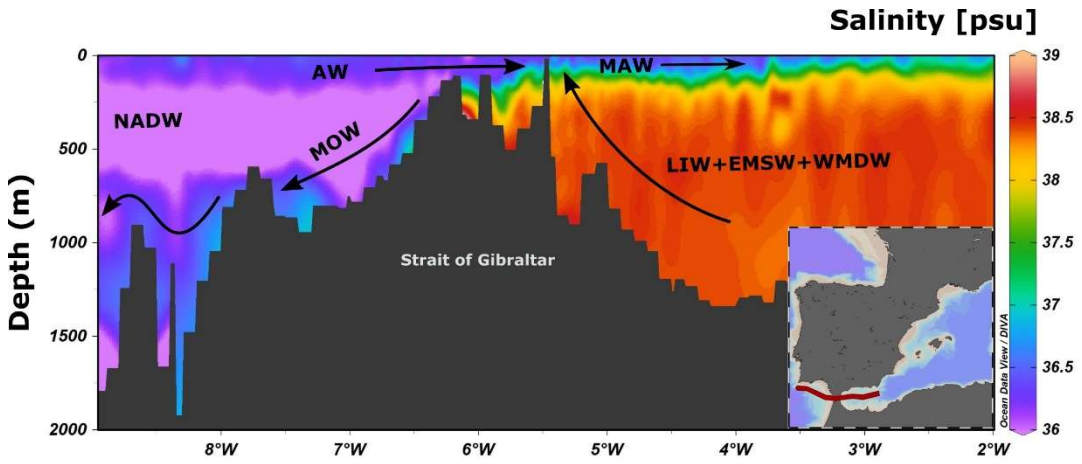

Fig. 4. Scheme of the surface and deep hydrology at the Strait of Gibraltar in terms of salinity based on Medatlas II acquired data and the map indicating with red line the profile section .

To evaluate these potential changes in the E – W Mediterranean exchange , this study uses a sediment core (NDT-6-2016) currently located in the main pathway of the Modified Atlantic Surface Water (MAW) towards the Strait of Sicily, at western flank of the Sicily channel. The NDT-6-2016 is located at 1066 m of water depth, which at present corresponds to the depth of the interphase layer in the region between water masses originated in the W- and E-Med. Therefore, this core is potentially suitable to evaluate changes in both surface and deep-water interconnection between the two sub-basins.

Changes in surface water properties are reconstructed through a multi-proxy approach combining planktic foraminifera ecology, major element analyses in bulk sediments, as well as stable oxygen isotopes measurements ($\delta^{18}O$) in both *Globigerina bulloides* and *Globigerinoides ruber* white variety. To evaluate potential changes in deep-water hydrology, we present a high-resolution record that combine major element analyses in bulk sediments, stable oxygen isotopes measurements ($\delta^{18}O$) in benthic foraminifera *Uvigerina mediterranea*, sedimentological grain size analyses, Mg/Ca measurements in *Uvigerina* ssp. (*Uvigerina mediterranea* and *Uvigerina peregrina*) and neodymium isotopes (εNd) analyses in Fe-Mn crusts formed over planktic foraminifera.

...Los nadies, los hijos de nadie, los dueños de nada

Que no son, aunque sean

Que no hablan idiomas, sino dialectos

Que no profesan religiones, sino supersticiones

Que no hacen arte, sino artesanía

Que no practican cultura, sino folklore

Que no son seres humanos, sino recursos humanos

Que no tienen cara, sino brazos

Que no tienen nombre, sino número

Que no figuran en la historia universal, sino en la crónica roja de la prensa local

Los nadies, que cuestan menos que la bala que los mata…

De “El libro de los abrazos” (Eduardo Galeano)

3 SURFACE HYDROGRAPHIC CHANGES AT THE WESTERN FLANK OF THE SICILY CHANNEL ASSOCIATED WITH THE LAST SAPROPEL*

Abstract

In the eastern Mediterranean Sea, the early Holocene was characterized by major climatic and oceanographic changes that led to the formation of the last sapropel (S1) between 10.8 – 6.1 kyr cal. BP. These hydrographic changes might have altered the water exchange between the eastern and western Mediterranean sub-basins through the Strait of Sicily, but the existing evidences are inconclusive. In the present study we show new evidence from sediment core NDT-6-2016 located at the western flank of the Sicily channel, a key location to monitor the surface/intermediate water exchange between the two Mediterranean sub-basins. We perform paleo-hydrographic reconstructions based on planktic foraminifera ecology for the last 15 kyr cal. BP, including the S1 deposition interval. In addition, $\delta^{18}O$ measurements in both *Globigerina bulloides* and *Globigerinoides ruber* and also major elements analyses in bulk sediment are presented. Our results show that significant changes in surface water properties occurred in W-Sicily characterized by a strong contrast in the seasonal hydrographic conditions during the S1 interval. This study proposes that the oceanographic changes in the eastern Mediterranean associated with the surface freshening promoted by the African monsoon likely triggered a restricted water exchange through the Strait of Sicily. This situation led to limited influence of the surface Atlantic waters into the studied area that favored the development of intense summer stratification and vertical winter mixing. This situation changed at about 7 kyr cal. BP when a decrease in the summer stratification probably reflected the influence of the eastward path of the surface Atlantic Waters. This situation would suggest a reinforcement of the water exchange through the Strait of Sicily that marked the end of the extreme conditions that prevailed in the eastern Mediterranean during the S1 formation.

*Trias-Navarro, S., Cacho, I., De La Fuente, M., Pena, L. D., Frigola, J., Lirer, F., & Caruso, A. (2021). Surface hydrographic changes at the western flank of the Sicily Channel associated with the last sapropel. Global and Planetary Change, 204, 103582. https://doi.org/10.1016/j.gloplacha.2021.103582

3.1 INTRODUCTION

The Mediterranean Sea is a semi-enclosed sea formed by two sub-basins, the eastern Mediterranean (E-Med) and the western Mediterranean (W-Med), connected through the Strait of Sicily. Their physiographic characteristics make both of these sub-basins very sensitive to climatic variability as demonstrated by many paleoclimatic and paleoceanographic studies (Abrantes et al., 2012; Cacho et al., 2001; Mayewski et al., 2004; Rohling et al., 2015). An interesting phenomenon that attests this enhanced sensitivity in the E-Med corresponds to a series of rhythmic deep water anoxic-events that resulted in the deposition of high-organic carbon sedimentary layers, i.e. the so-called "Sapropel" events (Grant et al., 2016; Lourens et al., 1992; Murat, 1999; Rohling, 1994; Rohling et al., 2015; Rossignol-Strick, 1985; Toucanne et al., 2015). Sapropel events occurred as a consequence of major changes in the hydrological cycle associated with stronger runoff of north African river systems into the Mediterranean Sea due to a maximum in the northern hemisphere summer insolation and monsoon intensification. The rapid influx of fresh-water promoted a strong surface ocean stratification that led to the establishment of deep-basin anoxic conditions in parallel with an increased export productivity, which resulted in the formation of sapropel layers observed in the sedimentary record (Bianchi et al., 2006; De Lange et al., 2008; Grant et al., 2016; Grimm et al., 2015; Incarbona et al., 2011; Marino et al., 2009; Rohling, 1994; Rohling et al., 2015; Rossignol-Strick, 1985; Toucanne et al., 2015). The last sapropel (S1) took place during the Holocene between ~10.8 and ~6.1 kyr cal. BP in the E-Med (De Lange et al., 2008). Several studies have focused on the detailed analysis of the oceanographic conditions associated with the S1 formation in the E-Med (Bianchi et al., 2006; Checa et al., 2020; Filippidi et al., 2016; Grimm et al., 2015; Mercone et al., 2001; Tachikawa et al., 2015; Tesi et al., 2017; Wu et al., 2017). However, only a few studies have explored in detail the inter-basin connection during these episodes and its link with past climate variability (Cornuault et al., 2018; Martínez-Ruiz et al., 2003; Murat, 1999).

The large S1 change in the evaporation-precipitation balance of the E-Med and the consequent reduction in deep water convection might have ended in reduced water exchange between the two

Mediterranean sub-basins (Bethoux, 1993; Murat, 1999). Despite some modeling exercises have estimated the impact of S1 conditions in the water exchange through the Strait of Sicily (Myers et al., 1998), no paleoceanographic reconstructions have been able to identify the potential impact of such changes in the W-Med surface hydrology to date.

In this study, we present a new detailed characterization of past surface hydrography in the western edge of the Sicily channel (W-Sicily) in order to identify potential variations in the water exchange between the two Mediterranean sub-basins through the Sicily channel associated with the S1 formation. For this purpose, we use a sediment core currently located in the main pathway of the Modified Atlantic Surface Water (MAW) towards the Strait of Sicily. This study focuses in the analysis of the surface hydrographic expression in this area associated to the S1, which has been labeled with the ES1 acronym. Changes in surface water properties are reconstructed through a multi-proxy approach combining planktic foraminifera ecology, major element analyses in bulk sediments, as well as stable oxygen isotopes measurements ($\delta^{18}O$) in both *Globigerina bulloides* and *Globigerinoides ruber* white variety. The newly generated data are also compared to other available records from the central Mediterranean and the Alboran Sea for further discussion.

3.2 MATERIALS AND METHODS

3.2.1 Core description and sampling

The gravity core NDT-6-2016 (~4 m long) was recovered during the Next Data expedition that took place in 2016 on board of CNR-URANIA R/V. The core is located in the transition area between the W-Sicily channel and the southern Tyrrhenian Sea (38°0'26.60" N and 11°47'44.84"E, 1066 m water depth), i.e. at the easternmost region of the W-Med (Fig. 1a). This location is currently sensitive to inter-basin water exchange variability (Fig. 1b) and thus, appropriate to detect potential hydrological changes. Core NDT-6-2016 consists of homogeneous silty-clay sediments with no sedimentary irregularities along the whole sequence. The core was sampled every cm. Planktic foraminifera assemblages were counted every 1-5 cm for the intervals 1-61 cm and 123-340 cm and every 5-20 cm for the rest. Stable isotopes were analysed every 1-

2 cm for the interval between 1.20 and 2.60 m (corresponding chronologically to the deglacial-Holocene period) and at lower resolution (5-20 cm) for the rest of the core. Finally, elemental XRF analyses were carried out every cm all along the core.

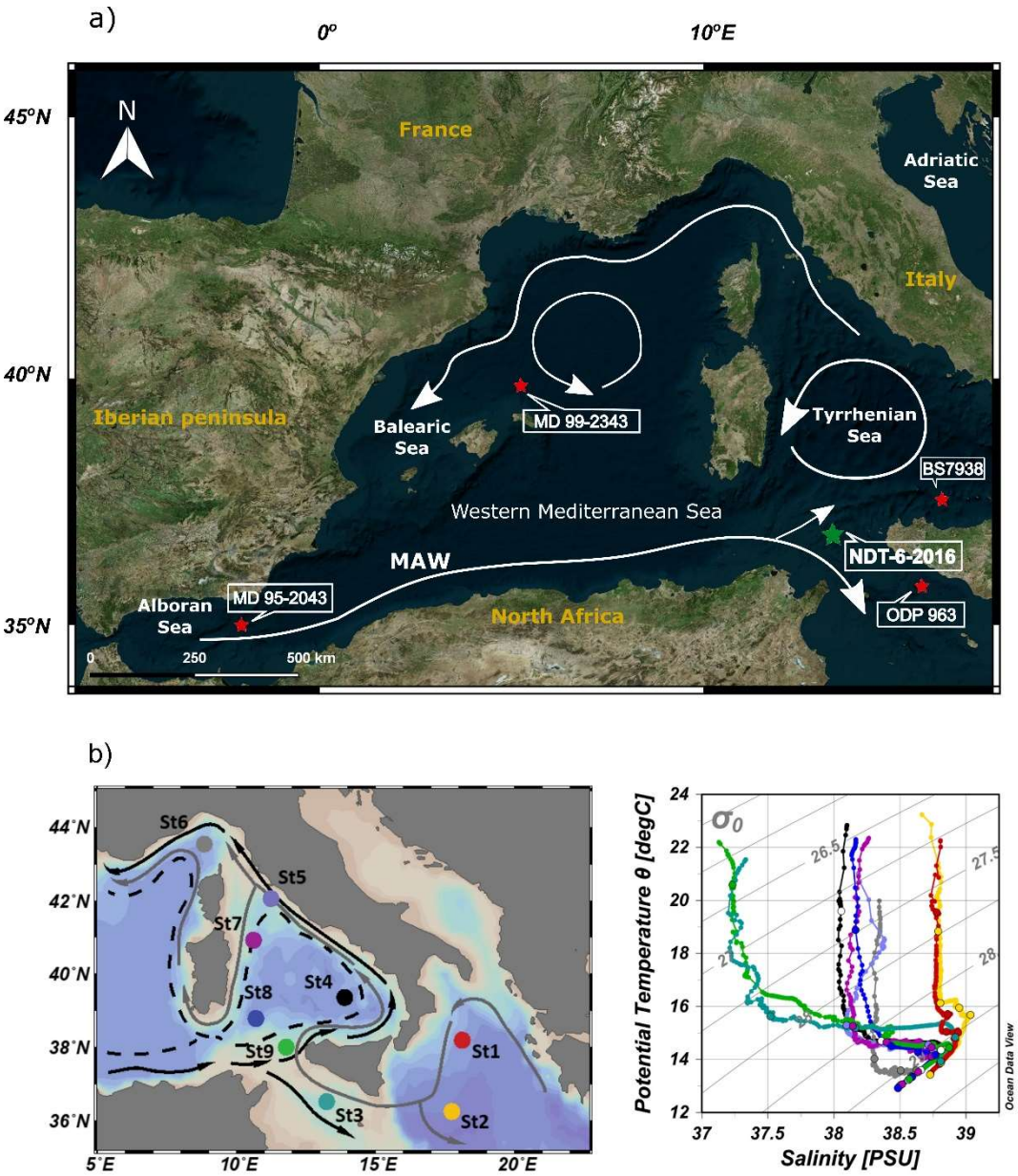

Fig. 1 a) Map of the study area in the western Mediterranean Sea. White arrows represent the Modified Atlantic waters (MAW) and stars represent the cores discussed in this manuscript. Green star represent the studied core NDT-6-2016 and red stars represent the other cores of the western and central Mediterranean Sea. b) Hydrographic stations around the Tyrrhenian Sea, Strait of Sicily and Ionian Sea and its properties in terms of temperature and salinity from Garcia-Solsona et al. (2020), note that location of St9 (green) corresponds to the studied site.

3.2.2 Radiocarbon dates and age model

The chronological framework of core NDT-6-2016 was established by twenty ^{14}C dates analysed in monospecific planktic foraminifera samples (>250µm, *Globorotalia inflata)*. Six ^{14}C ages (Table 1) were measured at The 14Chrono Centre of the Queen's University of Belfast (UK) using a National Electrostatic Corporation (NEC) compact model 0.5MV accelerator mass spectrometer (AMS). Samples were previously treated at the Godwin Laboratory for Palaeoclimate Research of the University of Cambridge (UK), where carbonate shells were turned into graphite following Freeman et al. (2016). Fourteen ^{14}C ages (Table 1) were measured at the ETH Laboratory of Ion Beam Physics (Zurich), using a 200 kV Mini Carbon Dating System (Micadas) with a gas ion source.

Radiocarbon ages were calibrated using MARINE20 calibration curve (Hunt et al., 2020). The age model was constructed using the Bayesian statistics software Bacon (Blaauw & Christeny, 2011) (Table 1). In addition to the ^{14}C dates of the lower part, three tie points were added based on an adjusted alignment between the studied $\delta^{18}O$ record from *G. bulloides* and the well-dated reference NGRIP isotope record (Rasmussen et al., 2006; Vinther et al., 2006). In particular, these selected tie points correlate the onset of the Bølling-Allerød (14.55 kyr BP) and the base and top of the Younger Dryas (YD, 12.89 and 11.57 kyr cal. BP, respectively) (Fig. 2). The sedimentation rates for the studied period (i.e. the last ~15 kyr cal. BP), oscillate between 5.70-76.34 cm/kyr, i.e. between 13.10-167.56 years per cm (Fig. 2). These results reveal a major decrease in sedimentations rates at around ~10 kyr BP which is validated by a large number of absolute dates supporting that it represents to a major change in the sedimentological processes at the studied location.

Depth (cm)	Species	Laboratory	Age ^{14}C (years BP)	2σ error	Calendar (years BP)	Age uncertainties interval (years BP)
6	*G. inflata*	ETH Zurich	434	44	103	0-245
61	*G. inflata*	Godwin Laboratory	3111	28	2972	2798-3148
83	*G. inflata*	Godwin Laboratory	3718	29	3722	3544-3896
121	*G. inflata*	ETH Zurich	5319	55	5705	5530-5989
126	*G. inflata*	Godwin Laboratory	5613	29	6030	5876-6196
141	*G. inflata*	Godwin Laboratory	6203	28	6659	6483-6835
151	*G. inflata*	Godwin Laboratory	7432	44	7906	7728-8070
161	*G. inflata*	Godwin Laboratory	9001	31	9764	9544-9968
166	*G. inflata*	ETH Zurich	9613	69	10599	10291-10891
172	*G. inflata*	ETH Zurich	9836	72	10927	10665-11174
177	*G. inflata*	ETH Zurich	9658	73	10669	10393-11006
182	*G. inflata*	ETH Zurich	10000	74	11151	10837-11399
230	*G. inflata*	ETH Zurich	10179	73	11388	11159-11690
242	*G. inflata*	ETH Zurich	9855	71	10951	10690-11186
255	*G. inflata*	ETH Zurich	9667	73	10683	10410-11018
259	*G. inflata*	ETH Zurich	11138	72	12685	12489-12867
271	Tie point		11570	200	11570	11413-12113
286	*G. inflata*	ETH Zurich	11650	76	13173	12960-13391
296	*G. inflata*	ETH Zurich	9959	70	11098	10792-11310
341	Tie point		12730	200	12730	12547-13323
360	*G. inflata*	ETH Zurich	11155	75	12700	12498-12890
391	*G. inflata*	ETH Zurich	12513	81	14227	13874-14649
415	Tie point		14550	200	14550	14394-15522

Table 1. ^{14}C ages with reservoir age corrections of core NDT-6-2016 and tie points based on the alignment between our stable oxygen isotopes records from *G. bulloides* and stable oxygen isotopes records from well-dated NGRIP (Rasmussen et al., 2006; Vinther et al., 2006). The ages were calibrated using Bayesian statistics software Bacon (Blaauw and Christen, 2011) and MARINE20 calibration (Hunt et al., 2020).

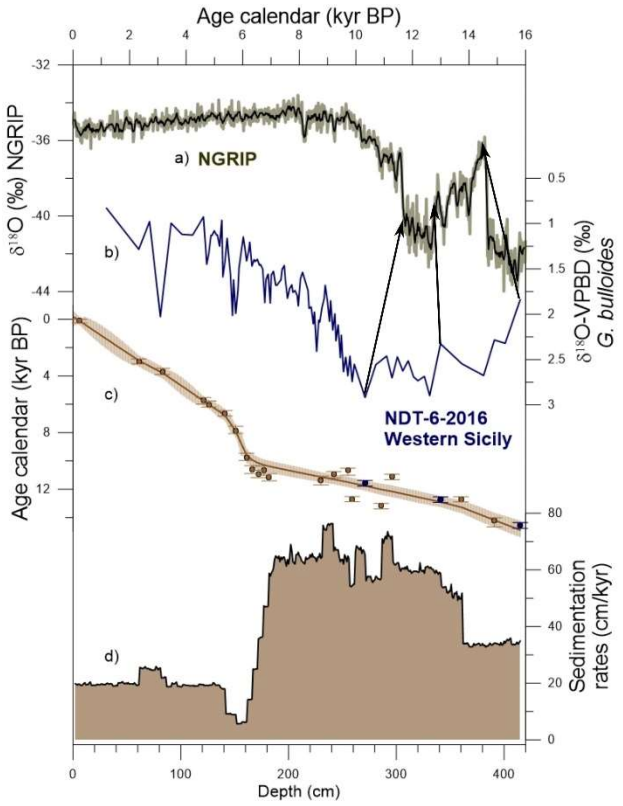

Fig. 2. a) Oxygen isotope record ($\delta^{18}O$) from NGRIP (Rasmussen et al., 2006; Vinther et al., 2006). b) Oxygen isotopes record measured in *G. bulloides* from sediment core NDT-6-2016. c) Age model based on ^{14}C calibrated dates from NDT-6-2016 (represented by brown circles) and three tie points (blue circles) based on the alignment between our *G. bulloides* $\delta^{18}O$ record and stable oxygen isotope record from well-dated NGRIP. d) sedimentation rates of sediment core NDT-6-2016. Note that all records are plotted in the same x axis which represents depth (cm), except the $\delta^{18}O$ record from NGRIP which is plotted in independent x axis representing the Age calendar (kyr BP).

3.2.3 Bulk sediment geochemistry

The analysis of the elemental geochemical composition of core NDT-6-2016 was performed on u-channels sections, with a 10×10 mm slit size, and at 1 cm resolution by means of an Avaatech XRF core-scanner at the CORELAB of the Universitat de Barcelona. Excitation conditions were established as follow: a) at 10kV, 0.5 mA, 10 s with no filter for major elements (Al, Si, S, K, Ca, Ti, Mn and Fe); b) 30 kV, 1 mA, 30 s and Pd-thick filter for heavier elements (mainly Br, Rb, Sr and Zr) and c) 50 kV, 1 mA, 40 s and a Cu filter for Ba. Previous to analysis, u-channels were imaged with a high-resolution line scan camera and covered with a 4 μm SPEXCerti Ultralene

foil, which prevents dehydration of the sediment and avoids contamination of the measurement prism.

3.2.4 Planktic foraminifera taxonomy

Planktic foraminifera species were counted every 2-5 cm for the discussed period (from YD to post-ES1) and between 5-20 cm for the rest, from the >125 μm fraction in order to minimise the loss of small species such as *Globigerinita glutinata* o *Turborotalita quinqueloba* (Sprovieri et al., 2003). To facilitate the counting, each sample was split between two and four times and a minimum of 300 specimens per sample were counted and normalized to 100. Nineteen groups were distinguished; *Globigerina bulloides* (including *Globigerina falconensis), Globoturborotalita ssp., Globigerinella siphonifera* (including *Globigerinella calida), Globigerinita glutinata, Globigerinoides elongatus, Globigerinoides ruber* white variety, *Globigerinoides ruber* pink variety, *Globigerinoides sacculifer* (including *Globigerinoides trilobus* and *Globigerinoides quadrilobatus*), *Globorotalia inflata, Globorotalia scitula* (dextral and sinistral coiling), *Globorotalia truncatulinoides* (dextral and sinistral coiling), *Neogloboquadrina incompta (*dextral coiling*), Neogloboquadrina pachyderma (*sinistral *coiling), Neogloboquadrina dutertrei, Neogloboquadrina sp., Orbulina universa, Turborotalita quinqueloba* and *Tenuitella spp.*, being *Globigerinita glutinata, Globorotalia inflata, Globigerina bulloides, Turborotalita quinqueloba, Globigerinoides ruber* white variety and *Neogloboquadrina incompta* the most abundant species. The ecological interpretation adopted in this study is based on previous works from Bé & Tolderlund, (1971), Hemleben et al., (1989), Pujol & Vergnaud-Grazzini (1995), Schiebel et al., (2001) and Kucera et al. (2005). Only species with an abundance of >10% of the total assemblages are discussed individually.

3.2.5 Stable Isotopes measurements

Between 10 and 12 specimens of the planktic foraminifera species *G. bulloides* and *G. ruber* white variety were handpicked from the 250-315 μm fraction to analyse the stable oxygen isotopic composition ($\delta^{18}O$) of surface waters. Samples were mechanically cleaned with methanol to remove any attached clay minerals, ultrasonicated for 30 seconds and dried out under a laminar

flood hood. The analyses were conducted using a Finnigan MAT 252 mass spectrometer in the Centre Científic i Tecnològic de la Universitat de Barcelona (CCiT-UB), whose analytical precision for $\delta^{18}O$ is better than 0.08‰. Calibration to Vienna Pee Dee Belemnite (VPDB) was carried out following NBS-19 standards (Coplen, 1996).

3.3 RESULTS

3.3.1 Downcore distribution of Planktic foraminifera assemblages

Planktic foraminifera live into the surface waters and are good indicators of climatic conditions since its distribution changes depending on salinity, temperature, vertical water-mixing and surface waters productivity (Bé & Hutson, 1977; Bé & Tolderlund, 1971; Capotondi et al., 1999; Hemleben et al., 1989; Pujol & Vergnaud-Grazzini, 1995; Schiebel & Hemleben, 2000). In this manuscript, we use the distribution of six planktic foraminifera species with different ecological preferences such as *T. quinqueloba, G. glutinata, N. incompta, G. bulloides, G. inflata* and *G. ruber* (Table 2) which allow us to identify four main time intervals (note that the here used ES1 acronym refers to the hydrographic expression of the S1 in the W-Sicily, i.e. changes in the surface hydrology associated to the eastern basin stagnation): 1) the YD (12.95-11.65 kyr cal. BP), characterized by the predominance of *T. quinqueloba* as well as *N. incompta,*; 2) the precedent period to the ES1 (pre-ES1 interval; 11.65-10.5 kyr cal. BP), distinguished by high abundance of both *G. glutinata* and *T. quinqueloba* while *N. incompta* decreased significantly; 3) the ES1 (10.5-7 kyr cal. BP) determined by high presence of *G. inflata* and *G. ruber*; and 4) the post-ES1 (7-6 kyr cal. BP) characterized by high abundance of both *G. inflata* and *N. incompta* and lower values of *G. ruber*. Furthermore, the ES1interval can be divided in two sub-stages: a) the ES1a, characterized by high abundance of *G. inflata* and increasing percentages of *G. ruber* while *T. quinqueloba* and *G. glutinata* tend to decrease and b) the ES1b, distinguished by the highest presence of *G. inflata, N. incompta* and *G. ruber* and the almost total disappearance of *T. quinqueloba* and *G. glutinata*.

Planktic foraminifera species	Ecological preferences
Turborotalita quinqueloba	Cold and well-mixed high-nutrient waters. Commonly associated with continental run-off.
Globigerinita glutinata	Temperate, well-mixed and high-nutrient waters.
Globigerina bulloides	Cold and temperate waters. High-nutrient and well-mixed waters. Upwelling areas.
Globorotalia inflata	Temperate species. Strong vertical water mixing. No deep chlorophyll maximum (DCM).
Neogloboquadrina incompta	Cold-temperate species. Presence of the DCM.
Globigerinoides ruber	Warm and oligotrophic species. Stratified surface waters.

Table 2. Summary of planktic foraminifera ecological preferences based on works of (Bé & Tolderlund, 1971), (Hemleben et al., 1989), Pujol & Grazzini (1995), (Schiebel et al., 2001) and Kucera et al. (2005).

Maximum abundance of both *T. quinqueloba* (25-40%) and *G. glutinata* (15-25%) during the YD suggests the prevalence of cold conditions and high-nutrient waters (Fig. 3e and f) (Schmidt et al., 2004). In the modern Mediterranean, both *T. quinqueloba* and *G. glutinata* proliferate during spring as a response to enhanced phytoplankton production, as well as during fall when surface enhanced vertical water column mixing increases and the chlorophyll accumulated during summer in the so-called Deep Chlorophyll Maximum (DCM) is redistributed uniformly in the surface waters (Schiebel et al., 2001). During the same period, the high presence of *N. incompta* (12-20%, Fig. 3f) suggests the presence of a shallow mixed layer and the DCM development, since it proliferated below the thermocline at the end of summer and over fall, when the presence of a shallow nutricline favors the phytoplankton spread (Bé & Hutson, 1977; Pérez-Folgado et al., 2003; Pujol & Vergnaud-Grazzini, 1995; Schiebel et al., 2001). Therefore, during the YD, both *T. quinqueloba* and *G. glutinata* likely predominated during winter/spring when a moderate vertical water-mixing occurred, while *N. incompta* might have prevailed during summer/fall associated with more stratified conditions.

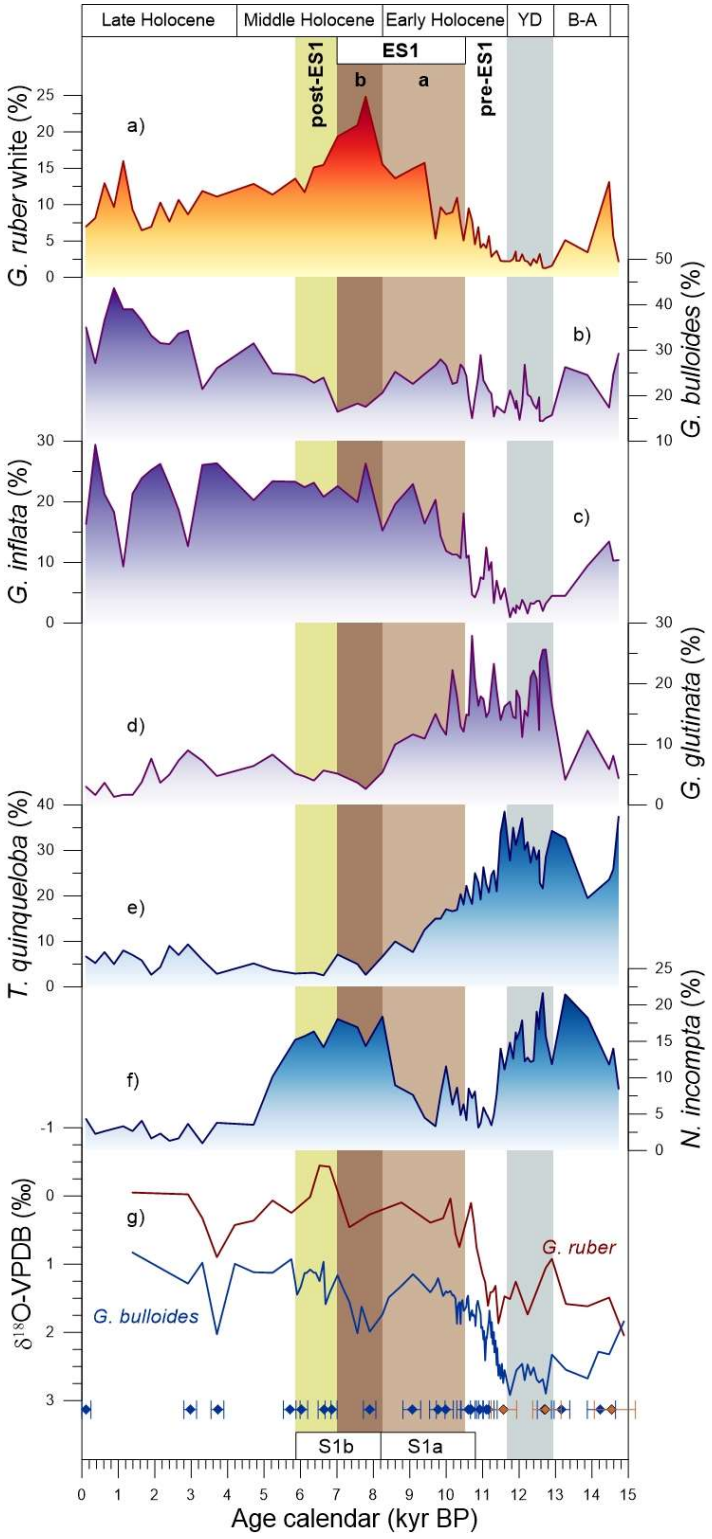

Fig. 3. a-f) Planktic foraminifera distribution and g) $\delta^{18}O$ of planktic foraminifera species *G. bulloides* and *G. ruber* and their ^{14}C calibrated dates with the corresponding errors (blue rhombs) and applied tie points including their uncertainties (orange rhombs). Grey bar represents YD (Younger Dryas), light-brown bar the ES1a, dark-brown bar the ES1b and greenish-yellow bar the post-ES1 (ES1: W-Sicily expression of the S1).

During the pre-ES1 high abundance of both *G. glutinata* (12.5-27.5%) and *T. quinqueloba* (15-25%) (Fig. 3d and e) indicates well-mixed waters and eutrophic conditions (Pujol & Vergnaud-Grazzini, 1995; Sprovieri et al., 2003) as during the YD. But the sharp decrease of *N. incompta* during this period probably indicates a moderate vertical-mixing from the end of summer, which promote the redistribution of nutrients from the DCM favoring the *G. glutinata* and *T. quinqueloba* spread. At the same time, *G. inflata,* that proliferates as a result of thermocline erosion due to the strong vertical mixing conditions (Pujol & Vergnaud-Grazzini, 1995; Sprovieri et al., 2003), show a relatively low abundances (from ~5 to ~10%) (Fig. 3c). Then, planktonic foraminifera distribution during the pre-ES1 suggests an annual homogeneity of the oceanographic conditions, with a weakly developed seasonality.

The ES1 was characterized by maximum abundance of the subtropical species *G. ruber* (10-25%), characteristic of oligotrophic waters (Bonfardeci et al., 2018; Kucera, 2007; Numberger et al., 2009) (Fig. 3a). *G. ruber* grow preferentially during summer conditions in well stratified surface waters (Pujol & Vergnaud-Grazzini, 1995; Schiebel et al., 2001; Sprovieri et al., 2003). *G. inflata* also reaches its highest abundance during this period (oscillating between 12 and 27%) (Fig. 3c). Thus, the ES1 is distinguished by an increase in seasonality with strong winter water-mixing as high abundances of *G. inflata* suggest and by strong summer stratification as *G. ruber* increase point out. The high presence of *N. incompta* (~15%) during the ES1b (Fig. 3f) may suggest the dominance of rather stratified summer/fall conditions with a shallow mixed layer and a DCM development. A different situation than that developed before, during the ES1a, when strong vertical mixing presumably took place during autumn, redistributing the nutrients accumulated in the DCM and favouring the growth of *G. inflata* instead of *N. incompta*. (Bé & Hutson, 1977; Pérez-Folgado et al., 2003; Pujol & Vergnaud-Grazzini, 1995; Schiebel et al., 2001).

During the post-ES1 predominated both *G. inflata* (~22%) and *N. incompta* (~15%) in parallel with a decrease of *G. ruber* (from 20 to 12%) (Fig. 3c and f). While *G. ruber* decrease suggests lower summer-water stratification, *N. incompta* indicates reduced vertical water-mixing and the

development of a DCM during fall. During winter, vertical water-mixing would strongly increase as suggested by the high abundance of *G. inflata*.

3.3.2 Oxygen isotopic records ($\delta^{18}O$)

Oxygen isotopic records ($\delta^{18}O$) from *G. bulloides* and *G. ruber* (Fig. 3g) show a general transition from heavier (glacial) to lighter (interglacial) isotopic values, consistent with the overall global warming and ice sheet melting associated with the last deglaciation (Cacho et al., 2001; Frigola et al., 2007; Rohling et al., 1998; Sbaffi et al., 2004). From ~15 to ~11.7 kyr cal. BP, $\delta^{18}O$ of *G. bulloides* presents a general transition from lighter (~2‰) to heavier values (~3‰). During the YD, heaviest values were dominant ranging between 2.5 and 3‰. Along the pre-ES1 a progressive lightening of 1.5‰ took place (Fig. 3g). During the first part of the ES1 interval (ES1a) $\delta^{18}O$ of *G. bulloides* oscillated between 1 and 1.5‰, while the second part (ES1b) was characterized by a remarkable $\delta^{18}O$ enrichment (~1‰). From the end of the ES1b, $\delta^{18}O$ progressively returned to lighter values. In the case of the *G. ruber* $\delta^{18}O$ record, the evolution was very similar to that of *G. bulloides* but with lighter values (1-2‰), which is consistent with the habitat differences of the two planktic foraminifera; *G. ruber* register the signal of warm and stratified waters, while *G. bulloides* record the signal of colder and mixed waters. The heaviest *G. ruber* $\delta^{18}O$ values were registered between 15 and 11 kyr cal. BP oscillating between 2 and 1.2‰ (except for the onset of the YD where 1‰ was reached). The pre-ES1 was characterized by a progressive lightening of ~2‰. Along the ES1, $\delta^{18}O$ values were rather constant oscillating between 0 and 0.5‰, while during the post-ES1 a significant depletion took place (from 0.4 to -0.4‰). In general terms, it is remarkable that the overall $\delta^{18}O$ gradient between the two planktic species reached its maximum values during the ES1b interval and the minimum along the pre-ES1 (Fig. 3g).

3.3.3 Elemental analyses

Profiles of Ti/Al and K/Al ratios present very similar trends throughout the studied interval. These ratios are usually interpreted as indicators of the arrival of terrestrial source material likely reflecting increased sediment supply by river runoff (Frigola et al., 2008; Wehausen & Brumsack,

1998, 2000; Wu et al., 2016). Both ratios reached their maximum values during the pre-ES1 while the ES1 is represented by a relative minimum (Fig. 4a-b). Ba/Ti ratios are often used as an indicator of export primary productivity, since the deposition of barite is associate with primary productivity, although Ba can also have some detrital sources (Martínez-Ruiz et al., 2003; Murray et al., 2000; Paytan & Griffith, 2007). In the case of core NDT-6-2016, the maximum values of Ba/Ti are also reached during the pre-ES1 showing a similar evolution to the previously described ratios (Fig. 4c). During the ES1, however, the Ba/Ti evolution is very distinctive to that of the other ratios, supporting its interpretation in terms of export productivity. In this regard, Ba/Ti ratios present relatively high values during the early ES1 to progressively decrease along that period. From the end of the ES1 to the rest of the record, a general decreasing trend is observed (Fig. 4c). It is interesting to note that the relatively low values in the Ti/Al and K/Al ratios during the ES1 coincides with a major reduction in the sedimentation rates of the NDT-6-2016 core (Fig. 4e), pointing to a decrease in the arrival of detrital source sedimentary particles as a potential cause of these sedimentary changes.

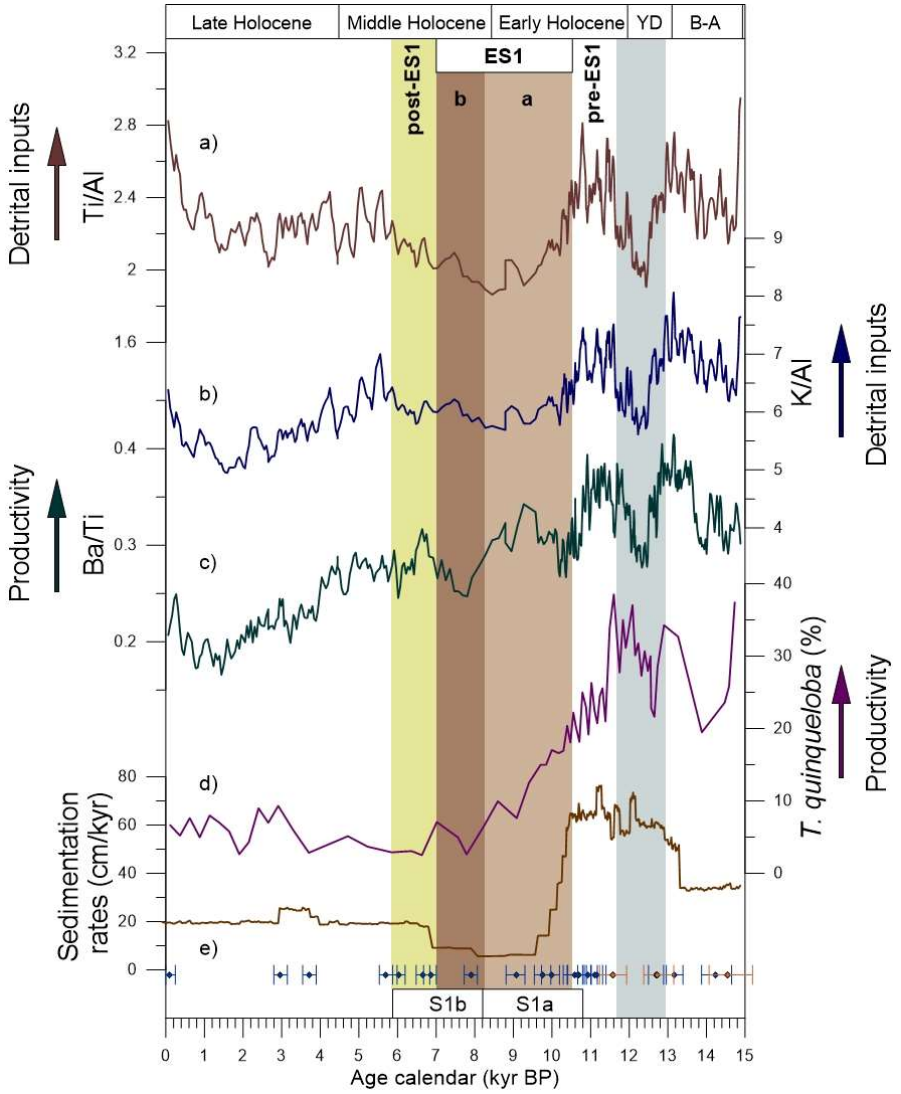

Fig. 4. a-c) Major and minor elements distribution, d) planktic foraminifera distribution of *T. quinqueloba* and e) sedimentation rates of sediment core NDT-6-2016. Blue rhombs represent ^{14}C calibrated dates and orange rhombs represent tie points. Grey bar represents YD, light-brown bar the ES1a, dark-brown bar the ES1b and greenish-yellow bar the post-ES1.The S1 (a and b) according to de Lange (2008).

3.4 DISCUSSION

3.4.1 Deglacial-Holocene evolution of surface oceanography in W-Sicily

The overall evolution of $\delta^{18}O$ records is consistent with the described deglacial warming trend in the W-Mediterranean (Budillon et al., 2009; Cacho et al., 2001; Català et al., 2019; Kallel et al., 1997; Sbaffi et al., 2001). Nevertheless, one of the outstanding findings in our studied core is the

distinctive characteristics of the ES1 period (between ~10.5 and ~7 kyr cal. BP) in comparison to those developed before (pre-ES1 and YD) and after it.

The predominant high values of both Ti/Al and K/Al ratios during the pre-ES1 (Fig. 4a-b) indicate the arrival of detrital particles to the core location likely due to enhanced continental runoff (Frigola et al., 2008; Wehausen & Brumsack, 2000; Wu et al., 2016). The parallel evolution in Ba/Ti profiles (Fig. 4c) could reflect a relatively high biological productivity (Martínez-Ruiz et al., 2003; Paytan & Griffith, 2007) probably related to the increase in river discharge and the consequent nutrient increase. This interpretation is consistent with a high abundance of planktic foraminifera species with a strong affinity for nutrient-rich surface waters such as *T. quinqueloba* (Fig. 4d) (Margaritelli et al., 2016; Schiebel et al., 2001; Sprovieri et al., 2003). The described high arrival of the detrital particles could be related to the strong African Monsoon activity that started at around 15 kyr BP (Ménot et al., 2020). The general north African humid conditions were interrupted during the YD (Ménot et al., 2020), probably causing the relative minimum in our both Ti/Al and K/Al ratios during this period (Fig. 4a-b). Our core location is currently far from the direct influence of any major river system, but this situation might have been very different during the pre-ES1 coincident with the African humid period, when currently fossil river systems along the North Africa coast were active (Wu et al., 2016, 2017). Considering the local oceanography, detrital particles and nutrients transported by these rivers could reach the studied location through the outflowing intermediate waters from the Strait of Sicily. During the pre–ES1, summer stratification and winter vertical mixing should have been weak according to the low presence of both *G. ruber* and *G. inflata* (Kucera, 2007; Pujol & Vergnaud-Grazzini, 1995). This data, along with the lowest $\delta^{18}O$ gradient between *G. bulloides* and *G. ruber,* support a rather annual homogeneity with a weakly developed seasonality (Fig. 5) since such species represent winter-spring and summer conditions, respectively. Thus, similar values of $\delta^{18}O$ should involve similar conditions across an entire year.

Both bulk sediment chemistry and surface hydrography at the NDT-6-2016 location in the W-Sicily strongly changed at the onset of the ES1. Both Ti/Al and K/Al ratios show minimum values during the whole interval (Fig. 4a-b) while the African humid conditions and associated sediment

delivery by the north African river system prevailed (Ménot et al., 2020; Wu et al., 2016). The major reduction in the arrival of detrital source particles is in good agreement with the large reduction of the sediment rates during the whole ES1 (Fig. 4e). However, since this sedimentary change cannot be explained by reduced river runoff, we suggest that it might reflect a major change in the deep water hydrology, likely related to reduction of water exchange through the Strait of Sicily. Consistently, the parallel increment during the ES1 of both *G. inflata*, that predominate with strong water-mixing (typically during winter), and *G. ruber*, that prefer strong surface water stratification conditions (typically during summer), supports the development of a strong seasonality (Fig. 3a,c and Fig. 5) (Hemleben et al., 1989; Pujol & Vergnaud-Grazzini, 1995). This stronger seasonality reached its maxim expression during the ES1b accordingly to the maximum *G. ruber* percentages and it is further supported by the maximum $\delta^{18}O$ gradient between *G. ruber* and *G. bulloides* records (Fig. 3g). The *G. bulloides* $\delta^{18}O$ enrichment observed during the ES1b could reflect the development of extreme winter vertical water-mixing and colder SST (Fig. 7). In contrast, *G. ruber* $\delta^{18}O$ record represented stratified (low nutrient) summer conditions and warmer Sea Surface Temperatures (SST) (Fig. 5).

During the post-ES1, a significant decrease in *G. ruber* points to a decrease in surface water stratification during summer, while the high presence of both *N. incompta* and *G. inflata* suggest, on the one hand, relatively stratified conditions with the presence of the DCM during fall and, on the other hand, an intense water-mixing during winter. During the rest of the Holocene period, after post-ES1, a progressive increase in *G. bulloides* parallel with a gradual decrease in *G. ruber* and a sharp decline in *N. incompta* suggests that surface water stratification progressively decreased during summer while more intense water-mixing took place during fall and winter. Furthermore, the sedimentation rates are higher after the ES1, although not as high as during the pre-ES1 (Fig. 4e). These changes in both sedimentary conditions and surface hydrography were probably related to the end of the extreme stagnation in the E-Med and might reflect the arrival of detrital material transported by intermediate waters through the Strait of Sicily, although it was never as high as that during the African humid period that preceded the S1 stagnation.

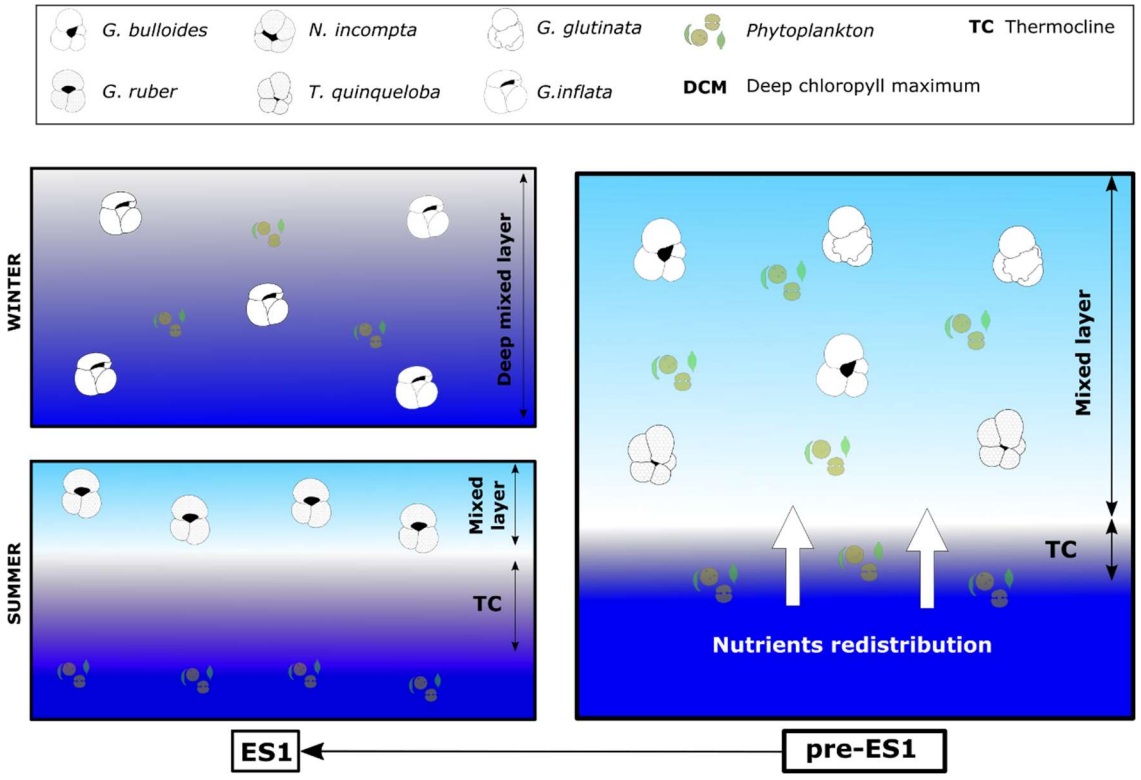

Fig. 5. Scheme representing the planktic foraminifera distribution in the W-Sicily (core NDT-6-2016) during the pre-ES1 and the ES1. Figure represents only the main species dominating each period. It must be noted that changes in planktic foraminifera distribution between periods were progressive.

3.4.2 Implications of the E-Med S1 stagnation in the central Mediterranean surface oceanography

Our results from W-Sicily during the last ~15 kyr cal. BP can be framed in a broader regional context by comparing our planktic foraminifera results with previously published records from the Alboran Sea (Pérez-Folgado et al., 2003), the southern Tyrrhenian Sea (Sbaffi et al., 2004) and the Strait of Sicily (Sprovieri et al., 2003) (Fig. 6). We also compare the *G. bulloides* $\delta^{18}O$ records from the same locations (Fig. 7), with the exception of the Sicily channel where no isotopic records are available, and also with an additional record from the Balearic Sea (Català et al., 2019; Frigola et al., 2007).

Our results from W-Sicily during the last ~15 kyr cal. BP can be framed in a broader regional context by comparing our planktic foraminifera results with previously published records from the Alboran Sea (Pérez-Folgado et al., 2003), the southern Tyrrhenian Sea (Sbaffi et al., 2004)

and the Strait of Sicily (Sprovieri et al., 2003). We also compare the *G. bulloides* $\delta^{18}O$ records from the same locations (Fig. 7), with the exception of the Sicily channel where no isotopic records are available, and also with an additional record from the Balearic Sea (Català et al., 2019; Frigola et al., 2007).

Oceanographic surface conditions during the YD appear to be rather homogeneous along the considered locations with weak summer stratification conditions (low abundance of *G. ruber*) and weak surface winter water-mixing (low abundance of *G. inflata*). With the onset of the Holocene period (pre-ES1) the surface hydrology conditions begin to differ within the compared locations according to the planktic foraminifera distributions (Fig. 6). In the Strait of Sicily and the southern Tyrrhenian Sea an increased seasonality developed with stronger winter water-mixing conditions (an increase of *G. inflata*) and greater summer water-stratification (an increase of *G. ruber*) (Sbaffi et al., 2004; Sprovieri et al., 2003). In contrast, these species remained relatively low in the Alboran Sea and W-Sicily, probably suggesting the commune influence of the eastward path of the surface Atlantic Waters (MAW). This oceanographic situation would be comparable to that currently observed in the region (Fig. 1b) (Garcia-Solsona et al., 2020), where the station located in in the W-Sicily shows the direct influence of the eastward flow of the surface MAW while the southern Tyrrhenian Sea records a more modified signal in terms of salinity.

During the ES1 interval, significant differences are observed between the Strait of Sicily and our W-Sicily location (Fig. 6). Stratified conditions along the whole year predominated in the Strait of Sicily, as the high abundance of *G. ruber* and low presence of *G. inflata* suggests, while a marked seasonality with winter water-mixing and summer stratification, (high *G. inflata* and *G. ruber* abundance) dominated in W-Sicily (Hemleben et al., 1989; Kucera, 2007; Pujol & Vergnaud-Grazzini, 1995). Therefore, hydrographic conditions in W-Sicily resembled more to those already developed in the southern Tyrrhenian Sea during the pre-ES1 and become very distinctive to those in the Alboran Sea (Fig. 6). The comparison of the $\delta^{18}O$ records also supports the distinctive conditions between the W-Sicily and the Alboran Sea with closer similitudes to the

southern Tyrrhenian Sea location where both of them (W-Sicily and southern Tyrrhenian Sea) registered a significant $\delta^{18}O$ enrichment (Fig. 7).

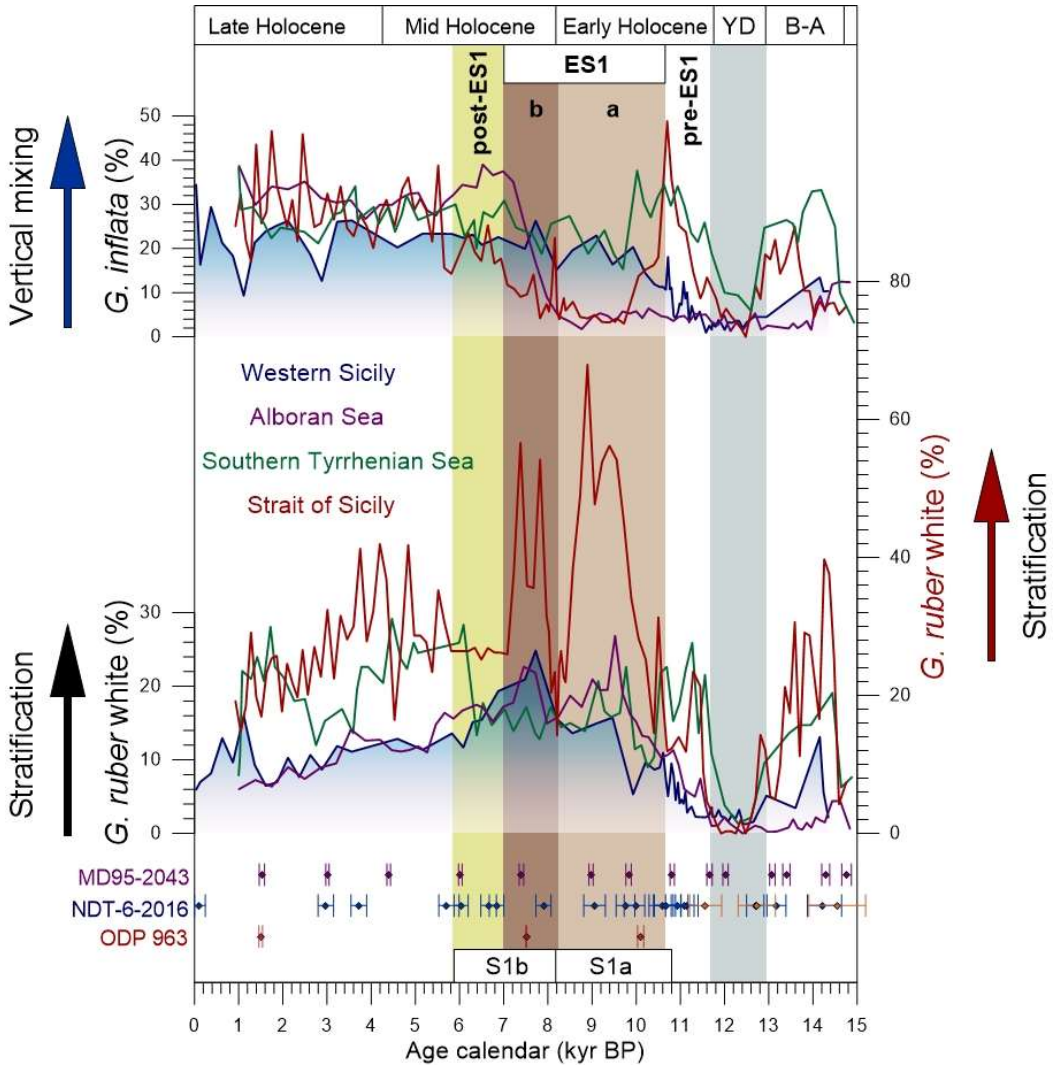

Fig. 6. Planktic foraminifera distribution in the western and central Mediterranean from the studied core NDT-6-2016 and cores BS7938 (Sbaffi et al., 2003), MD95-2043 (Pérez-Folgado et al., 2003) and ODP963 (Sprovieri et al., 2003). Blue line is for the NDT-6-2016, green line for the BS-7938, violet line for MD95-2043 and red line for the ODP963. It must be noted that *G. ruber* distribution from core ODP963 is plotted in independent *y* axis in order to help the figure compression. The ^{14}C calibrated dates used for each chronology are colored accordingly to the corresponding record. In the sediment core NDT-6-2016, blue rhombs represent ^{14}C calibrated dates and orange rhombs represent tie points. Grey bar represents YD, light-brown bar the ES1a, dark-brown bar the ES1b and greenish-yellow bar the post-ES1.

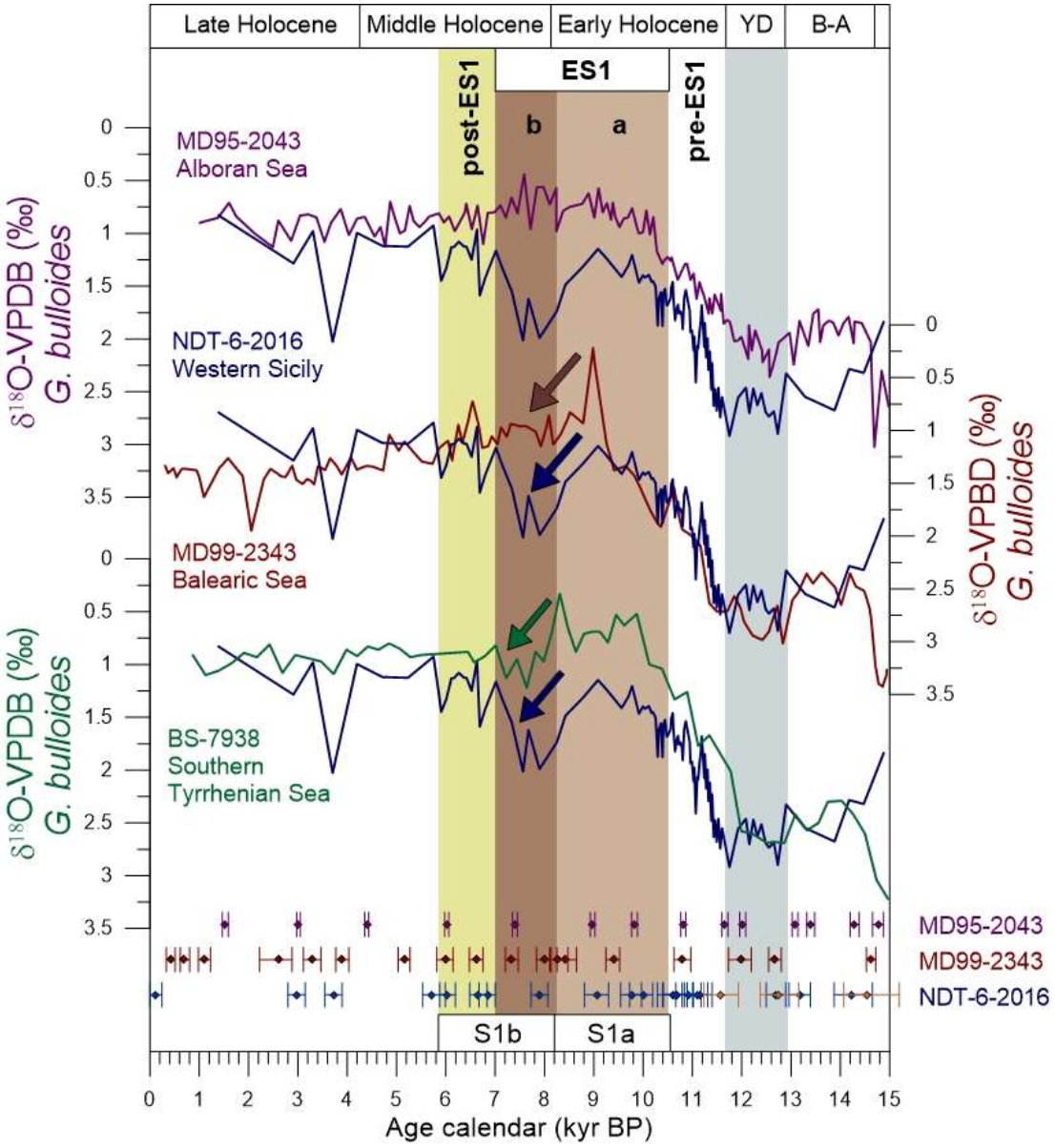

Fig. 7. Comparison of $\delta^{18}O$ (VPDB) records from different locations of the western Mediterranean Sea throughout the last 15 kyr cal. BP and chronological control for individual records. Blue line represents the $\delta^{18}O$ record from the studied core NDT-6-2016. From the top to the base in violet, red and green color $\delta^{18}O$ records from the cores MD95-2043 (Cacho et a., 1999), MD99-22343 (Frigola et al., 2007; Català et al., 2019) and BS-7938 (Sbaffi et al., 2003) respectively. The ^{14}C calibrated dates used for each chronology are colored accordingly to the corresponding record. For core NDT-6-2016, blue rhombs represent ^{14}C calibrated dates and orange rhombs represent tie points. Grey bar represents YD, light-brown bar the ES1a, dark-brown bar the ES1b and greenish-yellow bar the post-ES1.

In consequence, this site comparison highlights the singular character of the W-Sicily oceanographic conditions during the ES1 and, to some extent, during the pre-ES1. During the YD and after the ES1 the data agree in indicating a good surface interconnection between the W and E-Mediterranean basins, letting the W-Sicily and Strait of Sicily locations under the direct influence of the eastern path of the surface Modified Atlantic Waters (MAW). This would be a comparable oceanographic situation to that of the present day (Fig.1b). During the ES1 a major oceanographic reorganization occurred at the W-Sicily location that we attribute to a restricted sea surface interconnection between the E-Med and the W-Med. While the sea surface conditions in the Sicily channel are coherent with strong annual stratification, likely reflecting the freshening promoted by the African monsoon (Mercone et al., 2001; Rohling et al., 2015; Tachikawa et al., 2015; Tesi et al., 2017), the surface conditions in the W-Sicily were closer to those in the southern Tyrrhenian Sea, probably reflecting the major influence of the predominant climatic conditions in central Europe (Davis et al., 2003; Walker, 1995). This change in the sea surface interconnection between the W-E Med during the ES1 might be a response to the reduced exit of E-Med waters masses through the Strait of Sicily as a consequence of the reduced deep convection in the E-Med (Cornuault et al., 2018; Vadsaria et al., 2019; Wu et al., 2019). This would agree with the observed major reduction in the detrital particles transport toward the studied site detected by the Ti/Al and K/Al ratios and sedimentation rates (Fig. 4a-b, e). Although our data cannot provide any direct insight into the intermediate and deep circulation, the parallel changes in sea surface condition and in sedimentary patterns support a tided link between them, which is consistent with a major weakening in the Strait of Sicily exchange at both surface and deep layers..

3.5 SUMMARY AND CONCLUSIONS

Our new data from sediment core NDT-6-2016 in the W-Sicily allow the characterization of very distinctive oceanographic conditions during the ES1 interval (10.5-7 kyr cal. BP), as compared to the pre-ES1 and post-ES1. During the pre-ES1 interval, the W-Sicily records reflect low seasonality that progressively increased at the onset of the ES1 with summer stratification and winter mixing. These conditions turned more extreme during the ES1b and changed progressively

along the post-ES1 toward lower seasonality. A comparison of our $\delta^{18}O$ and planktic foraminifera distribution results, with similar records from the Alboran Sea, Balearic Sea, Tyrrhenian Sea and Strait of Sicily reveals that the ES1 conditions in our location contrasted to those developed in the Sicily channel and also in the Alboran Sea, showing higher similarity to those of the Tyrrhenian Sea. This is an opposite situation to that developed during YD when conditions in W-Sicily were closer to those of the Sicily channel and the Alboran Sea, a situation coherent with the current oceanography at these locations directly affected by the eastern path of the MAW. Consequently, we propose that during the ES1 a reduced surface water interconnection between E-Med and W-Med prevailed likely driven by the E-Med stagnation. This oceanographic condition resulted in a reduced thermohaline circulation that caused a weakening of the eastward flow of Atlantic source surface waters, reducing its entrance through the Strait of Sicily and over the studied W-Sicily site. In consequence, the predominant conditions that prevailed in central-southern Europe during the ES1 interval played an essential role, promoting the observed high seasonality in the W-Sicily oceanographic conditions. Therefore, our data provide a solid support for a major surface oceanographic reorganization in the central Mediterranean associated with the S1 formation in the Eastern Mediterranean Sea.

3.6 ACKNOWLEDGEMENTS

This work was founded by the projects TIMED (683237) of the European Research Council (Consolidator Grants) and NextData PNR 2011–2013 (http://www.nextdataproject.it/). The GRC Geociències Marines thank the Generalitat de Catalunya for the Grups de Recerca Consolidats grant 2017 SGR 315. Leopoldo D. Pena acknowledges support from the Ramón y Cajal program (MINECO, Spain), Isabel Cacho from the ICREA Academia programme from the Generalitat de Catalunya, Jaime Frigola from the Serra Húnter Programme (Generalitat de Catalunya). We thank the doctoral school in Earth and Sea Sciences from University of Palermo which supported the research. We also thank ISMAR-CNR (Napoli) for core NDT-6-2016 which it was recovered by the NEXTDATA expedition on board R/V CNR-Urania in 2014. Finally, we acknowledge

Montse Guart (Dept. Dinàmica de la Terra i de l'Oceà, Universitat de Barcelona) and Joaquim Perona (Centres Científics i Tecnològics, CCiT-UB) for their support with the laboratory work..

3.7 References

Abrantes, F., Voelker, A., Sierro, F. J., Naughton, F., Rodrigues, T., Cacho, I., Ariztegui, D., Brayshaw, D., Sicre, M. A., & Batista, L. (2012). Paleoclimate variability in the mediterranean region. In *The Climate of the Mediterranean Region* (First Edit). Elsevier Inc. https://doi.org/10.1016/B978-0-12-416042-2.00001-X

Bé, A. W. H., & Hutson, W. H. (1977). Ecology of Planktonic Foraminifera and Biogeographic Patterns of Life and Fossil Assemblages in the Indian Ocean. *Micropaleontology*, *23*(4), 369. https://doi.org/10.2307/1485406

Bé, A. W. H., & Tolderlund, D. S. (1971). Distribution and ecology of living planktonic foraminifera in surface waters of the Atlantic and Indian oceans. *The Micropalaentology of the Oceans*, 105–149.

Bethoux, J. P. (1993). Mediterranean sapropel formation, dynamic and climatic viewpoints. *Oceanologica Acta*, *16*(2), 127–133.

Bianchi, D., Zavatarelli, M., Pinardi, N., Capozzi, R., Capotondi, L., Corselli, C., & Masina, S. (2006). Simulations of ecosystem response during the sapropel S1 deposition event. *Palaeogeography, Palaeoclimatology, Palaeoecology*, *235*(1–3), 265–287. https://doi.org/10.1016/j.palaeo.2005.09.032

Blaauw, M., & Christeny, J. A. (2011). Flexible paleoclimate age-depth models using an autoregressive gamma process. *Bayesian Analysis*, *6*(3), 457–474. https://doi.org/10.1214/11-BA618

Bonfardeci, A., Caruso, A., Bartolini, A., Bassinot, F., & Blanc-Valleron, M. M. (2018). Distribution and ecology of the Globigerinoides ruber — Globigerinoides elongatus morphotypes in the Azores region during the late Pleistocene-Holocene. *Palaeogeography,*

Palaeoclimatology, Palaeoecology, *491*(November), 92–111. https://doi.org/10.1016/j.palaeo.2017.11.052

Budillon, F., Lirer, F., Iorio, M., Macrì, P., Sagnotti, L., Vallefuoco, M., Ferraro, L., Garziglia, S., Innangi, S., Sahabi, M., & Tonielli, R. (2009). Integrated stratigraphic reconstruction for the last 80 kyr in a deep sector of the Sardinia Channel (Western Mediterranean). *Deep-Sea Research Part II: Topical Studies in Oceanography*, *56*(11–12), 725–737. https://doi.org/10.1016/j.dsr2.2008.07.026

Cacho, I., Grimalt, J. O., Canals, M., Sbaffi, L., Shackleton, N., Schönfeld, J., & Zahn, R. (2001). Variability of the western Mediterranean Sea surface temperature during the last 25,000 years and its connection with the northern hemisphere climatic changes. *Climatic Changes*, *16*(1), 40–52. https://doi.org/10.1029/sp010

Capotondi, L., Maria Borsetti, A., & Morigi, C. (1999). Foraminiferal ecozones, a high resolution proxy for the late Quaternary biochronology in the central Mediterranean Sea. *Marine Geology*, *153*(1–4), 253–274. https://doi.org/10.1016/S0025-3227(98)00079-6

Català, A., Cacho, I., Frigola, J., Pena, L. D., & Lirer, F. (2019). Holocene hydrography evolution in the Alboran Sea: A multi-record and multi-proxy comparison. *Climate of the Past*, *15*(3), 927–942. https://doi.org/10.5194/cp-15-927-2019

Checa, H., Margaritelli, G., Pena, L. D., Frigola, J., Cacho, I., Rettori, R., & Lirer, F. (2020). High resolution paleo-environmental changes during the Sapropel 1 in the North Ionian Sea, central Mediterranean. *Holocene*. https://doi.org/10.1177/0959683620941095

Cornuault, M., Tachikawa, K., Vidal, L., Guihou, A., Siani, G., Deschamps, P., Bassinot, F., & Revel, M. (2018). Circulation Changes in the Eastern Mediterranean Sea Over the Past 23,000 Years Inferred From Authigenic Nd Isotopic Ratios. *Paleoceanography and Paleoclimatology*, *33*(3), 264–280. https://doi.org/10.1002/2017PA003227

Davis, B. A. S., Brewer, S., Stevenson, A. C., Guiot, J., Allen, J., Almqvist-Jacobson, H.,

Ammann, B., Andreev, A. A., Argant, J., Atanassova, J., Balwierz, Z., Barnosky, C. D., Bartley, D. D., De Beaulieu, J. L., Beckett, S. C., Behre, K. E., Bennett, K. D., Berglund, B. E. B., Beug, H. J., … Zernitskaya, V. P. (2003). The temperature of Europe during the Holocene reconstructed from pollen data. *Quaternary Science Reviews*, *22*(15–17), 1701–1716. https://doi.org/10.1016/S0277-3791(03)00173-2

De Lange, G. J., Thomson, J., Reitz, A., Slomp, C. P., Speranza Principato, M., Erba, E., & Corselli, C. (2008). Synchronous basin-wide formation and redox-controlled preservation of a Mediterranean sapropel. *Nature Geoscience*, *1*(9), 606–610. https://doi.org/10.1038/ngeo283

Filippidi, A., Triantaphyllou, M. V., & De Lange, G. J. (2016). Eastern-Mediterranean ventilation variability during sapropel S1 formation, evaluated at two sites influenced by deep-water formation from Adriatic and Aegean Seas. *Quaternary Science Reviews*, *144*, 95–106. https://doi.org/10.1016/j.quascirev.2016.05.024

Freeman, E., Skinner, L. C., Reimer, R., Scrivner, A., & Fallon, S. (2016). Graphitization of small carbonate samples for paleoceanographic research at the godwin radiocarbon laboratory, University of Cambridge. *Radiocarbon*, *58*(1), 89–97. https://doi.org/10.1017/RDC.2015.8

Frigola, J., Moreno, A., Cacho, I., Canals, M., Sierro, F. J., Flores, J. A., & Grimalt, J. O. (2008). Evidence of abrupt changes in Western Mediterranean Deep Water circulation during the last 50 kyr: A high-resolution marine record from the Balearic Sea. *Quaternary International*, *181*(1), 88–104. https://doi.org/10.1016/j.quaint.2007.06.016

Frigola, J., Moreno, A., Cacho, I., Canals, M., Sierro, F. J., Flores, J. A., Grimalt, J. O., Hodell, D. A., & Curtis, J. H. (2007). Holocene climate variability in the western Mediterranean region from a deepwater sediment record. *Paleoceanography*, *22*(2), 1–16. https://doi.org/10.1029/2006PA001307

Garcia-Solsona, E., Pena, L. D., Paredes, E., Pérez-Asensio, J. N., Quirós-Collazos, L., Lirer, F.,

& Cacho, I. (2020). Rare earth elements and Nd isotopes as tracers of modern ocean circulation in the central Mediterranean Sea. *Progress in Oceanography*, *185*(December 2019), 102340. https://doi.org/10.1016/j.pocean.2020.102340

Grant, K. M., Grimm, R., Mikolajewicz, U., Marino, G., Ziegler, M., & Rohling, E. J. (2016). The timing of Mediterranean sapropel deposition relative to insolation, sea-level and African monsoon changes. *Quaternary Science Reviews*, *140*, 125–141. https://doi.org/10.1016/j.quascirev.2016.03.026

Grimm, R., Maier-reimer, E., Mikolajewicz, U., Schmiedl, G., Mu, K., Adloff, F., Grant, K. M., Ziegler, M., Lourens, L. J., & Emeis, K. (2015). *Late glacial initiation of Holocene eastern Mediterranean sapropel formation*. https://doi.org/10.1038/ncomms8099

Hemleben, C., Spindler, M., & Anderson, O. R. (1989). Modern Planktonic Foraminifera. In *Springer-Verlag*. https://doi.org/10.1017/CBO9781107415324.004

Hunt, C. O., Farrell, M., Fenech, K., French, C., McLaughlin, R., Blaauw, M., Bennett, J., *et al.* "Chronology and stratigraphy of the valley system" in Temple landscapes: Fragility, change and resilience of Holocene environments in the Maltese Islands, James Barrett, Ed. (McDonald Institute for Archaeological Research, 2020), pp. 35-71.

Incarbona, A., Sprovieri, M., Lirer, F., & Sprovieri, R. (2011). Surface and deep water conditions in the Sicily channel (central Mediterranean) at the time of sapropel S5 deposition. *Palaeogeography, Palaeoclimatology, Palaeoecology*, *306*(3–4), 243–248. https://doi.org/10.1016/j.palaeo.2011.04.030

Kallel, N., Paterne, M., Labeyrie, L., Duplessy, J. C., & Arnold, M. (1997). Temperature and salinity records of the Tyrrhenian Sea during the last 18,000 years. *Palaeogeography, Palaeoclimatology, Palaeoecology*, *135*(1–4), 97–108. https://doi.org/10.1016/S0031-0182(97)00021-7

Kucera, M. (2007). Chapter Six Planktonic Foraminifera as Tracers of Past Oceanic

Environments. *Developments in Marine Geology*, *1*(07), 213–262. https://doi.org/10.1016/S1572-5480(07)01011-1

Kucera, M., Weinelt, M., Kiefer, T., Pflaumann, U., Hayes, A., Weinelt, M., Chen, M. Te, Mix, A. C., Barrows, T. T., Cortijo, E., Duprat, J., Juggins, S., & Waelbroeck, C. (2005). Reconstruction of sea-surface temperatures from assemblages of planktonic foraminifera: Multi-technique approach based on geographically constrained calibration data sets and its application to glacial Atlantic and Pacific Oceans. *Quaternary Science Reviews*, *24*(7-9 SPEC. ISS.), 951–998. https://doi.org/10.1016/j.quascirev.2004.07.014

Lourens, L. J., Hilgen, F. J., Gudjonsson, L., & Zachariasse, W. J. (1992). Late Pliocene to early Pleistocene astronomically forced sea surface productivity and temperature variations in the Mediterranean. *Marine Micropaleontology*, *19*(1–2), 49–78. https://doi.org/10.1016/0377-8398(92)90021-B

Margaritelli, G., Vallefuoco, M., Di Rita, F., Capotondi, L., Bellucci, L. G., Insinga, D. D., Petrosino, P., Bonomo, S., Cacho, I., Cascella, A., Ferraro, L., Florindo, F., Lubritto, C., Lurcock, P. C., Magri, D., Pelosi, N., Rettori, R., & Lirer, F. (2016). Marine response to climate changes during the last five millennia in the central Mediterranean Sea. *Global and Planetary Change*, *142*, 53–72. https://doi.org/10.1016/j.gloplacha.2016.04.007

Marino, G., Rohling, E. J., Sangiorgi, F., Hayes, A., Casford, J. L., Lotter, A. F., Kucera, M., & Brinkhuis, H. (2009). Early and middle Holocene in the Aegean Sea: interplay between high and low latitude climate variability. *Quaternary Science Reviews*, *28*(27–28), 3246–3262. https://doi.org/10.1016/j.quascirev.2009.08.011

Martínez-Ruiz, F., Paytan, A., Kastner, M., González-Donoso, J. M., Linares, D., Bernasconi, S. M., & Jimenez-Espejo, F. J. (2003). A comparative study of the geochemical and mineralogical characteristics of the S1 sapropel in the western and eastern Mediterranean. *Palaeogeography, Palaeoclimatology, Palaeoecology*, *190*, 23–37. https://doi.org/10.1016/S0031-0182(02)00597-7

Mayewski, P. A., Rohling, E. J., Stager, J. C., Karlén, W., Maasch, K. A., Meeker, L. D., Meyerson, E. A., Gasse, F., van Kreveld, S., Holmgren, K., Lee-Thorp, J., Rosqvist, G., Rack, F., Staubwasser, M., Schneider, R. R., & Steig, E. J. (2004). Holocene climate variability. *Quaternary Research*, *62*(3), 243–255. https://doi.org/10.1016/j.yqres.2004.07.001

Ménot, G., Pivot, S., Bouloubassi, I., Davtian, N., Hennekam, R., Bosch, D., Ducassou, E., Bard, E., Migeon, S., & Revel, M. (2020). Timing and stepwise transitions of the African Humid Period from geochemical proxies in the Nile deep-sea fan sediments. *Quaternary Science Reviews*, *228*. https://doi.org/10.1016/j.quascirev.2019.106071

Mercone, D., Thomson, J., Abu-Zied, R. H., Croudace, I. W., & Rohling, E. J. (2001). High-resolution geochemical and micropalaeontological profiling of the most recent eastern Mediterranean sapropel. *Marine Geology*, *177*(1–2), 25–44. https://doi.org/10.1016/S0025-3227(01)00122-0

Murat, A. (1999). Pliocene – Pleistocene occurrence of sapropels in the western Mediterranean Sea and their relation to eastern Mediterranean sapropels. *Proceedings of the Ocean Drilling Program, Scientific Results*, *161*, 519–527.

Murray, R. W., Knowlton, C., Leinen, M., Mix, A. C., & Polsky, C. H. (2000). Export production and carbonate dissolution in the central equatorial Pacific Ocean over the past 1 Myr. *Paleoceanography*, *15*(6), 570–592. https://doi.org/10.1029/1999PA000457

Myers, P. G., Haines, K., & Rohling, E. J. (1998). Modeling the paleocirculation of the Mediterranean: The last glacial maximum and the Holocene with emphasis on the formation of sapropel S1. *Paleoceanography*, *13*(6), 586–606. https://doi.org/10.1029/98PA02736

Numberger, L., Hemleben, C., Hoffmann, R., Mackensen, A., Schulz, H., Wunderlich, J. M., & Kucera, M. (2009). Habitats, abundance patterns and isotopic signals of morphotypes of the planktonic foraminifer Globigerinoides ruber (d'Orbigny) in the eastern Mediterranean

Sea since the Marine Isotopic Stage 12. *Marine Micropaleontology*, *73*(1–2), 90–104. https://doi.org/10.1016/j.marmicro.2009.07.004

Paytan, A., & Griffith, E. M. (2007). Marine barite: Recorder of variations in ocean export productivity. *Deep-Sea Research Part II: Topical Studies in Oceanography*, *54*(5–7), 687–705. https://doi.org/10.1016/j.dsr2.2007.01.007

Pérez-Folgado, M., Sierro, F. J., Flores, J. A., Cacho, I., Grimalt, J. O., Zahn, R., & Shackleton, N. (2003). Western Mediterranean planktonic foraminifera events and millennial climatic variability during the last 70 kyr. *Marine Micropaleontology*, *48*(1–2), 49–70. https://doi.org/10.1016/S0377-8398(02)00160-3

Pujol, C., & Vergnaud-Grazzini, C. (1995). Distribution patterns of live planktic foraminifers as related to regional hydrography and productive systems of the Mediterranean Sea. *Marine Micropaleontology*, *25*(2–3), 187–217. https://doi.org/10.1016/0377-8398(95)00002-I

Rasmussen, S. O., Andersen, K. K., Svensson, A. M., Steffensen, J. P., Vinther, B. M., Clausen, H. B., Johnsen, S. J., Larsen, L. B., Bigler, M., Ro, R., & Fischer, H. (2006). *A new Greenland ice core chronology for the last glacial termination*. *111*, 1–16. https://doi.org/10.1029/2005JD006079

Rohling, E. J. (1994). Review and new aspects concerning the formation of eastern Mediterranean sapropels. *Marine Geology*, *122*(1–2), 1–28. https://doi.org/10.1016/0025-3227(94)90202-X

Rohling, E. J., Hayes, A., De Rijk, S., Kroon, D., Zachariasse, W. J., & Eisma, D. (1998). Abrupt cold spells in the northwest Mediterranean. *Paleoceanography*, *13*(4), 316–322. https://doi.org/10.1029/98PA00671

Rohling, E. J., Marino, G., & Grant, K. M. (2015). Mediterranean climate and oceanography, and the periodic development of anoxic events (sapropels). *Earth-Science Reviews*, *143*, 62–97. https://doi.org/10.1016/j.earscirev.2015.01.008

Rossignol-Strick, M. (1985). Mediterranean Quaternary sapropels, an immediate response of the African monsoon to variation of insolation. *Palaeogeography, Palaeoclimatology, Palaeoecology*, *49*(3–4), 237–263. https://doi.org/10.1016/0031-0182(85)90056-2

Sbaffi, L., Wezel, F. C., Curzi, G., & Zoppi, U. (2004). Millennial- to centennial-scale palaeoclimatic variations during Termination I and the Holocene in the central Mediterranean Sea. *Global and Planetary Change*, *40*(1–2), 201–217. https://doi.org/10.1016/S0921-8181(03)00111-5

Sbaffi, L., Wezel, F. C., Kallel, N., Paterne, M., Cacho, I., Ziveri, P., & Shackleton, N. (2001). Response of the pelagic environment to palaeoclimatic changes in the central Mediterranean Sea during the Late Quaternary. *Marine Geology*, *178*(1–4), 39–62. https://doi.org/10.1016/S0025-3227(01)00185-2

Schiebel, R., & Hemleben, C. (2000). Interannual variability of planktic foraminiferal populations and test flux in the eastern North Atlantic Ocean (JGOFS). *Deep-Sea Research Part II: Topical Studies in Oceanography*, *47*(9–11), 1809–1852. https://doi.org/10.1016/S0967-0645(00)00008-4

Schiebel, R., Waniek, J., Bork, M., & Hemleben, C. (2001). Planktic foraminiferal production stimulated by chlorophyll redistribution and entrainment of nutrients. *Deep-Sea Research Part I: Oceanographic Research Papers*, *48*(3), 721–740. https://doi.org/10.1016/S0967-0637(00)00065-0

Schmidt, D. N., Renaud, S., Bollmann, J., Schiebel, R., & Thierstein, H. R. (2004). Size distribution of Holocene planktic foraminifer assemblages: Biogeography, ecology and adaptation. *Marine Micropaleontology*, *50*(3–4), 319–338. https://doi.org/10.1016/S0377-8398(03)00098-7

Sprovieri, R., Di Stefano, E., Incarbona, A., & Gargano, M. E. (2003). A high-resolution record of the last deglaciation in the Sicily Channel based on foraminifera and calcareous nannofossil quantitative distribution. *Palaeogeography, Palaeoclimatology,*

Palaeoecology, *202*(1–2), 119–142. https://doi.org/10.1016/S0031-0182(03)00632-1

Tachikawa, K., Vidal, L., Cornuault, M., Garcia, M., Pothin, A., Sonzogni, C., Bard, E., Menot, G., & Revel, M. (2015). Eastern Mediterranean Sea circulation inferred from the conditions of S1 sapropel deposition. *Climate of the Past*, *11*(6), 855–867. https://doi.org/10.5194/cp-11-855-2015

Tesi, T., Asioli, A., Minisini, D., Maselli, V., Dalla Valle, G., Gamberi, F., Langone, L., Cattaneo, A., Montagna, P., & Trincardi, F. (2017). Large-scale response of the Eastern Mediterranean thermohaline circulation to African monsoon intensification during sapropel S1 formation. *Quaternary Science Reviews*, *159*, 139–154. https://doi.org/10.1016/j.quascirev.2017.01.020

Toucanne, S., Angue Minto'o, C. M., Fontanier, C., Bassetti, M. A., Jorry, S. J., & Jouet, G. (2015). Tracking rainfall in the northern Mediterranean borderlands during sapropel deposition. *Quaternary Science Reviews*, *129*, 178–195. https://doi.org/10.1016/j.quascirev.2015.10.016

Vadsaria, T., Ramstein, G., Dutay, J. C., Li, L., Ayache, M., & Richon, C. (2019). Simulating the Occurrence of the Last Sapropel Event (S1): Mediterranean Basin Ocean Dynamics Simulations Using Nd Isotopic Composition Modeling. *Paleoceanography and Paleoclimatology*, *34*(2), 237–251. https://doi.org/10.1029/2019PA003566

Vinther, B. M., Clausen, H. B., Johnsen, S. J., Rasmussen, S. O., Andersen, K. K., Buchardt, S. L., Seierstad, I. K., Steffensen, J. P., Svensson, A., Olsen, J., & Heinemeier, J. (2006). *A synchronized dating of three Greenland ice cores throughout the Holocene*. *111*, 1–11. https://doi.org/10.1029/2005JD006921

Walker, M. J. C. (1995). Climatic changes in Europe during the last glacial/interglacial transition. *Quaternary International*, *28*(C), 63–76. https://doi.org/10.1016/1040-6182(95)00030-M

Wehausen, R., & Brumsack, H. J. (1998). The formation of Pliocene Mediterranean sapropels: Constraints from high-resolution major and minor element studies. *Proceedings of the Ocean Drilling Program: Scientific Results*, *160*, 207–218. https://doi.org/10.2973/odp.proc.sr.160.004.1998

Wehausen, R., & Brumsack, H. J. (2000). Chemical cycles in Pliocene sapropel-bearing and sapropel-barren eastern Mediterranean sediments. *Palaeogeography, Palaeoclimatology, Palaeoecology*, *158*(3–4), 325–352. https://doi.org/10.1016/S0031-0182(00)00057-2

Wu, J., Böning, P., Pahnke, K., Tachikawa, K., & de Lange, G. J. (2016). Unraveling North-African riverine and eolian contributions to central Mediterranean sediments during Holocene sapropel S1 formation. *Quaternary Science Reviews*, *152*, 31–48. https://doi.org/10.1016/j.quascirev.2016.09.029

Wu, J., Liu, Z., Stuut, J. B. W., Zhao, Y., Schirone, A., & de Lange, G. J. (2017). North-African paleodrainage discharges to the central Mediterranean during the last 18,000 years: A multiproxy characterization. *Quaternary Science Reviews*, *163*(May), 95–113. https://doi.org/10.1016/j.quascirev.2017.03.015

Wu, J., Pahnke, K., Böning, P., Wu, L., Michard, A., & de Lange, G. J. (2019). Divergent Mediterranean seawater circulation during Holocene sapropel formation – Reconstructed using Nd isotopes in fish debris and foraminifera. *Earth and Planetary Science Letters*, *511*, 141–153. https://doi.org/10.1016/j.epsl.2019.01.036

El navegante no tiene más remedio que seguir navegando

hasta encontrar el lugar donde poder recalar,

o hasta que el mar se lo devore,

porque así fue dispuesto desde el comienzo de todas las cosas…

Extracto de “El navegante” (Morris West)

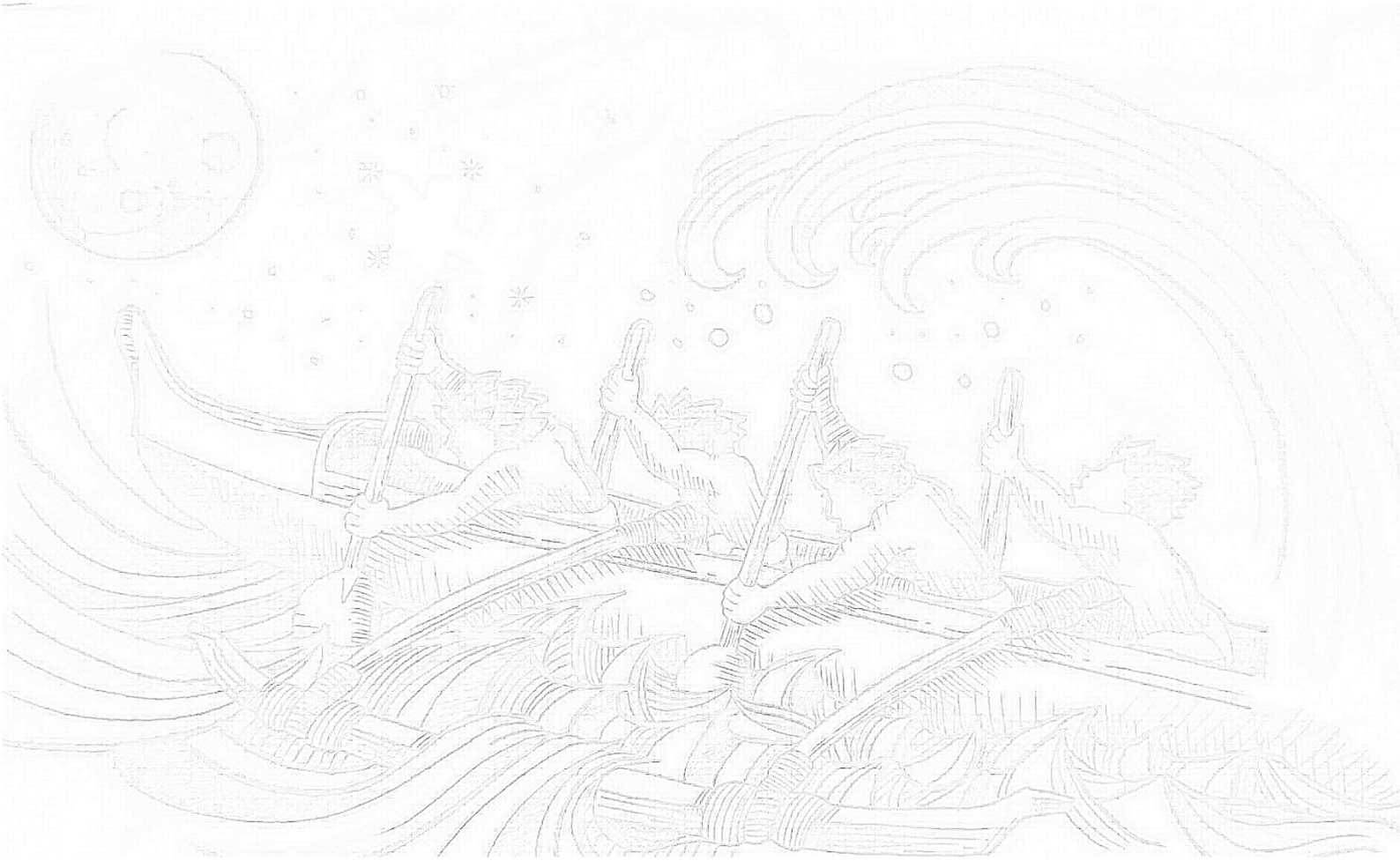

4 WATER EXPORT CHANGES THROUGH THE STRAIT OF SICILY DURING THE LAST DEGLACIAL PERIOD *

Abstract

The intermediate and deep water convection of the Eastern Mediterranean has been proved to be highly sensitive to varying fresh water fluxes, associated with increased rainfall during the African Humid period (15-6 kyr BP). Here we investigate for the first time, changes in the export rates of eastern Mediterranean sourced water masses (EMSW) into the western basin for the last ~15 kyr BP. For this purpose, we analyze $^{143}Nd/^{144}Nd$ isotope ratios (εNd) in planktic foraminifera coatings, a quantitative tracer of water mass provenance, from a sediment core recovered at the western flank of the Sicily channel (NDT-6-2016, 1066 m depth). At present, this site is located below the hydrographic boundary layer between the eastern and western source water-masses. The measured εNd values were then used to elucidate changes in EMSW export rates through late deglacial and Holocene periods applying an endmember mixing model. Our results indicate that EMSW export rates were maximum during the Younger Dryas (YD) period, about three times higher than during the S1, supporting the limited formation of both intermediate and deep water masses in the eastern basin during the S1 as suggested by previous studies. We propose that the enhanced EMSW outflow into the western Mediterranean over the YD was the result of the combined effect of (1) enhanced climate-driven convection in the Aegean Sea and (2) the reduced convection of western deep water during this period, when the last Organic Rich Layer deposited in the deepest areas of the western basin.

4.1 INTRODUCTION

The Mediterranean Sea hydrography is typically characterized by a negative precipitation-evaporation (P-E) net balance across the basin. As a result of this, the Mediterranean Sea thermohaline circulation system (Med-THC) presents an anti-estuarine pattern, where the inflowing fresh and cold Atlantic surface waters (AW) entering through the Strait of Gibraltar, progressively transform into saltier surface waters, that eventually sink to intermediate depths at

*Submitted at PNAS (2022-01997) as Trias-Navarro, S., Pena, L.D., de la Fuente, M., Paredes, E., Garcia-Solsona, E., Frigola, J., Català, A., Caruso, A., Pérez-Asensio, J.N., Haghipour, N., Lirer, F. and Cacho, I.

the Levantine Sea as Levantine Intermediate Water (LIW). The LIW contributes to preconditioning deep water convection both in the Adriatic Sea and the Aegean Sea, where the Eastern Mediterranean Deep Water (EMDW) is formed. EMDW and LIW outflow together through the Strait of Sicily, hereafter called eastern Mediterranean Source Waters (EMSW), contributing in the deep water convection at Gulf of Lions to produce Western Mediterranean Deep Water (WMDW). These three water masses (WMDW, LIW and EMDW), eventually exit into the Atlantic Ocean through the Strait of Gibraltar forming the so-called Mediterranean Outflow Water (MOW), thus closing Med-THC system (Fig. 1a) (Gacic et al., 2001; Lascaratos et al., 1993; Millot, 1987, 1999; Pinardi & Masetti, 2000).

Proxy evidence show that the intensity of the Med-THC system is highly sensitive to past climate oscillations at different timescales and in some particular periods (Cacho et al., 2001; Frigola et al., 2008; Rohling et al., 2015; Schmiedl et al., 2010). In this regard, deglacial seal level rise has often been proposed as the main cause of deep water convection weakening in the Western Mediterranean Sea (W-Med), that, for instance, led to the formation of the last Organic Rich layer in the deep western basin (ORL: 15-8.9 kyr BP) (Cacho et al., 2002; Pérez-Asensio et al., 2020; Rogerson et al., 2008). In the Eastern Mediterranean Sea (E-Med), however, it has been well documented the existence of a major deep water formation perturbation associated with the intensification of the African Monsoon over north Africa during the African Humid Period (AHP; from ~15 to 6 kyr BP) (Shanahan et al., 2015). Some evidence suggests that an enhanced rainfall during the AHP led to increased runoff from north African riverine systems into the Eastern Mediterranean (E-Med) basin, thus, inducing stronger sea surface density stratification, that might have weakened the intermediate and deep water convection in the region (Grimm et al., 2015).

Interestingly, it has also been proposed that the AHP underwent an “interruption” phase during the Younger Dryas (YD; from 12.95 to 11.65 kyr BP), when colder and more arid conditions were predominant over the E-Med (Grimm et al., 2015; Ménot et al., 2020; Revel et al., 2015; Shanahan et al., 2015). Although there are inconclusive evidence at the moment, some studies have

proposed that such conditions could have favoured a partial reactivation of the intermediate and/or deep water convection in the E-Med (Grimm et al., 2015; McCulloch et al., 2010).

In the E-Med basin there are clear sedimentary expressions of reduced/collapsed intermediate- and/or deep water convection, that consist of a deposition of an organic-rich sediment layer, such as the one that occurred during the so-called last sapropel or S1. (De Lange et al., 2008; Grant et al., 2016; Lourens et al., 1992; Mercone et al., 2001; Rohling, 1994; Rohling et al., 2015; Rossignol-Strick, 1985; Schmiedl et al., 2010; Toucanne et al., 2015). It is commonly accepted that the S1 occurred between 10.8 and 6.1 kyr BP (De Lange et al., 2008), although several authors have proposed that the end of S1 was asynchronous in the water column, with intermediate depths in the E-Med being "re-ventilated" between 7.7 and 7 kyr BP (Checa et al., 2020; Filippidi et al., 2016; Tesi et al., 2017).

The hydrographic conditions associated with the S1 have been widely studied in the E-Med (Bianchi et al., 2006; Checa et al., 2020; De Lange et al., 2008; Filippidi et al., 2016; Grimm et al., 2015; Incarbona et al., 2019; Mercone et al., 2001; Revel et al., 2014; Rohling et al., 2015; Tesi et al., 2017) and the potential impact of the S1 in the water exchange between the E- and W-Med sub-basins has also been previously suggested (Colin et al., 2021; Dubois-Dauphin et al., 2017; Duhamel et al., 2020; Murat, 1999). However, no quantitative estimates of changes in the E-W water exchange through the Strait of Sicily during the deglacial and Holocene periods are available so far.

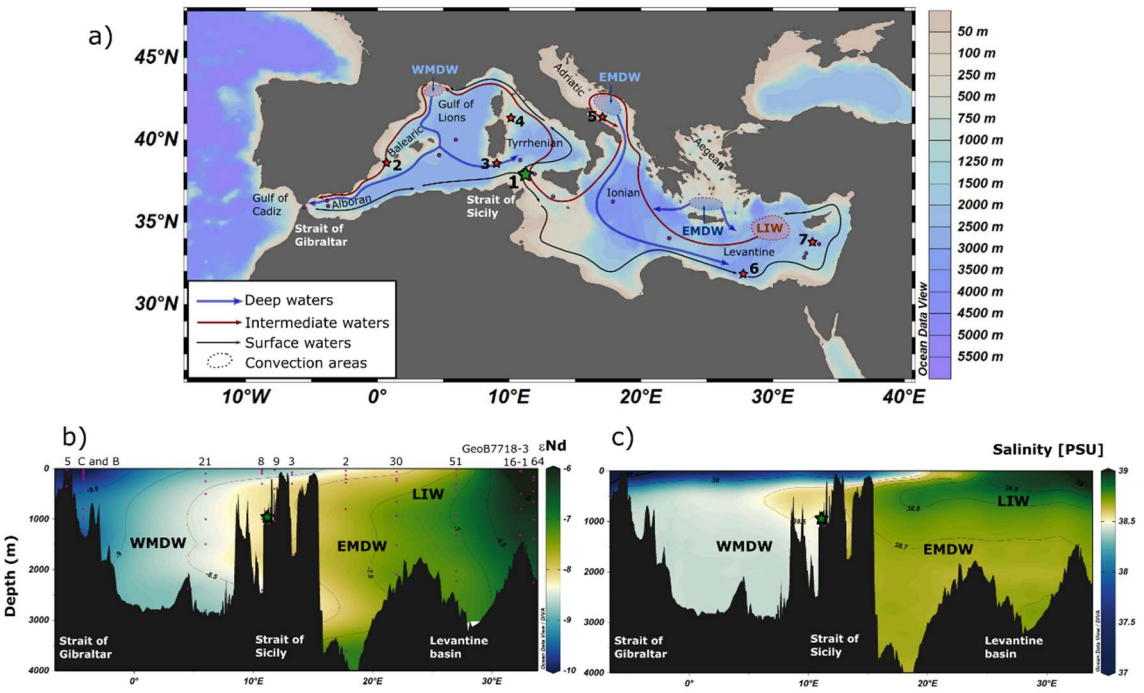

Fig. 1. a) Map of the study area in the Mediterranean Sea. The green star represents the studied core NDT-6-2016 (1) and red stars represent the other cores discussed in this manuscript located in both the western and eastern Mediterranean Sea: 2) SU92-33 and 3) RECORD23 (Dubois-Dauphin et al., 2017), 4) MD01-2472 and 5) MD90-917 (Colin et al., 2021), 6) MS27PT (Duhamel et al., 2020) and 7) BC07 (Freydier et al., 2001). Violet circles stand for the stations of the obtained present-day seawater ε_{Nd} values. Blue arrows indicate deep waters (Western -WMDW- and Eastern -EMDW- Mediterranean Deep Waters), red arrows represent Levantine Intermediate Water (LIW) and black ones the surface Modified Atlantic Water (MAW). b) Map of the seawater neodymium distribution in the Mediterranean Sea based on previous acquired data from stations (violet circles): B, C, 5, 51, 64 (Tachikawa et al., 2004); 8, 9, 3, 2 (Garcia-Solsona et al., 2020); GeoB7718-3, GeoB7716-1 (Vance et al., 2004); 21 (Garcia-Solsona & Jeandel, 2020). c) Map of the salinity distribution in the Mediterranean Sea based on Medatlas II acquired data.

In this work, we present for the first time, quantitative estimations of E-W Mediterranean water exchange through neodymium isotope (εNd) measurements on planktic foraminifera Fe-Mn crusts, which has been shown to well represent the Nd isotopic signature of the waters masses where foraminifera shells are deposited (Garcia-Solsona et al., 2020; Tachikawa et al., 2014; Vance et al., 2009). Present day chemical oceanography studies have shown that E-Med seawater ε_{Nd} values are typically higher than W-Med ε_{Nd} values and thus, establishing the basic ground for

the use of Nd isotopes as an extraordinary tracer of past changes in Med-THC (Fig.1b) (Ayache et al., 2016; Garcia-Solsona et al., 2020; Henry et al., 1994; Tachikawa et al., 2004; Vance et al., 2009).

Because of this, the gravity core NDT-6-2016 (38°0'26,60" N and 11°47'44,84"E) collected during the Next Data expedition (CNR-URANIA R/V, 2016) was recovered at the transition area between the W-Sicily channel and the southern Tyrrhenian Sea (38°0'26,60" N and 11°47'44,84"E) at 1066 m of water depth (Fig. 1b, c). The core depth is below the interphase between the WMDW and the EMSW outflowing through the Strait of Sicily, a suitable location to evaluate changes in the intermediate-deep water exchange between the two main Mediterranean sub-basins (Garcia-Solsona et al., 2020). Neodymium isotopes (ε_{Nd}) results are complemented with other published ε_{Nd} records from different regions of the Mediterranean Sea (Fig. 1a) (Colin et al., 2021; Dubois-Dauphin et al., 2017; Duhamel et al., 2020; Freydier et al., 2001; Wu et al., 2019). All together allowing the mixing rates between the outflowing EMSW and the WMDW during the late deglaciation and Holocene periods to be estimated.

4.2 RESULTS AND DISCUSSION

The new ε_{Nd} record from W-Sicily presents high variability along the late deglaciation and Holocene periods (the last ~15 kyr cal. BP). The highest ε_{Nd} values predominated during the YD (between -5.6 ± 0.4 and 6.3 ± 0.3; Fig. 2), while the lowest ε_{Nd} values are predominant during the S1 interval (from −7.8 ± 0.3 to −8. 4 ± 0.3; Fig. 2). The pre-S1 and the post-S1 were characterized by intermediate values ranging from -7.0 ± 0.4 to -7.4 ± 0.6 and from -7.3 ± 0.3 to -7.5 ± 0.3, respectively (Fig. 2).

4.2.1 Enhanced EMSW outflow during the Younger Dryas

The remarkably high ε_{Nd} values recorded at the west flank of Sicily channel during the YD are one of the most outstanding features recorded for the studied period (from -5.6 ± 0.4 to -6.3 ± 0.3; Fig. 2). We interpret these ε_{Nd} values as the result of 1) an enhanced EMSW contribution through the Strait of Sicily into the study area, given that W-Med sourced waters, such as WMDW, are

typically represented by more negative ε_{Nd} values (Fig.2) (Ayache et al., 2016; Garcia-Solsona et al., 2020; Henry et al., 1994; Tachikawa et al., 2004; Vance et al., 2009), 2) a shift towards more radiogenic composition in the EMSW end-members, i.e., EMDW and the LIW. Since outflowing EMSW comprises a mix between LIW and EMDW (Garcia-Solsona et al., 2020), any relative change in the ε_{Nd} endmember composition of either of these two water-masses could also have induced variations in the W-Sicily ε_{Nd} signature, regardless of any changes in the volume of water exported.

This later hypothesis would be in good agreement with previous data from the deep Levantine Sea, showing the presence of a more radiogenic EMDW during the YD than today and attributed to the intensification of Nile river discharge during the AHP (Fig. 2, Nile slope, MS27PT) (Duhamel et al., 2020). In addition, changes in the EMDW ε_{Nd} signature could have also been induced through changes in the relative contribution of both Adriatic Sea and Aegean Sea waters to the EMDW. The Adriatic Sea show relatively constant ε_{Nd} values along the studied period (Fig.2, MD90-917) (Colin et al., 2021), which are systematically more negative than those found in the Levantine Sea (Fig. 2, MS27PT, LC07) (Duhamel et al., 2020; Freydier et al., 2001). In contrast, present day Aegean Sea deep waters present similar ε_{Nd} values than those of the deep Levantine basin and significantly higher radiogenic than ε_{Nd} values of the Adriatic Sea (Tachikawa et al., 2004).Therefore, an intensification of the contribution of the Aegean waters to the EMDW in detriment to the Adriatic waters, cannot be discard as a potential source for the detected YD anomaly.

Relatively high ε_{Nd} values in the EMDW at the Levantine Sea, however, were recorded for the whole deglacial period and early Holocene (Fig. 2) (Duhamel et al., 2020), while at our W-Sicily site the highest ε_{Nd} anomaly is restricted to the YD period. Consequently, changes in the EMSW end-member composition cannot solely account for our observations. Thus, we propose that the ε_{Nd} anomaly recorded at our site during the YD likely resulted from the combined effect of 1) the

presence of more radiogenic EMSW end-members and 2) the increased contribution of EMSW into the W-Med over this period.

By considering that measured ε_{Nd} values in the W-Sicily site are the result from both changes in EMSW volume export rates as well as changes in EMSW ε_{Nd} end-member composition we present a new quantitative estimate of the mixing and export rates through the Strait of Sicily for the studied period. Export rates have been estimated applying a simple mixing model, using our new W-Sicily ε_{Nd} record in combination with previously published records as water mass ε_{Nd} end-members for WMDW (SU92-33), EMDW (MS27PT) and LIW (BC07) (32, 33, 42, respectivey). In order to account for uncertainties associated with mixing estimations and analytical errors, we have implemented a Monte-Carlo approach of the mixing equation (see details in section 4.3.1).

Mixing estimates calculations further support a larger proportion of EMSWs arriving into W-Sicily during the (Fig. 3b, c), as compared to the pre- and post-YD (in average: YD, 57 ± 5%, n=9; pre-YD, 23 ± 4%, n=9; post-YD, 33 ± 5%, n=15; Fig. 3a, b, c and Table S3). Our new mixing estimates are supported by previous results from model experiments and proxy compilations, that show a partial re-ventilation of the E-Med basin during the YD (Grimm et al., 2015), associated with increased cooling and aridity conditions in the Aegean Sea (Fig. 4e) (Dormoy et al., 2009; Kotthoff et al., 2011). Enhanced deep water convection in the Aegean Sea during the YD is also coherent with the higher ε_{Nd} values recorded in W-Sicily.

Interestingly, the higher ε_{Nd} values recorded during the YD at our site are in direct concurrence with maximum values in grain-size reported from both a shallower and distal core located at 501 m at the eastern flank of Corsica (Fig. 4d) (Toucanne et al., 2015) and also from an even further and deeper core in the Alboran Sea at 914 m (Fig. 4c) (Alonso et al., 2021). These grain size records suggest an increase in the currents velocity at intermediate depths in the W-Med at that moment, that is also synchronous with increased outflow speed of Mediterranean waters outflowing the Strait of Gibraltar as reported in contourite deposits of the Gulf of Cadiz (Lebreiro et al., 2018; Sierro et al., 2020).

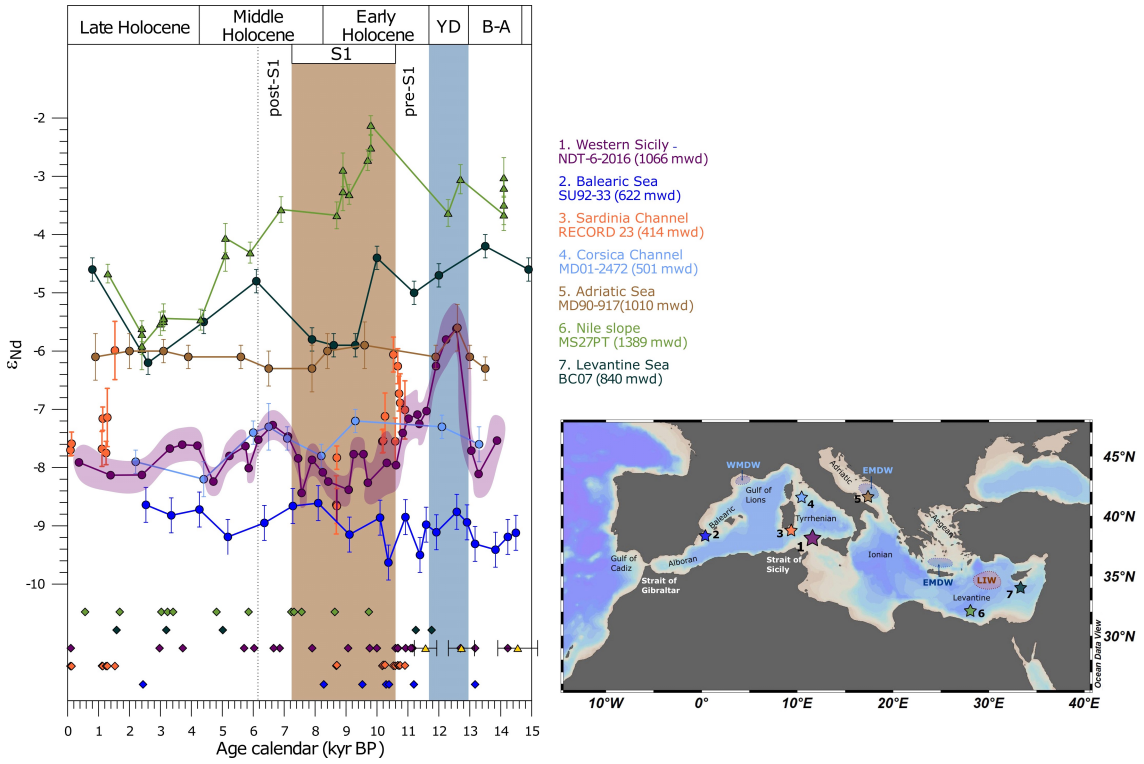

Fig. 2. Records of Neodymium isotopes in planktic foraminifera from NDT-6-2016 (this study), SU92-33 and RECORD23 (Dubois-Dauphin et al., 2017), MD01-2472 and MD90-917 (Colin et al., 2021), MS27PT (Duhamel et al., 2020) and BC07 (Freydier et al., 2001). The ^{14}C-calibrated dates used for each chronology are colored according to the corresponding record. In the sediment core NDT-6-2016, blue rhombs represent ^{14}C-calibrated dates and yellow triangles represent tie points. Grey-blue bar represents YD and light-brown bar, the S1.

Enhanced EMSW export rates during the YD occurred simultaneously with a major reduction of deep water convection and an associated weakening of deep-sea currents intensity in the W-Med (Frigola et al., 2008), which led to the last ORL formation in the Alboran Sea (Fig 4a) (Cacho et al., 2002; Martinez-Ruiz et al., 2000; Pérez-Asensio et al., 2020; Rogerson et al., 2008). We hypothesise that reduced W-Med deep water formation favoured the expansion of EMSW to greater depths into the W-Med replacing WMDW. This hypothesis is supported by evidence of re-ventilation processes at intermediate depths (~ 900 m) described in the Alboran Sea for the YD period (Fig. 5b) (Pérez-Asensio et al., 2020). All these evidence together would agree with the high ε_{Nd} values recorded at W-Sicily, suggesting an enhanced outflow of the EMSW into the W-Med during the YD.

4.2.2 Weakening in the westward flow of Eastern Mediterranean Source Waters during the last sapropel

In contrast to the high ε_{Nd} values described during the YD in the W-Sicily, our results show that the S1 period is identified by relatively low ε_{Nd} values, (Fig. 2; from -8.4 ± 0.3 to -7.8 ± 0.3), i.e., between ~2 and 3-unit lower than for the YD period (between -5.6 ± 0.4 and -6.3 ± 0.3). This relatively low ε_{Nd} values are interpreted as a response of a weaker outflow of EMSW into the W-Sicily during the S1 (Fig. 3a). This interpretation would be supported by the low percentages of EMSW obtained throughout the quantitative Monte-Carlo estimate (in average: 16 ± 6%, n=33; Fig. 3b and c; Table S3), i.e., approximately one half of EMSW exports estimated for the pre- and post-S1 (in average: pre-S1, 33 ± 5%, n=15; post-S1, 29 ± 2%, n=9; Fig. 3b and c).

Our relative low ε_{Nd} values recorded in the W-Sicily also agree with previous ε_{Nd} results from the Sardinia channel measured in deep-sea corals at 414 m, both of them showing a decrease in the ε_{Nd} records from the pre-S1 to the S1 (Fig. 2) (Dubois-Dauphin et al., 2017). Thus, ε_{Nd} data from both W-Sicily and Sardinia channel support moderate EMSW outflow rates during the pre-S1 but, especially, they show an important reduction in the export during the S1 period at both locations. Moreover, reduced westward outflow of the EMSW through the Sicily channel during the S1 is further supported by a major reduction in the sedimentation rates at the W-Sicily (Fig. 4e). All these indicators are consistent with a weaker export rates of EMSW during the S1, which presumably resulted in a larger volume of low ε_{Nd} WMDW occupying intermediate depths at the study site (Fig. 3a).

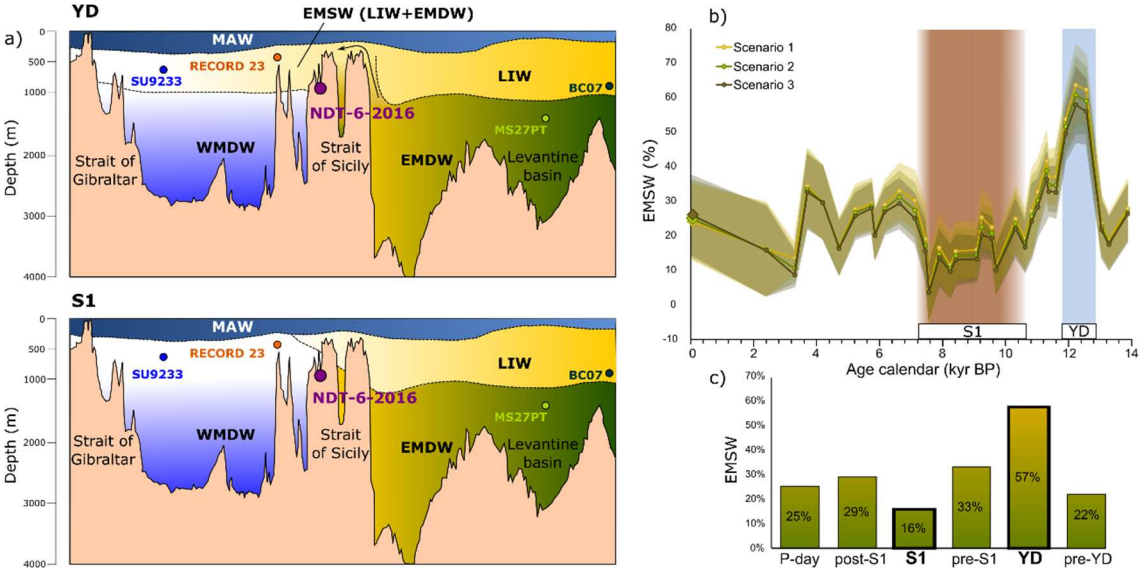

Fig. 3. a) Distribution of intermediate and deep water masses in the Mediterranean Sea during both the YD and S1 and the location of the main cores discussed in this work. b) Export rates of Eastern Mediterranean Source Water (EMSW) expressed as % contribution, with they range of uncertainty. Different scenarios corresponded with different proportions of EMDW and LIW; the first scenario characterized by the same contribution of each water mass, the second one considers a LIW contribution that doubles that of EMDW and the third one takes into account a double contribution of the EMDW with respect to the LIW. Grey-blue bar represents the YD and light-brown bar the S1. Current percentages of EMSW are calculated using present-day seawater ε_{Nd} values from WMDW, LIW, EMDW (Tachikawa et al., 2004) and South Tyrrhenian Sea (Garcia-Solsona et al., 2020) and are indicated with rhombs (see supplementary material, Table S2). c) Average values of EMSW export in the studied location for each period discussed in this work.

The end of the S1 period is shown as a transition in the ε_{Nd} values from -8.4 ± 0.3 to -7.5 ± 0.3 units (Fig. 2). Quantitative mixing estimates indicate that this transition accounted for an increase in the EMSW contribution from 4 ± 8% to 28 ± 8% at the W-Sicily (Fig. 3b). These results confirm an increase in the volume export of EMSW through the Strait of Sicily at the end of the S1, likely indicating the end of the deep water stagnant conditions that prevailed in the E-Med during the S1 interval.

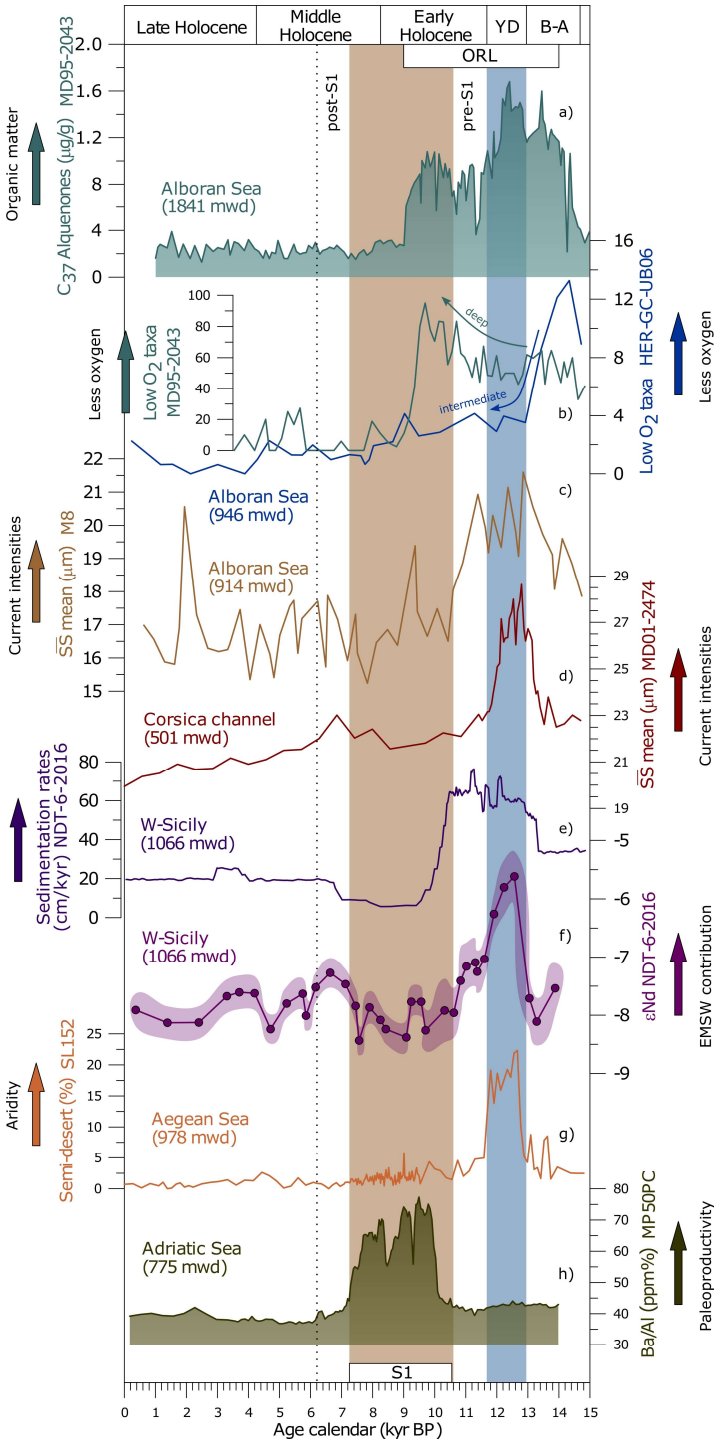

Fig. 4. Comparison between different marine records of the Mediterranean Sea from the late deglacial and Holocene periods. From the top to the base: a) C_{37} Alkenones from MD95-2043 (Cacho et al., 2002), b) Low oxygen benthic foraminiferal taxa percentages from intermediate record HER-GC-UB6 and deep MD95-2043 (Pérez-Asensio et al., 2020), c and d) Grain-size measurements from M8 (Alonso et al., 2021) and MD01-2474 (Toucanne et al., 2012), e) Sedimentation rates from NDT-6-2016 (this study), f) Neodymium isotope records from NDT-6-2016 (this study), g) Semi-desert taxa percentages obtained from SL152 (Dormoy et al., 2009; Kotthoff et al., 2008), h) Ba/Al profiles from MP50PC (Filippidi et al., 2016). Grey-blue bar represents the YD and light-brown bar the S1.

According to our age model (Trias-Navarro et al., 2021) (also see methods for details), the end of the S1 period occurred between 7.5-7 kyr BP. Our new results suggest that the interconnection between the E-W Mediterranean basins was re-established ~1 kyr before the absolute end of the S1 around 6.1 kyr cal. BP (De Lange et al., 2008). If this observation was confirmed, it would suggest that the re-activation of intermediate and deep water circulation might have not occurred synchronously across the eastern Mediterranean basin, but instead, intermediate waters would

have been re-ventilated before any other deeper water masses in the basin. This hypothesis is coherent with previous evidences for an earlier S1 re-ventilation between 7.7 to 7 kyr BP, both in the Adriatic and the Aegean Sea (Fig. 4h) (Cascella et al., 2021; Checa et al., 2020; Filippidi et al., 2016; Incarbona et al., 2019; Siani et al., 2013). Although this earlier re-ventilation at intermediate depths might have not affected the deep basin, our records indicate that it would have been strong enough to re-establish the water exchange between the E-Med and W-Med.

4.3 SUMMARY AND CONCLUSIONS

The new generated ε_{Nd} data from sediment core NDT-6-2016 at 1066m provide quantitative information on the export rates of ESMW towards the W-Med basin, during the last deglacial/Holocene periods and particularly over the YD and the S1, for the first time. The highest percentages of EMSW are identified at W-Sicily during the YD (57 ± 5%) indicating that an enhanced deep water interconnection prevailed between the E-Med and the W-Med. We speculate that this situation responded to the combined effect of climate-driven enhanced convection in the Aegean and Levantine basins and a weaker western deep water formation that led to a deeper expansion of the EMSW into the western basin. We propose that this enhanced western flow of EMSW also corresponded with the previous described stronger currents at intermediate depths of the W-Med, ceasing the stagnation at ~ 900m that had been initiated with the last ORL formation in the westernmost part of the Mediterranean Sea. Estimated export rates for the S1 provide the minimum values of the record (16 ± 6%), supporting a substantial weakening of the EMSW outflow through the Strait of Sicily. As a consequence, intermediate/deep water exchange between the two basins would have been significantly reduced. The reactivation of the interconnection between the E-Med and W-Med would have taken place around 1 kyr before the absolute end of the S1 (6.1 kyr cal. BP). We propose that the exit of the EMSW through the Strait of Sicily at 7.5-7 kyr BP agrees with the earlier convection enhancement in the Adriatic and Aegean Seas, that marked the end of the stagnant conditions at intermediate depths of the E-Med, while the re-activation of the deep basin would have taken longer.

4.4 MATERIALS AND METHODS

4.4.1 Core description

The gravity core NDT-6-2016 (~4 m long) was sampled every cm and consists of homogeneous silty-clay sediments with no sedimentary irregularities along the whole sequence. Neodymium isotopes were analysed every 2-6 cm for the interval between 1.20 and 1.62 m (corresponding chronologically to the S1) and at lower resolution (10-30 cm) for the rest of the core. Both sedimentological grain measurements and elemental XRF analyses were carried out every cm all along the core.

4.4.2 Radiocarbon dates and sedimentation rates

The chronological framework was established by twenty ^{14}C dates analysed in monospecific planktic foraminifera samples (>250µm, *Globoconella inflata)*. Radiocarbon ages were calibrated using MARINE20 calibration curve (Hunt et al., 2020). The age model was constructed using the Bayesian statistics software Bacon (Blaauw & Christeny, 2011). In addition to the ^{14}C dates of the lower part, three tie points were added based on an adjusted alignment between the studied $\delta^{18}O$ record from *Globigerina bulloides* and the well-dated reference NGRIP isotope record (Fig. S1 in supplementary material) (Rasmussen et al., 2006; Vinther et al., 2006). The age model is more detailed in Trias-Navarro et al. (2021).

4.4.3 Neodymium isotopes measurements

A total of 32 samples were selected for neodymium isotopes analyses. For each sample, 20 to 30 mg of mixed planktic foraminifera from the >212 µm fraction were handpicked, except for those samples where planktic foraminifera were scarce and only 4 to 12 mg were available. Each sample was processed individually and the specimens were crushed with extreme care to avoid the over-crushing using two glass slides under the microscope. Each sample was cleaned with Ultra-Pure water (Resistivity > 18 MΩ cm) as many times as necessary to remove the clay fraction, and then rinsed with methanol to eliminate particles that could have remained attached to the vial (Barker et al., 2003; Pena et al., 2005). Between each Ultra-Pure water and methanol cleanings, samples

were sonicated to re-suspend the clay fraction. Sample dissolution was carried out by adding 0.5 ml of Ultra-Pure water and 0.1 ml of acetic acid in each sample. Then, they were sonicated until completely dissolved. Finally, all samples were centrifuged to avoid possible undissolved particles and transferred to clean vials to carry out the sample purification.

They were treated and purified by column chromatography at Laboratori d'Isòtops Radioactius i Ambientals (LIRA) of the Universitat de Barcelona (UB) based on (Copard et al., 2010); 1) rare elements (REE) were separated and collected following the Tru-spec chemistry and 2) neodymium was isolated from other REE by means of the Ln-Spec chromatography. Measurements of ε_{Nd} were performed using a Plasma 3 Multi Collector Inductively Coupled Plasma Mass Spectrometer (Nu Instruments-AMETEK) at Centres Científics i Tecnològics of the Universitat de Barcelona (CCiTUB). Procedural blanks were systematically corrected and were always found to be negligible. The $^{143}Nd/^{144}Nd$ instrumental mass bias was corrected using the exponential law (Wombacher & Rchkämper, 2003), assuming a reference $^{146}Nd/^{144}Nd$ ratio of 0.7219. Furthermore, the JNdi-1 standard was analysed before and after each sample, and an additional sample-standard bracketing normalization of the mass bias corrected ratios was carried out, using the reference $^{143}Nd/^{144}Nd$ value of 0.512115 ± 0.000007 for this standard (Tanaka et al., 2000).

Nd isotopic composition is expressed as $\varepsilon Nd = ([(^{143}Nd/^{144}Nd)_{sample}/(^{143}Nd/^{144}Nd)_{CHUR}]-1)*10^4$, where CHUR is the Chondritic Uniform Reservoir and represents a present-day Earth value of $(^{143}Nd/^{144}Nd)_{CHUR} = 0.512638$ (Jacobsen & Wasserburg, 1980). Uncertainties of the εNd values correspond to the external reproducibility of the JNdi-1 analysis performed throughout each measurement session (2 sd, n = 12-20), and ranged between 0.25 and 0.58 εNd-units, depending on the Nd amounts in the samples. Only one sample, with the lowest neodymium concentration (~1 ng), present higher uncertainty (0.72 εNd-units).

4.4.4 Estimation of mixing rates

Mixing rates estimations were performed using our new W-Sicily ε_{Nd} record in combination with previously published W- and E-Med ε_{Nd} records as representative time-evolving water mass ε_{Nd}

end-members for WMDW (SU92-33), EMDW (MS27PT) and LIW (BC07) (32, 33, 42, respectively). For the EMSW estimations we applied a simple mixing model using the following equation; $\varepsilon_{Nd}mix = ((\varepsilon_{Nd\ \mathrm{WMDW}} * [Nd]_{\mathrm{WMDW}} * f_{\mathrm{WMDW}}) + (\varepsilon_{Nd\ \mathrm{LIW}} * [Nd]_{\mathrm{LIW}} * f_{\mathrm{LIW}}) + (\varepsilon_{Nd\ \mathrm{EMDW}} * [Nd]_{\mathrm{EMDW}} * f_{\mathrm{EMDW}}))/(([Nd]_{\mathrm{WMDW}} * f_{\mathrm{WMDW}}) + ([Nd]_{\mathrm{LIW}} * f_{\mathrm{LIW}}) + ([Nd]_{\mathrm{EMDW}} * f_{\mathrm{EMDW}}))$, where $\varepsilon Ndmix$ correspond to our neodymium values from core NDT-6-2016, while $\varepsilon_{\mathrm{Nd\ WMDW}}$, $\varepsilon_{\mathrm{Nd\ LIW}}$, $\varepsilon_{\mathrm{Nd3\ EMDW}}$ are the ε_{Nd} values from cores SU92-33, MSPT2 and BC07. $[Nd]$ corresponds to the neodymium concentration of WDWM, EMDW as well as LIW and f is the proportion of each water-mass, so that $f_1 + f_2 + f_3 = 1$ (Fig. 3a).

Whenever the ε_{Nd} values from our record were acquired at different ages compared to those from cores SU92-33, BC07, and MS27PT, we used a linear interpolation between the ε_{Nd} values determined at adjacent ages in these three cores to obtain the corresponding ε_{Nd} values to the same age as our records (Table S1 in supplementary material). To account for uncertainties derived from the lack of reliable past-seawater Nd concentration estimates as well as to account for analytical uncertainties, we have implemented a Monte-Carlo approach of the mixing equation, that also considers different scenarios in the mixing proportions between the eastern Mediterranean water masses contributing to the EMSW, i.e., LIW and EMDW. The first scenario is characterized by the same contribution of LIW and EMSW (i.e. $f_{\mathrm{LIW}} = f_{\mathrm{EMDW}}$), the second scenario the contribution of the LIW doubles that of the EMDW (i.e. $f_{\mathrm{LIW}} = 2*f_{\mathrm{EMDW}}$) and the third scenario considers that the proportion of EMDW doubles that of the LIW (i.e. $f_{\mathrm{EMDW}} = 2*f_{\mathrm{LIW}}$) (Table S3 in supplementary material). Nd concentrations used for WMDW, LIW and EMDW have been 23.05 ± 1.05, 27.8 ± 1.6 and 28.25 ± 3.35 respectively, based on present-day Nd concentrations measured in each water-mass (Tachikawa et al., 2004).

4.5 ACKNOWLEDGEMENTS

This work was founded by the projects TIMED (683237) of the European Research Council (Consolidator Grants) and NextData PNR 2011–2013 (http://www.nextdataproject.it/). The GRC Geociències Marines thank the Generalitat de Catalunya for the Grups de Recerca Consolidats

grant 2017 SGR 315. Leopoldo D. Pena acknowledges support from the Ramón y Cajal program (MINECO, Spain), Isabel Cacho from the ICREA Academia programme from the Generalitat de Catalunya, Jaime Frigola from the Serra Húnter Programme (Generalitat de Catalunya). We thank the doctoral school in Earth and Sea Sciences from University of Palermo which supported the research. We also thank ISMAR-CNR (Napoli) for core NDT-6-2016 which it was recovered by the NEXTDATA expedition on board R/V CNR-Urania in 2014. Finally, we acknowledge Montse Guart (Dept. Dinàmica de la Terra i de l'Oceà, Universitat de Barcelona) and Joaquim Perona (Centres Científics i Tecnològics, CCiT-UB) for their support with the laboratory work.

4.6 REFERENCES

Alonso, B., Juan, C., Ercilla, G., Cacho, I., López-González, N., Rodríquez-Tovar, F. J., Dorador, J., Francés, G., Casas, D., Vandorpe, T., & Vázquez, J. T. (2021). Paleoceanographic and paleoclimatic variability in the Western Mediterranean during the last 25 cal. kyr BP. New insights from contourite drifts. *Marine Geology*, *437*. https://doi.org/10.1016/j.margeo.2021.106488

Ayache, M., Dutay, J. C., Arsouze, T., Révillon, S., Beuvier, J., & Jeandel, C. (2016). High-resolution neodymium characterization along the Mediterranean margins and modelling of Nd distribution in the Mediterranean basins. *Biogeosciences*, *13*(18), 5259–5276. https://doi.org/10.5194/bg-13-5259-2016

Barker, S., Greaves, M., & Elderfield, H. (2003). A study of cleaning procedures used for foraminiferal Mg/Ca paleothermometry. *Geochemistry, Geophysics, Geosystems*, *4*(9), 1–20. https://doi.org/10.1029/2003GC000559

Bianchi, D., Zavatarelli, M., Pinardi, N., Capozzi, R., Capotondi, L., Corselli, C., & Masina, S. (2006). Simulations of ecosystem response during the sapropel S1 deposition event. *Palaeogeography, Palaeoclimatology, Palaeoecology*, *235*(1–3), 265–287. https://doi.org/10.1016/j.palaeo.2005.09.032

Blaauw, M., & Christeny, J. A. (2011). Flexible paleoclimate age-depth models using an

autoregressive gamma process. *Bayesian Analysis*, *6*(3), 457–474. https://doi.org/10.1214/11-BA618

Cacho, I., Grimalt, J. O., & Canals, M. (2002). Response of the Western Mediterranean Sea to rapid climatic variability during the last 50,000 years: A molecular biomarker approach. *Journal of Marine Systems*, *33–34*, 253–272. https://doi.org/10.1016/S0924-7963(02)00061-1

Cacho, I., Grimalt, J. O., Canals, M., Sbaffi, L., Shackleton, N., Schönfeld, J., & Zahn, R. (2001). Variability of the western Mediterranean Sea surface temperature during the last 25,000 years and its connection with the northern hemisphere climatic changes. *Climatic Changes*, *16*(1), 40–52. https://doi.org/10.1029/sp010

Cascella, A., Bonomo, S., Lirer, F., Margaritelli, G., Checa, H., Cacho, I., Pena, L. D., & Frigola, J. (2021). The response of calcareous plankton to the Sapropel S1 interval in North Ionian Sea. *Global and Planetary Change*, *205*(November 2020), 103599. https://doi.org/10.1016/j.gloplacha.2021.103599

Checa, H., Margaritelli, G., Pena, L. D., Frigola, J., Cacho, I., Rettori, R., & Lirer, F. (2020). High resolution paleo-environmental changes during the Sapropel 1 in the North Ionian Sea, central Mediterranean. *Holocene*. https://doi.org/10.1177/0959683620941095

Colin, C., Duhamel, M., Siani, G., Dubois-Dauphin, Q., Ducassou, E., Liu, Z., Wu, J., Revel, M., Dapoigny, A., Douville, E., Taviani, M., & Montagna, P. (2021). Changes in the Intermediate Water Masses of the Mediterranean Sea During the Last Climatic Cycle—New Constraints From Neodymium Isotopes in Foraminifera. *Paleoceanography and Paleoclimatology*, *36*(4), 1–28. https://doi.org/10.1029/2020PA004153

Copard, K., Colin, C., Douville, E., Freiwald, A., Gudmundsson, G., De Mol, B., & Frank, N. (2010). Nd isotopes in deep-sea corals in the North-eastern Atlantic. *Quaternary Science Reviews*, *29*(19–20), 2499–2508. https://doi.org/10.1016/j.quascirev.2010.05.025

De Lange, G. J., Thomson, J., Reitz, A., Slomp, C. P., Speranza Principato, M., Erba, E., & Corselli, C. (2008). Synchronous basin-wide formation and redox-controlled preservation of a Mediterranean sapropel. *Nature Geoscience*, *1*(9), 606–610. https://doi.org/10.1038/ngeo283

Dormoy, I., Peyron, O., Nebout, N. C., Goring, S., Kotthoff, U., Magny, M., & Pross, J. (2009). Terrestrial climate variability and seasonality changes in the Mediterranean region between 15000 and 4000 years BP deduced from marine pollen records. *Climate of the Past*, *5*(4), 615–632. https://doi.org/10.5194/cp-5-615-2009

Dubois-Dauphin, Q., Montagna, P., Siani, G., Douville, E., Wienberg, C., Hebbeln, D., Liu, Z., Kallel, N., Dapoigny, A., Revel, M., Pons-Branchu, E., Taviani, M., & Colin, C. (2017). Hydrological variations of the intermediate water masses of the western Mediterranean Sea during the past 20 ka inferred from neodymium isotopic composition in foraminifera and cold-water corals. *Climate of the Past*, *13*(1), 17–37. https://doi.org/10.5194/cp-13-17-2017

Duhamel, M., Colin, C., Revel, M., Siani, G., Dapoigny, A., Douville, E., Wu, J., Zhao, Y., Liu, Z., & Montagna, P. (2020). Variations in eastern Mediterranean hydrology during the last climatic cycle as inferred from neodymium isotopes in foraminifera. *Quaternary Science Reviews*, *237*, 106306. https://doi.org/10.1016/j.quascirev.2020.106306

Filippidi, A., Triantaphyllou, M. V., & De Lange, G. J. (2016). Eastern-Mediterranean ventilation variability during sapropel S1 formation, evaluated at two sites influenced by deep-water formation from Adriatic and Aegean Seas. *Quaternary Science Reviews*, *144*, 95–106. https://doi.org/10.1016/j.quascirev.2016.05.024

Freydier, R., Michard, A., De Lange, G., & Thomson, J. (2001). Nd isotopic compositions of Eastern Mediterranean sediments: Tracers of the Nile influence during sapropel S1 formation? *Marine Geology*, *177*(1–2), 45–62. https://doi.org/10.1016/S0025-3227(01)00123-2

Frigola, J., Moreno, A., Cacho, I., Canals, M., Sierro, F. J., Flores, J. A., & Grimalt, J. O. (2008). Evidence of abrupt changes in Western Mediterranean Deep Water circulation during the last 50 kyr: A high-resolution marine record from the Balearic Sea. *Quaternary International*, *181*(1), 88–104. https://doi.org/10.1016/j.quaint.2007.06.016

Gacic, M., Manca, B. B., & Mantziafou, A. (2001). Physical Oceanography of the Adriatic Sea. In *Physical Oceanography of the Adriatic Sea* (Issue February 2019). https://doi.org/10.1007/978-94-015-9819-4

Garcia-Solsona, E., Pena, L. D., Paredes, E., Pérez-Asensio, J. N., Quirós-Collazos, L., Lirer, F., & Cacho, I. (2020). Rare earth elements and Nd isotopes as tracers of modern ocean circulation in the central Mediterranean Sea. *Progress in Oceanography*, *185*(December 2019), 102340. https://doi.org/10.1016/j.pocean.2020.102340

Grant, K. M., Grimm, R., Mikolajewicz, U., Marino, G., Ziegler, M., & Rohling, E. J. (2016). The timing of Mediterranean sapropel deposition relative to insolation, sea-level and African monsoon changes. *Quaternary Science Reviews*, *140*, 125–141. https://doi.org/10.1016/j.quascirev.2016.03.026

Grimm, R., Maier-reimer, E., Mikolajewicz, U., Schmiedl, G., Mu, K., Adloff, F., Grant, K. M., Ziegler, M., Lourens, L. J., & Emeis, K. (2015). *Late glacial initiation of Holocene eastern Mediterranean sapropel formation*. https://doi.org/10.1038/ncomms8099

Henry, F., Jeandel, C., Dupré, B., & Minster, J. F. (1994). Particulate and dissolved Nd in the western Mediterranean Sea: Sources, fate and budget. *Marine Chemistry*, *45*(4), 283–305. https://doi.org/10.1016/0304-4203(94)90075-2

Hunt, C. O., et al., “Chronology and stratigraphy of the valley system” in Temple landscapes: Fragility, change and resilience of Holocene environments in the Maltese Islands, James Barrett, Ed. (McDonald Institute for Archaeological Research, 2020), pp. 35-71.

Incarbona, A., Abu-Zied, R. H., Rohling, E. J., & Ziveri, P. (2019). *Reventilation Episodes*

During the Sapropel S1 Deposition in the Eastern Mediterranean Based on Holococcolith Preservation Paleoceanography and Paleoclimatology. 1–13. https://doi.org/10.1029/2019PA003626

Jacobsen, S. B., & Wasserburg, G. J. (1980). Sm-Nd isotopic evolution of chondrites. *Earth and Planetary Science Letters*, *50*(1), 139–155. https://doi.org/10.1016/0012-821X(80)90125-9

Kotthoff, U., Koutsodendris, A., Pross, J., Schmiedl, G., Bornemann, A., Kaul, C., Marino, G., Peyron, O., & Schiebel, R. (2011). Impact of Lateglacial cold events on the northern Aegean region reconstructed from marine and terrestrial proxy data. *Journal of Quaternary Science*, *26*(1), 86–96. https://doi.org/10.1002/jqs.1430

Lascaratos, A., Williams, R. G., & Tragou, E. (1993). A mixed-layer study of the formation of Levantine Intermediate Water. *Journal of Geophysical Research*, *98*(C8). https://doi.org/10.1029/93jc00912

Lebreiro, S. M., Antón, L., Reguera, M. I., & Marzocchi, A. (2018). *Paleoceanographic and climatic implications of a new Mediterranean Outflow branch in the southern Gulf of Cadiz*. *197*. https://doi.org/10.1016/j.quascirev.2018.07.036

Lourens, L. J., Hilgen, F. J., Gudjonsson, L., & Zachariasse, W. J. (1992). Late Pliocene to early Pleistocene astronomically forced sea surface productivity and temperature variations in the Mediterranean. *Marine Micropaleontology*, *19*(1–2), 49–78. https://doi.org/10.1016/0377-8398(92)90021-B

Martinez-Ruiz, F., Kastner, M., Paytan, A., Ortega-Huertas, M., & Bernasconi, S. M. (2000). Geochemical evidence for enhanced productivity during S1 sapropel deposition in the eastern Mediterranean. *Paleoceanography*, *15*(2), 200–209. https://doi.org/10.1029/1999PA000419

McCulloch, M., Taviani, M., Montagna, P., López Correa, M., Remia, A., & Mortimer, G. (2010). Proliferation and demise of deep-sea corals in the Mediterranean during the

Younger Dryas. *Earth and Planetary Science Letters*, *298*(1–2), 143–152. https://doi.org/10.1016/j.epsl.2010.07.036

Ménot, G., Pivot, S., Bouloubassi, I., Davtian, N., Hennekam, R., Bosch, D., Ducassou, E., Bard, E., Migeon, S., & Revel, M. (2020). Timing and stepwise transitions of the African Humid Period from geochemical proxies in the Nile deep-sea fan sediments. *Quaternary Science Reviews*, *228*. https://doi.org/10.1016/j.quascirev.2019.106071

Mercone, D., Thomson, J., Abu-Zied, R. H., Croudace, I. W., & Rohling, E. J. (2001). High-resolution geochemical and micropalaeontological profiling of the most recent eastern Mediterranean sapropel. *Marine Geology*, *177*(1–2), 25–44. https://doi.org/10.1016/S0025-3227(01)00122-0

Millot, C. (1987). Circulation in the Hydrodynamics General circulation Mediterranean Sea Mesoscale phenomena. *Oceanologica Acta*, *10*(2), 143–149.

Millot, C. (1999). Circulation in the Western Mediterranean Sea. *Journal of Marine Systems*, *20*(1–4), 423–442. https://doi.org/10.1016/S0924-7963(98)00078-5

Murat, A. (1999). Pliocene – Pleistocene occurrence of sapropels in the western Mediterranean Sea and their relation to eastern Mediterranean sapropels. *Proceedings of the Ocean Drilling Program, Scientific Results*, *161*, 519–527.

Pena, L. D., Calvo, E., Cacho, I., Eggins, S., & Pelejero, C. (2005). Identification and removal of Mn-Mg-rich contaminant phases on foraminiferal tests: Implications for Mg/Ca past temperature reconstructions. *Geochemistry, Geophysics, Geosystems*, *6*(9). https://doi.org/10.1029/2005GC000930

Pérez-Asensio, J. N., Frigola, J., Pena, L. D., Sierro, F. J., Reguera, M. I., Rodríguez-Tovar, F. J., Dorador, J., Asioli, A., Kuhlmann, J., Huhn, K., & Cacho, I. (2020). Changes in western Mediterranean thermohaline circulation in association with a deglacial Organic Rich Layer formation in the Alboran Sea. *Quaternary Science Reviews*, *228*.

https://doi.org/10.1016/j.quascirev.2019.106075

Pinardi, N., & Masetti, E. (2000). Variability of the large scale general circulation of the Mediterranean Sea from observations and modelling: A review. *Palaeogeography, Palaeoclimatology, Palaeoecology*, *158*(3–4), 153–173. https://doi.org/10.1016/S0031-0182(00)00048-1

Rasmussen, S. O., Andersen, K. K., Svensson, A. M., Steffensen, J. P., Vinther, B. M., Clausen, H. B., Johnsen, S. J., Larsen, L. B., Bigler, M., Ro, R., & Fischer, H. (2006). *A new Greenland ice core chronology for the last glacial termination*. *111*, 1–16. https://doi.org/10.1029/2005JD006079

Revel, M., Colin, C., Bernasconi, S., Combourieu-Nebout, N., Ducassou, E., Grousset, F. E., Rolland, Y., Migeon, S., Bosch, D., Brunet, P., Zhao, Y., & Mascle, J. (2014). 21,000 Years of Ethiopian African monsoon variability recorded in sediments of the western Nile deep-sea fan. *Regional Environmental Change*, *14*(5), 1685–1696. https://doi.org/10.1007/s10113-014-0588-x

Revel, M., Ducassou, E., Skonieczny, C., Colin, C., Bastian, L., Bosch, D., Migeon, S., & Mascle, J. (2015). 20,000 years of Nile River dynamics and environmental changes in the Nile catchment area as inferred from Nile upper continental slope sediments. *Quaternary Science Reviews*, *130*, 200–221. https://doi.org/10.1016/j.quascirev.2015.10.030

Rogerson, M., Cacho, I., Jimenez-Espejo, F., Reguera, M. I., Sierro, F. J., Martinez-Ruiz, F., Frigola, J., & Canals, M. (2008). A dynamic explanation for the origin of the western Mediterranean organic-rich layers. *Geochemistry, Geophysics, Geosystems*, *9*(7). https://doi.org/10.1029/2007GC001936

Rohling, E. J. (1994). Review and new aspects concerning the formation of eastern Mediterranean sapropels. *Marine Geology*, *122*(1–2), 1–28. https://doi.org/10.1016/0025-3227(94)90202-X

Rohling, E. J., Marino, G., & Grant, K. M. (2015). Mediterranean climate and oceanography, and the periodic development of anoxic events (sapropels). *Earth-Science Reviews*, *143*, 62–97. https://doi.org/10.1016/j.earscirev.2015.01.008

Rossignol-Strick, M. (1985). Mediterranean Quaternary sapropels, an immediate response of the African monsoon to variation of insolation. *Palaeogeography, Palaeoclimatology, Palaeoecology*, *49*(3–4), 237–263. https://doi.org/10.1016/0031-0182(85)90056-2

Schmiedl, G., Kuhnt, T., Ehrmann, W., Emeis, K. C., Hamann, Y., Kotthoff, U., Dulski, P., & Pross, J. (2010). Climatic forcing of eastern Mediterranean deep-water formation and benthic ecosystems during the past 22 000 years. *Quaternary Science Reviews*, *29*(23–24), 3006–3020. https://doi.org/10.1016/j.quascirev.2010.07.002

Shanahan, T. M., Mckay, N. P., Hughen, K. A., Overpeck, J. T., Otto-Bliesner, B., Heil, C. W., King, J., Scholz, C. A., & Peck, J. (2015). The time-transgressive termination of the African humid period. *Nature Geoscience*, *8*(2), 140–144. https://doi.org/10.1038/ngeo2329

Siani, G., Magny, M., Paterne, M., Debret, M., & Fontugne, M. (2013). Paleohydrology reconstruction and Holocene climate variability in the South Adriatic Sea. *Climate of the Past*, *9*(1), 499–515. https://doi.org/10.5194/cp-9-499-2013

Sierro, F. J., Hodell, D. A., Andersen, N., & Azibeiro, L. A. (2020). *Mediterranean Over fl ow Over the Last 250 kyr : Freshwater Forcing From the Tropics to the Ice Sheets Paleoceanography and Paleoclimatology*. 1–31. https://doi.org/10.1029/2020PA003931

Tachikawa, K., Piotrowski, A. M., & Bayon, G. (2014). Neodymium associated with foraminiferal carbonate as a recorder of seawater isotopic signatures. *Quaternary Science Reviews*, *88*, 1–13. https://doi.org/10.1016/j.quascirev.2013.12.027

Tachikawa, K., Roy-Barman, M., Michard, A., Thouron, D., Yeghicheyan, D., & Jeandel, C. (2004). Neodymium isotopes in the Mediterranean Sea: Comparison between seawater and

sediment signals. *Geochimica et Cosmochimica Acta*, *68*(14), 3095–3106. https://doi.org/10.1016/j.gca.2004.01.024

Tanaka, T., Togashi, S., Kamioka, H., Amakawa, H., Kagami, H., Hamamoto, T., Yuhara, M., Orihashi, Y., Yoneda, S., Shimizu, H., Kunimaru, T., Takahashi, K., Yanagi, T., Nakano, T., Fujimaki, H., Shinjo, R., Asahara, Y., Tanimizu, M., & Dragusanu, C. (2000). JNdi-1: A neodymium isotopic reference in consistency with LaJolla neodymium. *Chemical Geology*, *168*(3–4), 279–281. https://doi.org/10.1016/S0009-2541(00)00198-4

Tesi, T., Asioli, A., Minisini, D., Maselli, V., Dalla Valle, G., Gamberi, F., Langone, L., Cattaneo, A., Montagna, P., & Trincardi, F. (2017). Large-scale response of the Eastern Mediterranean thermohaline circulation to African monsoon intensification during sapropel S1 formation. *Quaternary Science Reviews*, *159*, 139–154. https://doi.org/10.1016/j.quascirev.2017.01.020

Toucanne, S., Angue Minto'o, C. M., Fontanier, C., Bassetti, M. A., Jorry, S. J., & Jouet, G. (2015). Tracking rainfall in the northern Mediterranean borderlands during sapropel deposition. *Quaternary Science Reviews*, *129*, 178–195. https://doi.org/10.1016/j.quascirev.2015.10.016

Trias-Navarro, S., Cacho, I., De La Fuente, M., Pena, L. D., Frigola, J., Lirer, F., & Caruso, A. (2021). Surface hydrographic changes at the western flank of the Sicily Channel associated with the last sapropel. *Global and Planetary Change*, *204*, 103582. https://doi.org/10.1016/j.gloplacha.2021.103582

Vance, D., Scrivner, A. E., Beney, P., Staubwasser, M., Henderson, G. M., & Slowey, N. C. (2009). The use of foraminifera as a record of the past neodymium isotope composition of seawater. *Paleoceanography*, *19*(2), 1–17. https://doi.org/10.1029/2003PA000957

Vinther, B. M., Clausen, H. B., Johnsen, S. J., Rasmussen, S. O., Andersen, K. K., Buchardt, S. L., Seierstad, I. K., Steffensen, J. P., Svensson, A., Olsen, J., & Heinemeier, J. (2006). *A synchronized dating of three Greenland ice cores throughout the Holocene*. *111*, 1–11.

https://doi.org/10.1029/2005JD006921

Wombacher, F., & Rchkämper, M. (2003). Investigation of the mass discrimination of multiple collector ICP-MS using neodymium isotopes and the generalised power law. *Journal of Analytical Atomic Spectrometry*, *18*(11), 1371–1375. https://doi.org/10.1039/b308403e

Wu, J., Pahnke, K., Böning, P., Wu, L., Michard, A., & de Lange, G. J. (2019). Divergent Mediterranean seawater circulation during Holocene sapropel formation – Reconstructed using Nd isotopes in fish debris and foraminifera. *Earth and Planetary Science Letters*, *511*, 141–153. https://doi.org/10.1016/j.epsl.2019.01.036

4.7 SUPLEMENTARY MATERIAL OF "WATER EXPORT CHANGES THROUGH THE STRAIT OF SICILY DURING THE LAST DEGLACIAL PERIOD"

Age calendar BP (kyr)	ε_{Nd} Lin interp Balearic Sea (WMDW)	2sd	ε_{Nd} Lin interp Levantine Sea (LIW)	2sd	ε_{Nd} Lin interp Levantine Sea (EMSW)	2sd	ε_{Nd} NDT-6-2016	2sd
Present-day	-9.2	0.2	-6.6	0.2	-7.0	0.2	-8.5	0.2
2.4	-8.6	0.3	-6.0	0.2	-5.8	0.2	-8.1	0.3
3.3	-8.8	0.3	-5.9	0.2	-5.5	0.2	-7.7	0.3
3.7	-8.8	0.3	-5.8	0.2	-5.5	0.2	-7.6	0.3
4.2	-8.7	0.3	-5.6	0.2	-5.5	0.2	-7.6	0.3
4.7	-9.0	0.3	-5.4	0.2	-4.8	0.2	-8.2	0.3
5.2	-9.2	0.3	-5.2	0.2	-4.2	0.3	-7.8	0.3
5.7	-9.1	0.3	-4.9	0.2	-4.3	0.2	-7.6	0.3
5.9	-9.1	0.3	-4.9	0.2	-4.3	0.2	-8.0	0.3
6.2	-9.0	0.3	-4.8	0.2	-4.1	0.2	-7.5	0.3
6.6	-8.9	0.3	-5.1	0.2	-3.8	0.2	-7.3	0.3
7.1	-8.7	0.3	-5.4	0.2	-3.6	0.2	-7.5	0.3
7.5	-8.6	0.3	-5.6	0.2	-3.6	0.2	-7.8	0.3
7.6	-8.6	0.3	-5.6	0.2	-3.6	0.2	-8.4	0.3
7.9	-8.6	0.3	-5.8	0.2	-3.6	0.2	-7.9	0.3
8.2	-8.7	0.3	-5.8	0.2	-3.6	0.2	-8.1	0.3
8.4	-8.8	0.3	-5.9	0.2	-3.7	0.2	-8.2	0.3
9.1	-9.1	0.3	-5.9	0.2	-3.3	0.2	-8.4	0.3
9.2	-9.1	0.3	-5.9	0.2	-3.2	0.2	-7.8	0.3
9.6	-9.0	0.3	-5.3	0.2	-2.9	0.2	-7.8	0.3
9.7	-9.0	0.3	-5.0	0.2	-2.7	0.2	-8.3	0.4
10.3	-9.5	0.3	-4.6	0.2	-2.6	0.2	-7.9	0.5
10.6	-9.3	0.3	-4.7	0.2	-2.7	0.2	-8.0	0.4
10.8	-9.0	0.3	-4.8	0.2	-2.9	0.2	-7.4	0.6
11.0	-9.0	0.3	-4.9	0.2	-3.0	0.2	-7.2	0.4
11.3	-9.4	0.3	-5.0	0.2	-3.1	0.2	-7.1	0.4
11.4	-9.5	0.3	-4.9	0.2	-3.1	0.2	-7.3	0.4
11.6	-9.0	0.3	-4.8	0.2	-3.3	0.2	-7.0	0.4
11.9	-9.1	0.3	-4.7	0.2	-3.4	0.2	-6.3	0.3
12.2	-8.9	0.3	-4.6	0.2	-3.6	0.2	-5.8	0.5
12.6	-8.8	0.3	-4.5	0.2	-3.2	0.3	-5.6	0.4
13.1	-9.1	0.3	-4.4	0.2	-3.1	0.3	-7.7	0.4
13.3	-9.3	0.3	-4.3	0.2	-3.2	0.3	-8.1	0.4
13.9	-9.4	0.3	-4.3	0.2	-3.3	0.3	-7.5	0.4

Table S1a. NDT-6-2016 ε_{Nd} record (this study) and those from sediment cores SU92-33 (Dubois-Dauphin et al., 2017), BC07 (Freydier et al., 2001; Wu et al., 2019) and MS27PT (Duhamel et al., 2020) as the end-members contributing in the W-Sicily, i.e. the WMDW, LIW and EMDW respectively and the associated error (2sd).

	Min [Nd] (pmols/Kg)	Max [Nd] (pmols/Kg)
WMDW	22.0	24.1
LIW	26.2	29.4
EMSW	24.9	31.6

Table S1b. Nd concentrations used for WMDW, LIW and EMDW, based on present-day Nd concentrations measured in each water-mass (Tachikawa et al. 2004).

	WMDW					ε_{Nd} average
ε_{Nd}	-9.3	-8.9	-8.9	-9.2	-9.5	**-9.2**
Depth (m)	800	950	400	800	1000	
Station	Station B		Station C			

	LIW				ε_{Nd} average
ε_{Nd}	-5.7	-6.5	-7	-7.1	**-6.6**
Depth (m)	403-504	606-707	272–352	429	
Station	Station 74		Station 51		

	EMDW				ε_{Nd} average
ε_{Nd}	-7	-7.5	-6.6	-7	**-7.0**
Depth (m)	857-1005	1213-1414	1009	1263–1516	
Station	Station 51		Station 74		

	South Tyrrhenian				ε_{Nd} average
ε_{Nd}	-7.68	-7.78	-9.38	-9.04	**-8.5**
Depth (m)	900	1000	1000	1036	
Station	St4	St7	St8	St9	

Table S2. Present-day sea water ε_{Nd} values from WMDW, LIW, EMSW (Tachikawa et al., 2004) and South Tyrrhenian Sea (Garcia-Solsona et al., 2020)

Age	ESMSW Mixing Scenario 1 (%)	ESMSW Mixing Scenario 2 (%)	ESMSW Mixing Scenario 3 (%)
0.0	25.2	26.2	24.3
2.4	16.1	15.9	16.3
3.3	10.7	8.8	13.8
3.7	33.6	32.8	34.5
4.2	29.8	29.7	29.8
4.7	16.8	16.5	17.1
5.2	26.8	25.8	27.9
5.7	28.8	28.1	29.4
5.9	20.6	20.2	21.0
6.2	28.0	27.1	29.1
6.6	31.3	29.5	33.2
7.1	27.6	25.2	30.4
7.5	17.2	15.7	19.2
7.6	4.0	3.7	4.5
7.9	14.9	13.7	16.7
8.2	10.6	9.8	11.6
8.4	14.3	13.1	15.7
9.1	14.6	13.4	16.1
9.2	22.6	20.3	25.4
9.6	20.8	19.4	22.6
9.7	10.7	10.2	11.3
10.3	23.7	22.2	25.1
10.6	17.9	16.8	19.4
10.8	25.8	24.3	27.4
11.0	30.3	28.3	32.8
11.3	39.0	36.5	41.7
11.4	34.8	33.0	37.1
11.6	34.8	32.7	37.3
11.9	51.8	49.6	53.9
12.2	60.8	58.0	63.7
12.6	59.1	56.1	62.3
13.1	22.8	21.8	23.8
13.3	18.1	17.6	18.9
13.9	27.0	26.5	28.0

Table S2. Eastern Mediterranean Source Waters (EMSW) estimations with different mixing proportions between the eastern Mediterranean water masses contributing to the EMSW (LIW and EMDW) based on ε_{Nd} values from our record (NDT-6-2016) and SU92-33 (Dubois-Dauphin et al., 2017), BC07 (Freydier et al., 2001; Wu et al., 2019) and MS27PT (Duhamel et al., 2020). The first scenario characterized by the same contribution of each water mass, the second one by double contribution of the LIW with respect to the EMDW and the third one by a double contribution of the EMDW with respect to the LIW.

References

Dubois-Dauphin, Q., Montagna, P., Siani, G., Douville, E., Wienberg, C., Hebbeln, D., Liu, Z., Kallel, N., Dapoigny, A., Revel, M., Pons-Branchu, E., Taviani, M., & Colin, C. (2017). Hydrological variations of the intermediate water masses of the western Mediterranean Sea during the past 20 ka inferred from neodymium isotopic composition in foraminifera and cold-water corals. *Climate of the Past*, *13*(1), 17–37. https://doi.org/10.5194/cp-13-17-2017

Duhamel, M., Colin, C., Revel, M., Siani, G., Dapoigny, A., Douville, E., Wu, J., Zhao, Y., Liu, Z., & Montagna, P. (2020). Variations in eastern Mediterranean hydrology during the last climatic cycle as inferred from neodymium isotopes in foraminifera. *Quaternary Science Reviews*, *237*, 106306. https://doi.org/10.1016/j.quascirev.2020.106306

Freydier, R., Michard, A., De Lange, G., & Thomson, J. (2001). Nd isotopic compositions of Eastern Mediterranean sediments: Tracers of the Nile influence during sapropel S1 formation? *Marine Geology*, *177*(1–2), 45–62. https://doi.org/10.1016/S0025-3227(01)00123-2

Garcia-Solsona, E., Pena, L. D., Paredes, E., Pérez-Asensio, J. N., Quirós-Collazos, L., Lirer, F., & Cacho, I. (2020). Rare earth elements and Nd isotopes as tracers of modern ocean circulation in the central Mediterranean Sea. *Progress in Oceanography*, *185*(December 2019), 102340. https://doi.org/10.1016/j.pocean.2020.102340

Tachikawa, K., Roy-Barman, M., Michard, A., Thouron, D., Yeghicheyan, D., & Jeandel, C. (2004). Neodymium isotopes in the Mediterranean Sea: Comparison between seawater and sediment signals. *Geochimica et Cosmochimica Acta*, *68*(14), 3095–3106. https://doi.org/10.1016/j.gca.2004.01.024

Wu, J., Pahnke, K., Böning, P., Wu, L., Michard, A., & de Lange, G. J. (2019). Divergent Mediterranean seawater circulation during Holocene sapropel formation – Reconstructed using Nd isotopes in fish debris and foraminifera. *Earth and Planetary Science Letters*, *511*, 141–153. https://doi.org/10.1016/j.epsl.2019.01.036

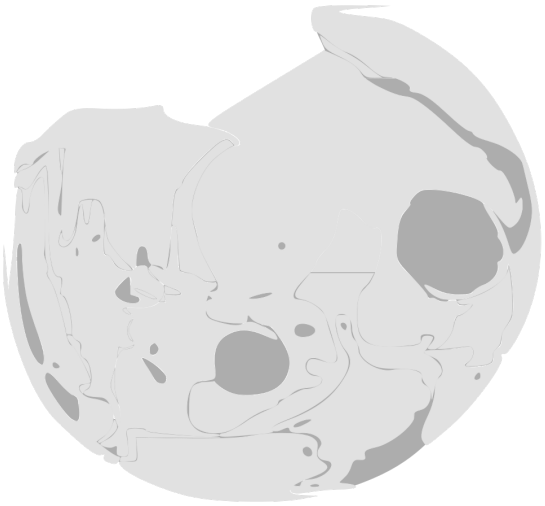

...nosotros nacimos de la noche

en ella vivimos

y moriremos en ella

pero la luz será mañana para los más,

para todos aquellos que hoy lloran la noche,

para quienes se niega el día.

Para todos la luz,

para todos todo…

...Techo, tierra, trabajo, pan, salud, educación, independencia, democracia, libertad,

estas fueran nuestras demandas en la larga noche de los 500 años,

estas son hoy nuestras exigencias.

Extracto del manifiesto zapatista

5 SURFACE AND DEEP WATER HYDROLOGY CHANGES IN THE WESTERN MEDITERRANEAN SEA DURING THE LATE DEGLACIAL AND THE HOLOCENE*

Abstract

During the last deglacial period, the sea level rise associated with the north Atlantic ice-melting resulted in enhanced fresh-water supply into the Mediterranean trhough the Strait of Gibraltar, promoting an important weakening of the western Mediterranean deep water convection. This situation culminated with the Organic Rich Layers (ORLs) deposition (14.4-8.9 kyr BP). Moreover, during the late deglacial and early/middle Holocene an intensified African monsoon (AHP, 15-6 kyr BP) promoted an important hydrographic perturbation in the eastern Mediterranean, that finished with the deposition of organic-rich layers, the so-called last Sapropel (S1). In this work, we investigate the impact of this two events in the Mediterranean thermohaline circulation. For that, we analyze $\delta^{18}O$ isotopes and Mg/Ca ratios from both benthic and planktic foraminifera from a sediment core recovered at the western flank of Sicily channel (NDT-6-2016, 1066 m depth). Our data reveal a general surface freshening across the early/middle Holocene in the central Mediterranean area. This situation wuold be promoted by 1) the progressive the sea level rise and the consequent enhanced inflow of atlantic waters and 2) an enhanced fresh water supply together with less evaporation in the area, associated with humid prevailing conditions during the AHP. We also proposed an important reduction of the contribution of eastern Mediterranean sourced waters into the W-Med during the S1. We hypothesize that the limited deep-water interconnection between the two basins might have resulted in a weakening of the surface water inflow toward de western Sicily. This situatuion would have promoted an intense seasonality in the studied area characterized by cold winter conditions, that presumably could have favored the formation of a new intermediate deep water mass in the Tyrrhenian Sea area during the ES1b.

*Intended for pubblication as Trias-Navarro, S., Pena, L.D., de la Fuente, M., Frigola, J., Català, A., Caruso, A., Lirer, F. and Cacho, I.

5.1 INTRODUCTION

The Mediterranean (Med-Sea) is a semi-enclosed sea, where evaporation exceeds the freshwater contribution by rainfall and river discharge, promoting an anti-estuarine circulation (Lionello, 2012) (Fig. 1). The Med-Sea is connected with the Atlantic Ocean through the Strait of Gibraltar, where cold and fresh Atlantic surface waters (AW) enter into the western Mediterranean Sea (W-Med). During its eastward path across the W-Med, AW progressively turn saltier as a result of intense evaporation (Modified Atlantic Waters, MAW) (Lermusiaux & Robinson, 2001; Millot, 1987, 1999). After passing the Sardinia channel, MAW splits into two branches, one flowing towards the Tyrrhenian Sea, the other entering the eastern Mediterranean (E-Med) through the Strait of Sicily and forming intermediate waters at Levantine Sea (Levantine intermediate Waters, LIW). LIW, in turn, contribute to the formation of Eastern Mediterranean Deep Water (EMDW) in both the Aegean and Adriatic Sea (Gacic et al., 2001; Lascaratos et al., 1993; Millot, 1999; Pinardi & Masetti, 2000). A percentage of EMDW and LIW outflow through the Strait of Sicily (Eastern Mediterranean Source Waters hereafter, EMSW) into the W-Med and contribute to the formation of Western Mediterranean Deep Water at Gulf of Lions (WMDW). Eventually, WMDW exit together with EMSW through the Strait of Gibraltar as Mediterranean Outflow Waters (MOW) (Millot, 2009; Pinardi & Masetti, 2000).

During the last deglacial period, the sea level rise associated to the north Atlantic ice-melting caused an increase of the inflow of fresh atlantic waters into the Mediterranean Sea through the Strait of Sicily. This enhanced supply of fresh water would have conditioned the formation of deep-water at Gulf of Lions causing a weakening of the WMDW convection, that triggered significant changes in the bottom water oxygen content. This changes led to the formation of the Organic Rich Layers (ORLs) in the Alboran Sea (14.4-8.9 kyr) (Cacho et al., 2002; Pérez-Asensio et al., 2020; Rogerson et al., 2008). At similar time, intensified African monsoon during the African Humid period (AHP, 15-6 kyr BP), caused an important perturbation of the hydrologic cycle in the E-Med. The associated enhanced freshwater supply from north African river systems into the E-Med promoted a surface water stratification increase, resulting in the intermediate and

deep water convection collapse (Checa et al., 2020; DeMenocal et al., 2000; Filippidi et al., 2016; Grimm et al., 2015; Incarbona et al., 2019; Ménot et al., 2020; Revel et al., 2015; Tesi et al., 2017; Wu et al., 2017). This situation led to the formation of the last sapropel (S1) between ~10.8 and ~6.1 kyr cal. BP (De Lange et al., 2008).

Recently, several studies have explored the inter-basin connection between the E-Med and the W-Med during the last deglacial period and the Holocene (Colin et al., 2021; Incarbona & Sprovieri, 2020; Trias-Navarro et al., 2021; Trias-Navarro et al, submitted). For example, previous studies from Trias-Navarro et al. (2021) proposed an enhanced surface water exchange between the E- and the W-Med during the Younger Dryas (YD) cold event (12.95-11.65 kyr BP), that was significantly reduced over the S1. According these authors, this limited flow of surface atlantic waters towards the E-Med led the W-Sicily under major influence of the predominant central-southern Europe cold/arid conditions (Davis et al., 2003; Walker, 1995). As a result, an intensification of seasonality would have occurred, with intense winter vertical water-mixing and stratified/warmer summer conditions. Other studies from Trias-Navarro et al. (in revision) explored potential oscillations in the export of the EMSW into the W-Med through the Strait of Sicily during the late deglacial period and the Holocene. They demonstrate that during the YD enhanced deep water interconnection prevailed between the E- and the W-Med, while a substantial weakening in the intermediate/deep water exchange between the two basins occurred during the S1.

In this work we present new data of sea surface (SST) and deep water temperature (DWT) based on Mg/Ca ratios, and also new oxygen stable isotopes records from surface and deep waters. All this data was obtained from gravity core NDT-6-2016 collected at the west flank of Sicily channel during the Next Data expedition at 1066 m of water depth (CNR-URANIA R/V, 2016). This data allows to explore for the first time changes in the regional evaporation-precipitation balance in the central Mediterranean during the late deglacial period and the Holocene. In addition, the new generated Mg/Ca-DWT record represent the first record of deep paleotemperatures in the W-Med for the deglacial period and the Holocene. These records, together with the obtained stable oxygen

isotopes records from benthic foraminifera, allow to determine changes in the deep water salinity at the W-Sicily. Then, since the recovered core is located at the present-day boundary between WMDW and EMSW (Garcia-Solsona et al., 2020) and EMSW are higher salinity than the WMDW (Lascaratos et al., 1993; Millot, 1987, 1999), changes in salinity could be interpreted as changes in the contribution of each water mass at the current location. Thus, allowing to evaluate changes in the intermediate-deep water exchange between this two sub-basins.

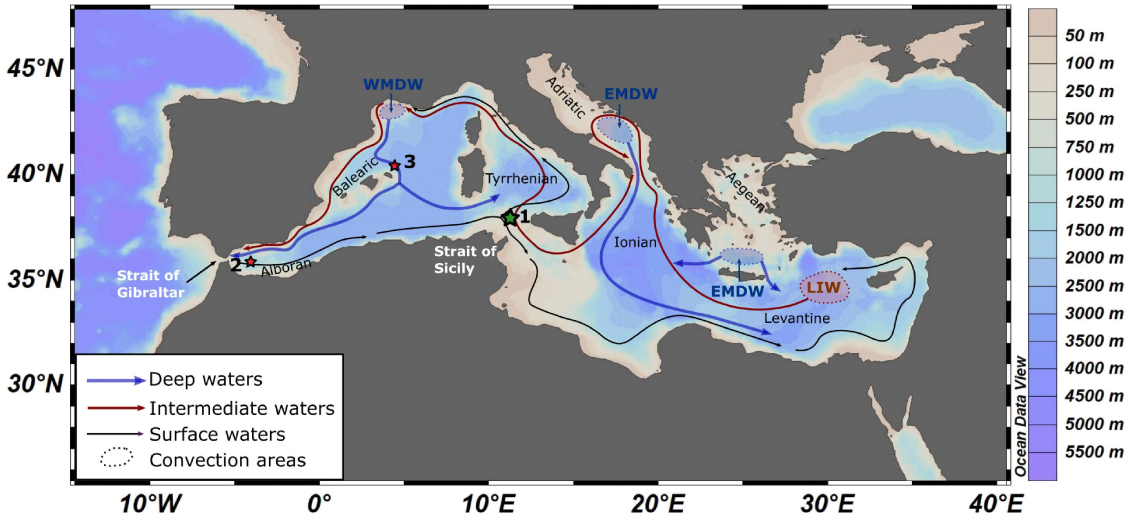

Fig. 1. a) Map of the study area in the Mediterranean Sea. Black arrows represent MAW, blue arrows represent WMDW and EMDW and red arrows represent LIW. Stars represent the cores discussed in this manuscript. Green star represent the studied core NDT-6-2016 (1) and red stars represent the HER-GC-ALB2 (2) and MD99-2343 (3).

5.2 MATERIALS AND METHODS

5.2.1 Core description and sampling

The gravity core NDT-6-2016 (~4 m long) was recovered during the Next Data expedition that took place in 2016 on board of CNR-URANIA R/V. The core is located in the transition area between the W-Sicily channel and the southern Tyrrhenian Sea (38°0'26,60" N and 11°47'44,84"E, 1066 m water depth), i.e. at the easternmost region of the W-Med (Fig. 1a). This location is currently sensitive to inter-basin water exchange variability and thus, appropriate to

detect potential hydrological changes. Core NDT-6-2016 consists of homogeneous silty-clay sediments with no sedimentary irregularities along the whole sequence.

5.2.2 Radiocarbon dates and age model

The chronological framework was established by twenty ^{14}C dates analyzed in monospecific planktic foraminifera samples (>250µm, *Globoconella inflata)*. Radiocarbon ages were calibrated using MARINE20 calibration curve (Hunt et al., 2020). The age model was constructed using the Bayesian statistics software Bacon (Blaauw & Christeny, 2011). In addition to the ^{14}C dates of the lower part, three tie points were added based on an adjusted alignment between the studied $\delta^{18}O$ record from *Globigerina bulloides* and the well-dated reference NGRIP isotope record (Rasmussen et al., 2006; Vinther et al., 2006). It is described in more detail in Trias-Navarro et al. (2021).

5.2.3 Trace elements analyses

Mg/Ca measurements were conducted in both benthic foraminifera species *Uvigerina* ssp. and planktic foraminifera species *G. bulloides*. Between 10-20 specimens were handpicked from the >250 µm fraction for *Uvigerina* ssp Mg/Ca measurements. For the samples where the presence of *Uvigerina* ssp. was scarce, a minimum of 5 specimens from the >212 µm fraction were handpicked. Mg/Ca analyses of *Uvigerina* ssp. were performed each 1-5 cm for the intervals 1-59 cm as well as 121-300 cm and between 10-20 cm for the rest of the interval. Mg/Ca measurements of planktonic foraminifera *G. bulloides* were performed each 1-10 cm for the interval between 123-259 cm and each 10-20 cm for the rest of the interval. Between 30-40 specimens were handpicked from the fraction between 250 and 315 µm. Each sample were processed individually. Before the cleaning procedure foraminifera of each sample were crushed using two glass slides under the microscope to observe the opening of the chambers. Crushing was done with extreme care to avoid the over-crushing which would accentuate sample loss during the cleaning procedure. The cleaning procedure, based on the works of Barker et al. (2003) and Pena et al. (2005), consisted in four steps; clay removal, reductive cleaning, oxidative cleaning and weak acid leaching. During the cleaning protocol a series of blanks (one blank every

~10 samples) were made in order to identify potential sample contamination. Sample dissolution was performed by adding ultra-pure 1% HNO3 with a Rh standard solution. After dissolution, samples were centrifuged to avoid any potential undissolved mineral particles. Trace elements analyses were measured on an inductively coupled plasma mass spectrometer (ICP-MS, Perkin Elmer ELAN 6000) in the CCiT-UB. In order to correct potential device calibration errors, standard solution with known elemental ratios was used for sample standard bracketing (SSB) as a correction for instrumental drift. The standard samples analytical reproducibility for Mg/Ca were 1.29% (1σ) and 1.21% in *U. mediterranea* and *G. bulloides*, respectively. Mg/Ca ratios were compared with both Mn/Ca and Al/Ca ratios to identify potential contamination from manganese oxides and aluminosilicates, respectively, since they could provide anomalous high Mg/Ca (Barker et al., 2003 and Pena et al., 2005). Mn/Ca ratios above 2σ were removed (0.11 and 0.09 mmol/mol for *G. bulloides* and *U. mediterranea*, respectively; over standard deviations of the averages Mn/Ca values). Also Al/Ca ratios, which are considered as potentially indicators of the presence of unremoved silicates, with values above 2σ were removed (0.64 and 0.37 mmol/mol for *G. bulloides* and *U. mediterranea*, respectively; over standard deviations of the averages Al/Ca values). Then, since any clear covariance with Mg/Ca ratios exist, all values bellow 2σ have been accepted as a good result. Mg/Ca ratios from *G. bulloides* were converted to SST by applying the calibration from Cisneros et al. (2016). Since this calibration was performed on non-reductive cleaned samples, our obtained Mg/Ca ratios with the reductive cleaning procedure were increased by 12% before to the calibration. This percentage considers the Mg calcite dissolution that introduces the reductive cleaning step (Barker et al., 2003; Rosenthal et al., 2004). Mg/Ca ratios from *U. mediterranea* were converted to DWT by applying the calibration from Lear et al. (2002).

5.2.4 Stable oxygen isotopes measurements

Between 8-12 specimens of planktic foraminifera species *G. bulloides* were handpicked from the 250-315 μm fraction and between 3 and 8 specimens of benthic foraminifera species *Uvigerina mediterranea* from the >212 μm fraction, for stable oxygen isotopic measurements ($\delta^{18}O$).

Samples were mechanically cleaned with methanol to remove any attached clay minerals, ultrasonicated for 30 seconds and dried out under a laminar flood hood. The analyses were conducted using a Finnigan MAT 252 mass spectrometer in the Centre Científic i Tecnològic de la Universitat de Barcelona (CCiT-UB), whose analytical precision for $\delta^{18}O$ is better than 0.08‰. Calibration to Vienna Pee Dee Belemnite (VPDB) was carried out following NBS-19 standards (Coplen, 1996).

5.2.5 Sea water oxygen isotopic composition

Sea water $\delta^{18}O$ ($\delta^{18}O_{sw}$) of both *U. mediterranea* and *G. bulloides* was calculated after removing the temperature effect, according to Mg/Ca-temperatures obtained for each foraminifera species. The effect that environmental temperature has in the foraminifera carbonate $\delta^{18}O$ was conducted in base to the Mg/Ca-temperature estimates and applying the equation from Shackleton (1974) in both planktic and benthic records. Results were transferred to SMOW (Standard Mean Ocean Water) using the correction of Craig (1965). Finally, to obtain the $\delta^{18}O_{sw}$ records that could reflect changes in the regional evaporation-precipitation balance, i. e., local salinity changes, the global-glacioeustatic effect was extracted using the sea level reconstructions from Lambeck et al.(2014).

5.2.6 Sedimentological measurements

Grain-size analyses of NDT-6-2016 sediment core were performed with a Coulter LS 230, which determines the volume percentage of particles with grain-sizes between 0.04 and 2000 μm (McCave et al., 1986; Agrawalet al., 1991). Grain-size measurements were performed on the terrigenous fraction (non-carbonate), after having removed both organic matter and carbonate fraction using H_2O_2 and HCl respectively. Since it does not include the biological production that mainly occurs in surface, it is considered the fraction that represents better the intensity of bottom currents (McCave et al., 1995). Grain size distribution is presented using the silt/clay (laser) ratios which is commonly interpreted as deep paleocurrent intensities (Frigola et al., 2008; Hall & McCave, 2000).

5.2.7 Bulk sediment geochemistry

The analysis of the elemental geochemical composition of core NDT-6-2016 was performed on u-channels sections, with a 10×10 mm slit size, and at 1 cm resolution by means of an Avaatech XRF core-scanner at the CORELAB of the Universitat de Barcelona. Excitation conditions were established as follow: a) at 10kV, 0.5 mA, 10 s with no filter for major elements (Al, Si, S, K, Ca, Ti, Mn and Fe); b) 30 kV, 1 mA, 30 s and Pd-thick filter for heavier elements (mainly Br, Rb, Sr and Zr) and c) 50 kV, 1 mA, 40 s and a Cu filter for Ba. Previous to analysis, u-channels were imaged with a high-resolution line scan camera and covered with a 4 µm SPEXCerti Ultralene foil, which prevents dehydration of the sediment and avoids contamination of the measurement prism.

5.3 RESULTS

5.3.1 Surface and deep temperature records

Mg/Ca-DWT records from benthic foraminifera *Uvigerina* ssp. present a relatively high variability from the YD to the post-S1 (Fig 2c). The lowest DWT were recorded during the YD (average of 11.32°C), while the warmest corresponded to the post-S1 (average of 15.5°C). The pre-S1 and the S1 were characterized by intermediate DWT in comparison with the YD and the post-S1 (average of 13.25°C) (Fig. 2c). Mg/Ca-SST records from planktic foraminifera *G. bulloides* show the lowest values during the YD and the post-S1 (Fig. 2d). During the onset of the S1 the warmest SST of the studied interval were recorded, showing a clear decreasing trend all over the period (Fig. 2d).

5.3.2 Oxygen isotopic records ($\delta^{18}O$ and $\delta^{18}Osw$)

Oxygen isotopic records ($\delta^{18}O$) from both planktic foraminifera *G. bulloides* and benthic *U. mediterranea* show a general transition from heavier to lighter isotopic values during the last ~15 kyr cal. BP (Fig. 2a, b). During the YD predominated the heaviest values in both planktic and benthic $\delta^{18}O$ records (~2.5‰ for *G. bulloides* and ~3.5 for *U. mediterranea*) and both of them show a progressive lightening along the Early Holocene (Fig. 2 a, b). During the ES1 (from ~8 to

~7.5 kyr cal. BP) took place a remarkable enrichment (~1‰) in both *G. bulloides* and *U. mediterranea* $\delta^{18}O$ records. Along the post-ES1 (from 7.2 to 6.5 kyr cal. BP) both benthic and planktic foraminifera show a significant depletion (~1‰).

The $\delta^{18}O_{sw}$ records from *G. bulloides*, interpreted as indicators of local surface salinity ($\delta^{18}O_{ssw}$), show a general decreasing or freshening trend from the YD to the of the post-S1. A relative salinity minimum is observed during the YD and the S1a, while a relative maximum salinity occurred during the S1b (Fig. 2f). $\delta^{18}O_{sw}$ records from *U. mediterranea,* interpreted as indicators of deep-water salinity ($\delta^{18}O_{dsw}$), show the highest values before and after the S1, but in this case also during the S1b, while the lowest $\delta^{18}O_{sw}$ values are recorded during the S1a (Fig. 2e).

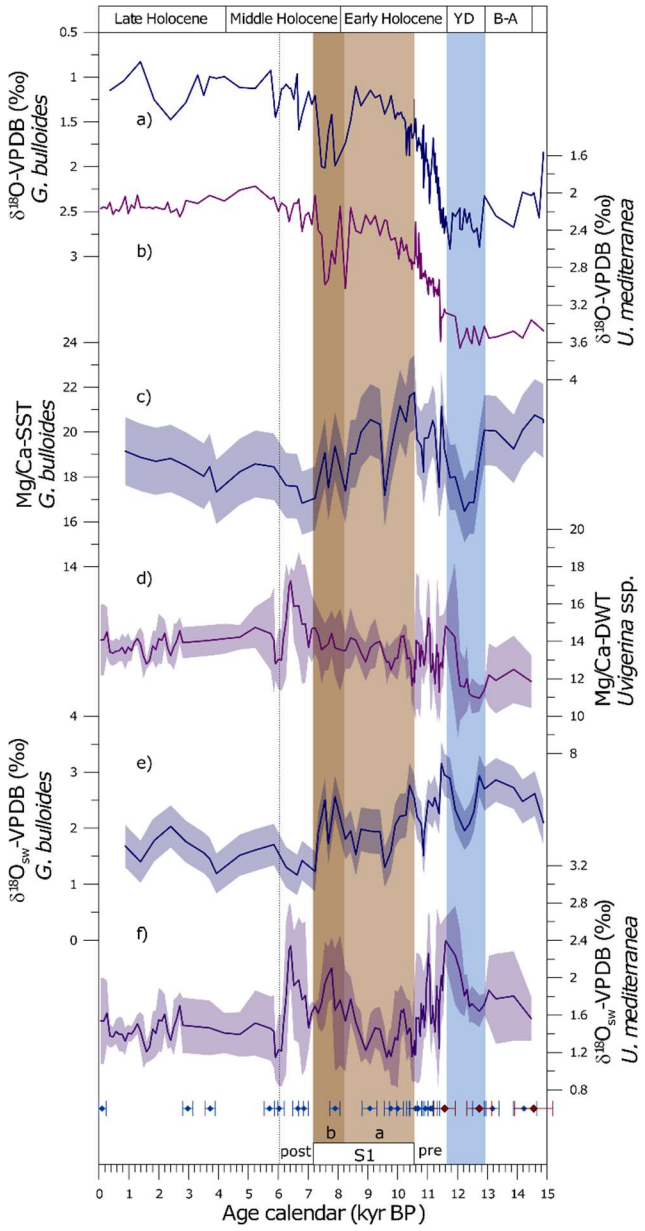

Fig. 2. Records of sediment core NDT-6-2016. From top to base; a) stable oxygen isotopes from *G. bulloides*, b) stable oxygen isotopes from *U. mediterranea*, c) Mg/Ca records from *G. bulloides*, d) Mg/Ca records from *U. mediterranea,* e) stable oxygen isotopes of sea water from *G. bulloides*, f) stable oxygen isotopes of sea water from *U. mediterranea.* Blue rhombs represent ^{14}C calibrated dates and red rhombs represent tie points. Blue bar represents YD, brown bar the ES1 and green bar the post-ES1.

5.3.3 Sedimentological and geochemmical records

Grain size distribution is presented using the silt/clay ratios, which are commonly interpreted as deep paleocurrent intensities (Frigola et al., 2008; Hall & McCave, 2000). Before the S1, silt/clay values were relatively high with the occurrence of a relative minimum associated to the YD. At the S1 onset a sharp decrease in silt/clay values occurred reaching a relative minimum and progressively rising to reach maximum values right after the S1b. After that, silt/clay values progressively reduced reaching minimum values during the late Holocene. In general terms, Si/Al records commonly interpreted as indicators of detrital contribution, are in good agreement with silt/clay profiles and only differ during the S1. During this period, Si/Al showed minimum values while silt/clay progressively increased, suggesting that detrital material supply by currents were different during this period at current location.

5.4 DISCUSSION

5.4.1 Surface and deep paleotemperatures of the Mediterranenan Sea

During the deglacial-Holocene period, the Mg/Ca SST records from W-Sicily are well coupled with those of the Balearic and Alboran Sea (Fig. 3b and c), likely reflecting the regional value of the Mg/Ca SST signal over the W-Med. However, while the YD was characterized by a significant SST decrease at W-Sicily and to a lesser extent in the Balearic Sea, this cooling is very slightly in the Alboran Sea. Instead, a cold/arid phase associated with the YD is clearly observed in planktic foraminifera assemblages from the Strait of Sicily (Sprovieri et al., 2003) as well as the Adriatic Sea (Siani et al., 2010) and also in the Aegean Sea pollen records (Dormoy et al., 2009; Kotthoff et al., 2008). We hypothesize that this data likely reflects the eastward amplification of the cold YD signal in the Med-Sea.

In the deep basin the YD is also characterized by cold water temperatures (Fig. 2d), that probably respond to the arrival of EMSW at W-Sicily. Cold and arid conditions detected in the Aegean Sea (Dormoy et al., 2009; Kotthoff et al., 2011) could have favored the formation of colder EMSW that reached the studied location. This hypothesis agrees with the previously described enhanced

flow of the EMSW into the W-Med exiting through the Strait of Sicily during the YD (Trias-Navarro, in revision). This situation changed at the end of the YD with a significant increment of DWT, coinciding with the earlier warming in the Mediterranean region (Cacho et al., 2001; Walker, 1995).

The general warming detected at W-Sicily as well as Balearic and Alboran Sea sites from the end of the YD was interrupted with a general cooling phase along the S1 (Fig. 2c, d). This cooling could be associated with the seasonality increase detected at W-Sicily during the S1. This period was characterized by colder winters and warm summers as high abundances of *G. inflata* and *G. ruber* suggest (Fig. 4f, g) (Trias-Navarro et al., 2021). Then, SST recorded by *G. bulloides* probably reflected colder surface-water spring conditions (Català et al., 2019). During the S1, the outflow of EMSW into the W-Med was significantly reduced. As a result, EMSW were likely replaced by WMDW at W-Sicily during that period (Trias-Navarro et al., in revision). Then, relatively warm and stable DWT at the studied site in comparison with the colder DWT recorded during the YD, might reflect the predominant warm and stable climatic conditions in the W-Med area (Cacho et al., 2002), that favored the formation of relatively warm WMDW. Since at present-day EMSW are warmer than the WMDW (Garcia-Sosona et al., 2020), a significant increment of the DWT during the post S1, probably reflected the exit of EMSW through the Strait of Sicily, suggesting the end of the prevailing stagnant conditions in the E-Med.

5.4.2 Comparison of surface stable oxygen isotopes records from western Mediterranean Sea

The $\delta^{18}O$ evolution from planktic foraminifera species *G. bulloides* observed at W-Sicily (Fig. 1b) is consistent with the global warming and ice sheet melting associated with the last deglaciation (Cacho et al., 2001; Frigola et al., 2008; Rohling et al., 1998). Here, we now compare our $\delta^{18}O$ records with previously published records from the Alboran Sea (Cacho et al., 2002; Català et al., 2019) and Balearic Sea (Català et al., 2019; Frigola et al., 2007) to obtain a regional view of the surface hydrographic evolution all over the W-Med (Fig. 2). In general terms, $\delta^{18}O$ records from both W-Sicily and Balearic Sea present heavier values than those from the Alboran Sea (Fig. 3a). This situation is reconcilable with the regional hydrology of the Mediterranean Sea,

since Atlantic waters enter at surface into the Mediterranean Sea through the Strait of Gibraltar flowing eastwards and increase its salinity as a result of intense evaporation and by mixing with the underlying LIW (Lacombe et al., 1981; Millot, 1999; Pinardi & Masetti, 2000; Skliris, 2014). This is supported by $\delta^{18}O_{ssw}$ estimates (Fig. 3d), which should better reflect the regional salinity, showing heavier values in both the W-Sicily and Balearic Sea in comparison with those recorded in the Alboran Sea (Fig. 3d).

During the S1, a general $\delta^{18}O_{sw}$ depletion observed at surface in the W-Sicily as well as in both Balearic and Alboran Sea, suggests that a gradual surface-water freshening occurred all over the W-Med (Fig. 3d). This situation might have promoted by the increase of cold and fresh atlantic waters flow entering in the W-Med through the Strait of Gibraltar(Lambeck & Chappell, 2001; Rogerson et al., 2008; Rohling & De Rijk, 1999), which likely resulted in a global salinity decrease (Melki et al., 2009; Rogerson et al., 2006). But also, the predominant humid conditions in the north Africa during the S1 (Bastian et al., 2017; Shanahan et al., 2015), could have promoted less evaporation and increasing fresh water supply, favoring a salinity decrease at current location.

The $\delta^{18}O$ decoupling observed between the W-Sicily and the Balearic Sea at 9 kyr BP (Fig 3a), might indicate an important reconfiguration of the surface hydrology in the W-Med. The reduced surface-water exchange between the E-Med and the W-Med during the S1 (Trias-Navarro et al., 2021), probably ended in a lesser MAW flowing eastwards. As a consequence, MAW mainly could have headed northwards reducing its influence in the W-Sicily (Fig. 6). The convergence in the $\delta^{18}O$ records from both the W-Sicily and Balearic Sea during the post-S1 (Fig. 3a and 3b), suggests the return to similar conditions which prevailed during the pre-S1, or in other words, the reactivation of the surface-water W-E connectivity.

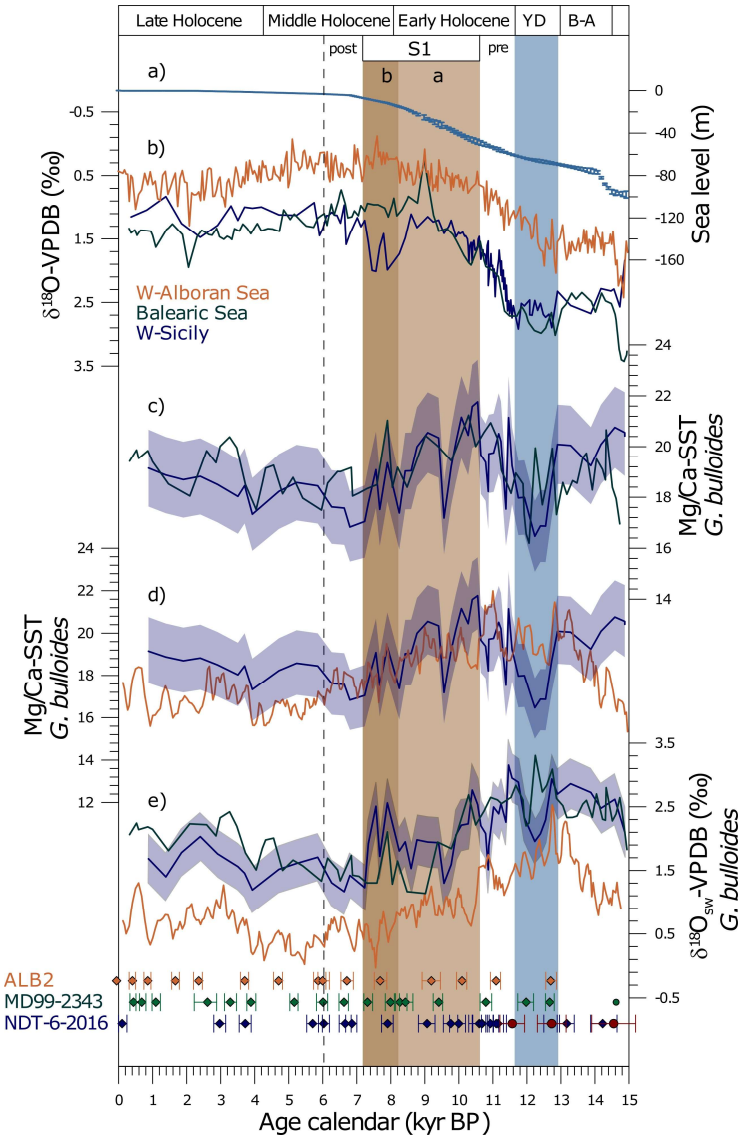

Fig. 3. Comparison of $\delta^{18}O$ (VPDB) records and their ^{14}C calibrated dates from the western Mediterranean Sea along the last 15 cal. kyr BP. a) Sea level (Lambeck et al., 2014), b) and c) Mg/Ca-Temperatures from *G. bulloides*, d) $\delta^{18}O_{sw}$ from *G. bulloides*. ^{14}C calibrated dates with the available errors from each record shown above. Each date is colored with the same color as the record excluding the red dots which represents the tie-points.

5.4.3 W-Med deep hydrology during deglacial-Holocene

Deep-water $\delta^{18}O_{sw}$ ($\delta^{18}O_{dsw}$) oscillations observed at W-Sicily probably respond to changes in the relative contribution of EMSWs and WMDW. Since EMSW is higher-salinity than WMDW (Lascaratos et al., 1993; Millot et al., 2006; Skliris, 2014), the predominating higher $\delta^{18}O_{dsw}$ values detected during the YD and the pre-S1 at current location would suggest major contribution

of the EMSW (Fig. 4a and 5). This hypothesis is in agreement with previous studies from Trias-Navarro et al. (in revision) based on neodymium isotopes records, that show relatively high εNd values during the YD, interpreted as an enhanced export of EMSW into the W-Med (Fig. 4b).

The enhanced westward outflow of EMSWs through the Strait of Sicily during the YD must have occurred necessarily by increased velocity in intermediate-deep water transport, given the more restricted section area in the Strait during a generally lower global sea-level time period (Grant et al., 2014). If that is the case, then we should expect an increase in the deep-current intensities. However, our records of Silt/Clay, commonly interpreted as proxies for paleo-currents intensities, show a relative minimum during the YD (Fig. 2c), apparently questioning our previous interpretation of enhanced EMSW outflow during this period.

Interestingly, such minimum in the grain-size (Silt/Clay) measurements during the YD at our site, is in direct contrast with the maximum values in grain-size reported from a shallower (501 m) and distal core located at the eastern flank of Corsica (Fig. 4f; Toucanne et al., 2015) and even further in the Alboran Sea (914 mwd) (Alonso et al., 2021). These grain size records suggest an increase in the current velocities at intermediate depths in the Western Mediterranean Sea. Thus, the lack of a relative maximum in the Silt/Clay record (Fig. 4c) from the W-Sicily would likely be explained by the fact that the depth of the main core of the outflowing EMSWs would be located at a shallower depth than the study site (1066 m).

During the S1a, the relatively low $\delta^{18}O_{dsw}$ values detected in the W-Sicily agree with lower ε_{Nd} values recorded at the same location (Fig. 4a, b and Fig. 5) (Trias-Navarro et al., submitted), both records suggesting an important decrease of the EMSW contribution at W-Sicily. This reduced westward flow of EMSW through the Sicily channel over the S1 would be further accompanied by a major reduction in detrital contribution at W-Sicily (Si/Al, Fig. 4d). In addition, it would also be coexistent with a rapid and intense reduction in the sediment rates (Fig. 2e) and a weakening of the deep-sea currents in the area at the onset of the S1a (low Silt/Clay in Fig. 2c). Since detrital particles arrived to W-Sicily transported within the EMSW (Trias-Navarro et al., 2021), it is very likely that a strong reduction in the EMSW contribution would have resulted in a large decrease

in the arrival of these particles, which consequently would get reflected in a large reduction of sedimentation rates. All these indicators are consistent with a reduced westward outflow of EMSW arriving to the W-Sicily, supporting the proposed S1 formation mechanisms linked to a major weakening of deep and intermediate overturning in the E-Med (Grimm et al., 2015; Rohling et al., 2015).

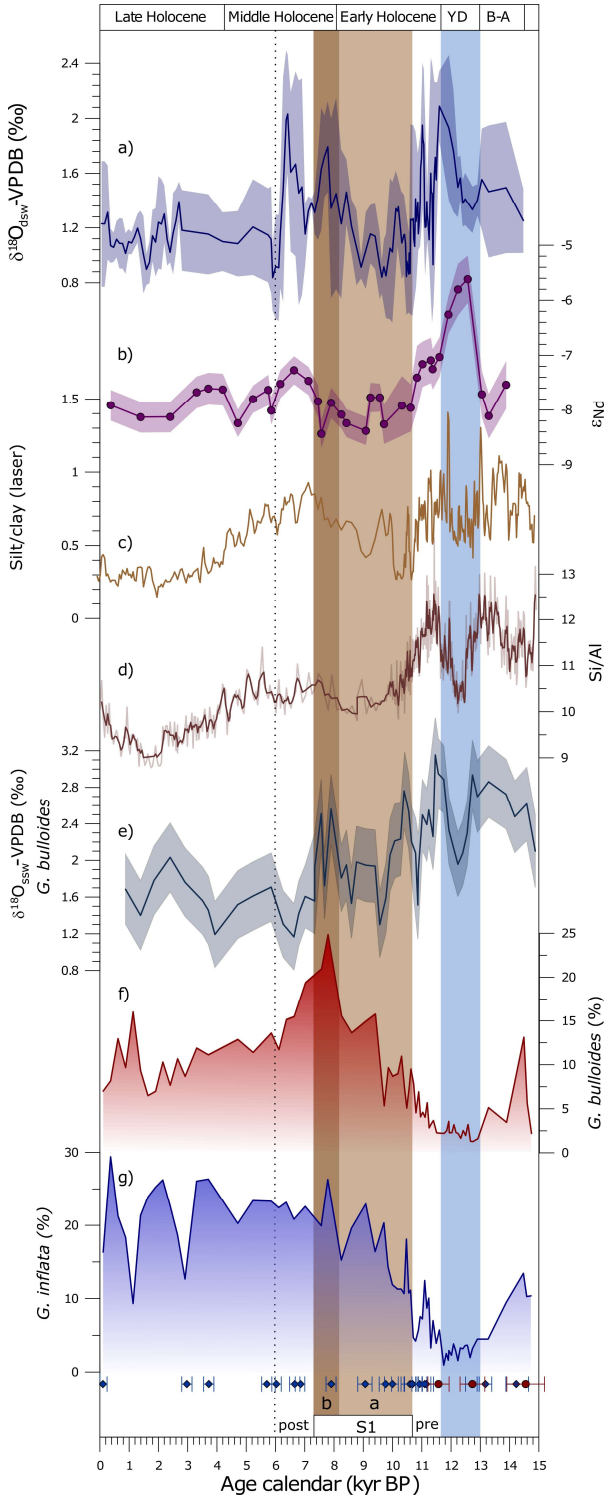

Fig. 4. Comparison of NDT-6-2016 proxies. From top to base; a) with blue line stable oxygen isotopic records of sea water from *U. mediterranea,* b) with violet line neodymium isotopes records c) with yellow-brownish line sortable silt records d) with red-brown line Si/Al ratios, e) with grey-blue line stable oxygen isotopic records of sea water from *G. bulloides*. Planktic foraminifera abundances of f) *G. ruber* and g) *G. inflata*. Blue rhombs represent ^{14}C calibrated dates and red rhombs represent tie points. Blue bar represents YD, brown bar the ES1 and green bar the post-ES1.

However, during the S1b, a significant $\delta^{18}O_{dsw}$ enrichment occurred at W-Sicily, while relatively low ε_{Nd} values still predominated (Fig. 4a and b) (Trias-Navarro et al., in revision). Therefore, although the S1b was characterized by lower contribution of the EMSW at the studied site as ε_{Nd} signature suggest (Trias-Navarro et al., in preparation), the higher $\delta^{18}O_{dsw}$ values might indicate the arrival of higher salinity western originated water-mass replacing the WMDW (Fig. 4 a, b). Furthermore, $\delta^{18}O_{dsw}$ increase is coexistent with a surface $\delta^{18}O_{sw}$ ($\delta^{18}O_{ssw}$) enrichment at the studied site, suggesting a narrow connection between surface and deep hydrology (Fig. 4a and e).

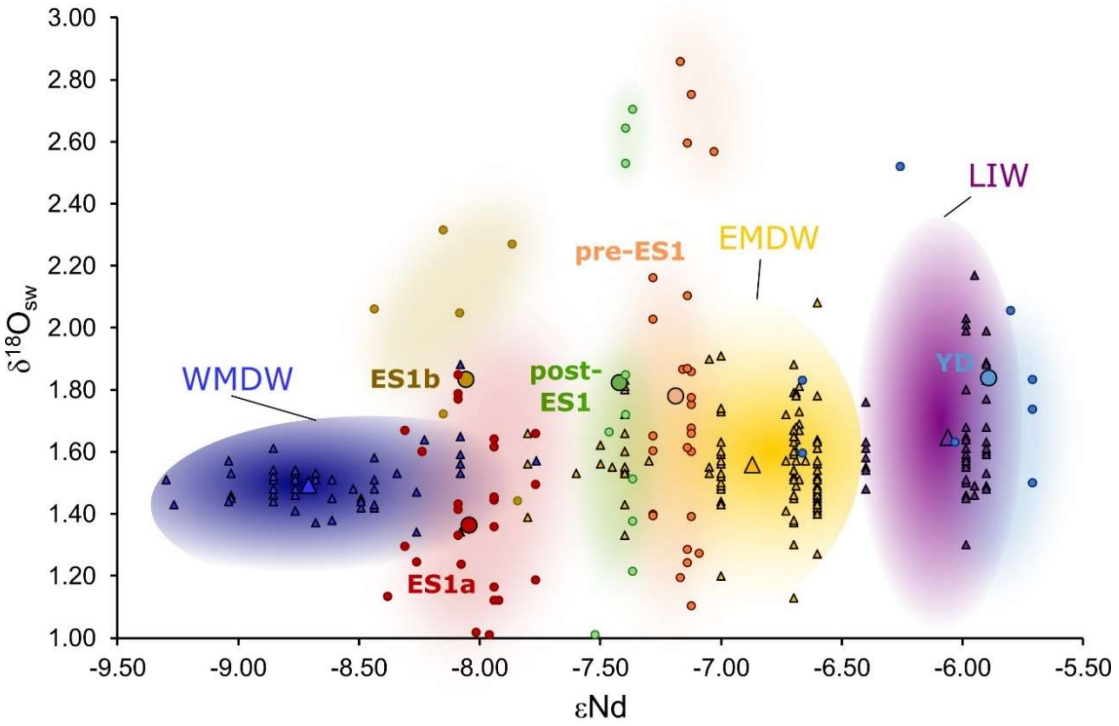

Fig. 5. Comparison between ε_{Nd} values and *U. mediterranea* $\delta^{18}O_{sw}$ values from sediment core NDT-6-2016 (this study) for the YD, pre-S1, S1a, S1b and post-S1 periods, represented by blue, orange, red, brown and green circles, respectively). Present-day ε_{Nd} (Tachikawa et al., 2004; Gracia-Solsona et al, 2020; Vance et al., 2004) and $\delta^{18}O_{sw}$ values for WMDW, LIW and EMDW (Gat et al., 1996; Pierre 1999; Stenni et al. 1995), represented by blue,yellow and violet triangles respectively.

Thus, this data might indicate that colder and dry surface conditions developed during winter at W-Sicily (Trias-Navarro et al., 2021), likely occurred over the Tyrrhenian Sea area, favoring the formation of higher-salinity intermediate-water mass. During the post-S1, the increase in both $\delta^{18}O_{dsw}$ and ε_{Nd} values might indicate the arrival of EMSW at W-Sicily, suggesting the end of the stagnant conditions which predominated in the eastern basin along the S1 (Trias-Navarro, submitted).

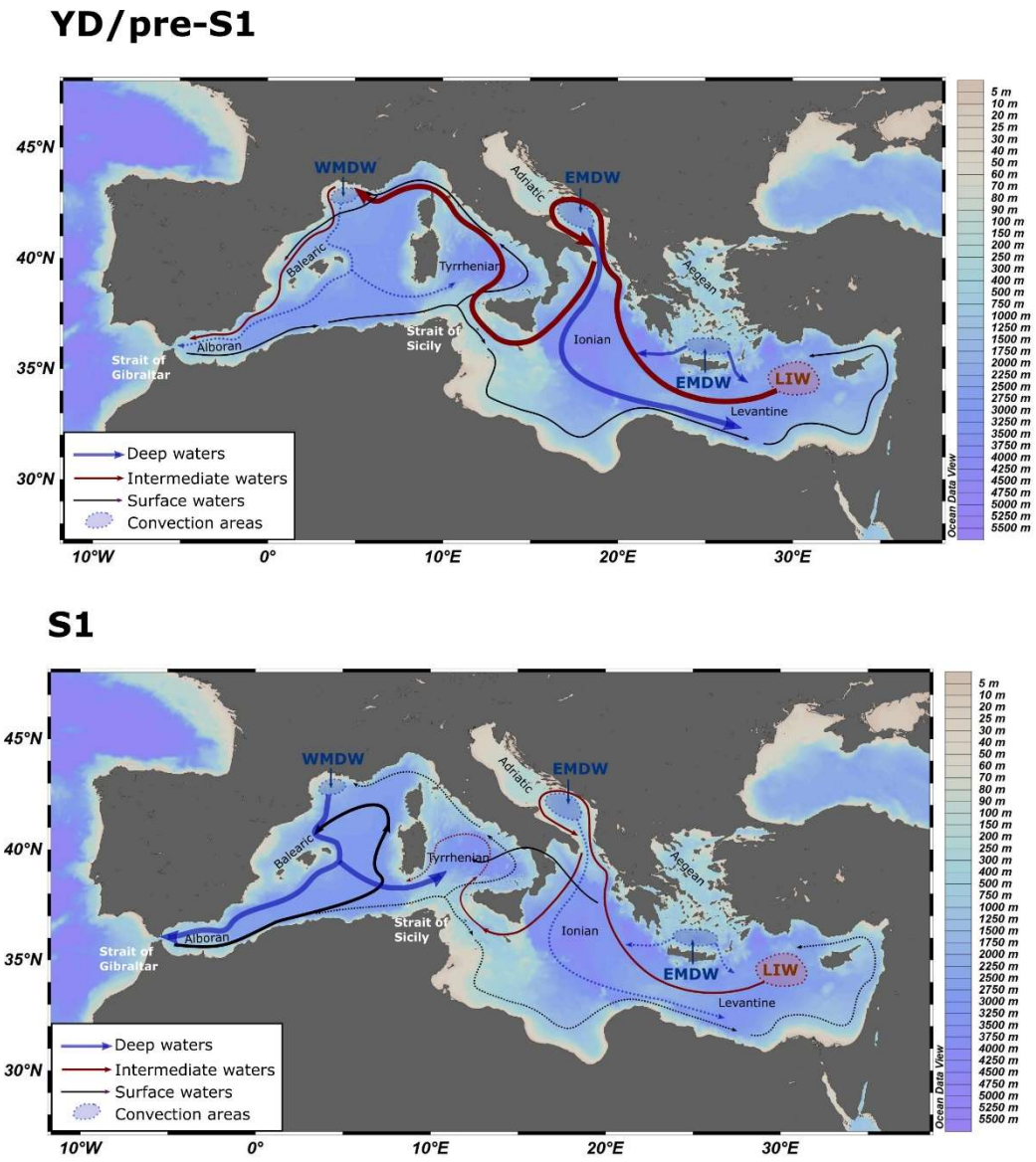

Figure. 6. Schematic map representing the predominant Med-THC during both the YD and the S1. Black arrows represent the Modified Atlantic waters (MAW), blue arrows deep-water and red arrows intermediate water (LIW).

5.5 CONCLUSIONS

The new generated data allow to distinguish important changes in the surface and deep hydrology of the Mediterranean Sea during the last deglacial and Holocene periods. A general surface freshening all over the Mediterranean Sea occurred from the YD to the end of the S1. This situation was likely promoted by the combined effect of 1) an increase of the sea level produced by the north Atlantic ice-melting and 2) enhanced fresh water supply together with less evaporation associated with humid prevailing conditions during the S1.

Although during the YD and the pre-S1 an enhanced surface and deep water interconnection between the E- and the W-Med prevailed, at the onset of the S1, EMSW reduced considerably its contribution in the W-Med. As a result, the WMDW replaced the EMSW occupying intermediate depths at W-Sicily. The limited exit of EMSW through the Strait of Sicily might have ended in reduced MAW flowing eastwards. As a consequence, MAW could mainly have headed northwards reducing its influence at W-Sicily. This particularly situation promoted an extreme seasonality in the current location with colder winters, that would have favored the formation of a higher salinity intermediate-water, likely produced in the Tyrrhenian Sea area. At ~7 kyr BP the higher salinity EMSW outflowed from the Strait of Sicily likely indicating the end of the prevailing stagnant conditions in the E-Med.

5.6 BIBLIOGRAPHY

Alonso, B., Juan, C., Ercilla, G., Cacho, I., López-González, N., Rodríquez-Tovar, F. J., Dorador, J., Francés, G., Casas, D., Vandorpe, T., & Vázquez, J. T. (2021). Paleoceanographic and paleoclimatic variability in the Western Mediterranean during the last 25 cal. kyr BP. New insights from contourite drifts. *Marine Geology*, *437*. https://doi.org/10.1016/j.margeo.2021.106488

Blaauw, M., & Christeny, J. A. (2011). Flexible paleoclimate age-depth models using an autoregressive gamma process. *Bayesian Analysis*, *6*(3), 457–474. https://doi.org/10.1214/11-BA618

Cacho, I., Grimalt, J. O., & Canals, M. (2002). Response of the Western Mediterranean Sea to rapid climatic variability during the last 50,000 years: A molecular biomarker approach. *Journal of Marine Systems*, *33–34*, 253–272. https://doi.org/10.1016/S0924-7963(02)00061-1

Cacho, I., Grimalt, J. O., Canals, M., Sbaffi, L., Shackleton, N., Schönfeld, J., & Zahn, R. (2001). Variability of the western Mediterranean Sea surface temperature during the last 25,000 years and its connection with the northern hemisphere climatic changes. *Climatic Changes*, *16*(1), 40–52. https://doi.org/10.1029/sp010

Català, A., Cacho, I., Frigola, J., Pena, L. D., & Lirer, F. (2019). Holocene hydrography evolution in the Alboran Sea: A multi-record and multi-proxy comparison. *Climate of the Past*, *15*(3), 927–942. https://doi.org/10.5194/cp-15-927-2019

Checa, H., Margaritelli, G., Pena, L. D., Frigola, J., Cacho, I., Rettori, R., & Lirer, F. (2020). High resolution paleo-environmental changes during the Sapropel 1 in the North Ionian Sea, central Mediterranean. *Holocene*. https://doi.org/10.1177/0959683620941095

De Lange, G. J., Thomson, J., Reitz, A., Slomp, C. P., Speranza Principato, M., Erba, E., & Corselli, C. (2008). Synchronous basin-wide formation and redox-controlled preservation of a Mediterranean sapropel. *Nature Geoscience*, *1*(9), 606–610.

https://doi.org/10.1038/ngeo283

DeMenocal, P., Ortiz, J., Guilderson, T., Adkins, J., Sarnthein, M., Baker, L., & Yarusinsky, M. (2000). *Abrupt onset and termination of the African Humid Period : rapid climate responses to gradual insolation forcing*. *19*.

Dormoy, I., Peyron, O., Nebout, N. C., Goring, S., Kotthoff, U., Magny, M., & Pross, J. (2009). Terrestrial climate variability and seasonality changes in the Mediterranean region between 15000 and 4000 years BP deduced from marine pollen records. *Climate of the Past*, *5*(4), 615–632. https://doi.org/10.5194/cp-5-615-2009

Emeis, K. C., Struck, U., Schulz, H. M., Rosenberg, R., Bernasconi, S., Erlenkeuser, H., Sakamoto, T., & Martinez-Ruiz, F. (2000). Temperature and salinity variations of Mediterranean Sea surface waters over the last 16,000 years from records of planktonic stable oxygen isotopes and alkenone unsaturation ratios. *Palaeogeography, Palaeoclimatology, Palaeoecology*, *158*(3–4), 259–280. https://doi.org/10.1016/S0031-0182(00)00053-5

Filippidi, A., Triantaphyllou, M. V., & De Lange, G. J. (2016). Eastern-Mediterranean ventilation variability during sapropel S1 formation, evaluated at two sites influenced by deep-water formation from Adriatic and Aegean Seas. *Quaternary Science Reviews*, *144*, 95–106. https://doi.org/10.1016/j.quascirev.2016.05.024

French, B. C., Hunt, C. O., & Grima, R. (2020). Temple landscapes Fragility , change and resilience of Holocene environments in the Maltese Islands Temple landscapes. In *Temple landscapes Fragility , change and resilience of Holocene environments in the Maltese Islands Temple landscapes* (Vol. 1, Issue November). https://doi.org/10.17863/CAM.59608

Frigola, J., Moreno, A., Cacho, I., Canals, M., Sierro, F. J., Flores, J. A., & Grimalt, J. O. (2008). Evidence of abrupt changes in Western Mediterranean Deep Water circulation during the last 50 kyr: A high-resolution marine record from the Balearic Sea. *Quaternary*

International, *181*(1), 88–104. https://doi.org/10.1016/j.quaint.2007.06.016

Frigola, J., Moreno, A., Cacho, I., Canals, M., Sierro, F. J., Flores, J. A., Grimalt, J. O., Hodell, D. A., & Curtis, J. H. (2007). Holocene climate variability in the western Mediterranean region from a deepwater sediment record. *Paleoceanography*, *22*(2), 1–16. https://doi.org/10.1029/2006PA001307

Gacic, M., Manca, B. B., & Mantziafou, A. (2001). Physical Oceanography of the Adriatic Sea. In *Physical Oceanography of the Adriatic Sea* (Issue February 2019). https://doi.org/10.1007/978-94-015-9819-4

Gat, R., & Tziperman, E. (1996). The stable isotope composition of waters of the eastern Mediterranean Sea. *Journal of Geophysical Research*, 101(95), 6441–6451.

Grant, K. M., Rohling, E. J., Bronk Ramsey, C., Cheng, H., Edwards, R. L., Florindo, F., Heslop, D., Marra, F., Roberts, A. P., Tamisiea, M. E., & Williams, F. (2014). Sea-level variability over five glacial cycles. *Nature Communications*, *5*. https://doi.org/10.1038/ncomms6076

Grimm, R., Maier-reimer, E., Mikolajewicz, U., Schmiedl, G., Mu, K., Adloff, F., Grant, K. M., Ziegler, M., Lourens, L. J., & Emeis, K. (2015). *Late glacial initiation of Holocene eastern Mediterranean sapropel formation*. https://doi.org/10.1038/ncomms8099

Hunt, C. O., Farrell, M., Fenech, K., French, C., McLaughlin, R., Blaauw, M., Bennett, J., et al. (2020). *Chronology and stratigraphy of the valley systems.* McDonald Institute for Archaeological Research, *Temple landscapes Fragility, change and resilience of Holocene environments in the Maltese Islands*. [Book chapter]. https://doi.org/10.17863/CAM.59608

Incarbona, A., Abu-Zied, R. H., Rohling, E. J., & Ziveri, P. (2019). *Reventilation Episodes During the Sapropel S1 Deposition in the Eastern Mediterranean Based on Holococcolith Preservation Paleoceanography and Paleoclimatology*. 1–13. https://doi.org/10.1029/2019PA003626

Kotthoff, U., Koutsodendris, A., Pross, J., Schmiedl, G., Bornemann, A., Kaul, C., Marino, G.,

Peyron, O., & Schiebel, R. (2011). Impact of Lateglacial cold events on the northern Aegean region reconstructed from marine and terrestrial proxy data. *Journal of Quaternary Science*, *26*(1), 86–96. https://doi.org/10.1002/jqs.1430

Lacombe, H., Gascard, J. C., Cornella, J., & Béthoux, J. P. (1981). Response of the Mediterranean to the water and energy fluxes across its surface, on seasonal and interannual scales. *Oceanologica Acta*, *4*(2), 247–255.

Lambeck, K., & Chappell, J. (2001). *Sea Level Change Through the Last Glacial Cycle*. *292*(April), 679–687.

Lascaratos, A., Williams, R. G., & Tragou, E. (1993). A mixed-layer study of the formation of Levantine Intermediate Water. *Journal of Geophysical Research*, *98*(C8). https://doi.org/10.1029/93jc00912

Lermusiaux, P. F. J., & Robinson, A. R. (2001). Features of dominant mesoscale variability, circulation patterns and dynamics in the strait of sicily. *Deep-Sea Research Part I: Oceanographic Research Papers*, *48*(9), 1953–1997. https://doi.org/10.1016/S0967-0637(00)00114-X

Lionello, P. (2012). *The Climate of the Mediterranean Region: From the Past to the Future* (1st ed.). Elsevier Inc.

Martinez-Ruiz, F., Kastner, M., Gallego-Torres, D., Rodrigo-Gámiz, M., Nieto-Moreno, V., & Ortega-Huertas, M. (2015). Paleoclimate and paleoceanography over the past 20,000yr in the Mediterranean Sea Basins as indicated by sediment elemental proxies. *Quaternary Science Reviews*, *107*, 25–46. https://doi.org/10.1016/j.quascirev.2014.09.018

Melki, T., Kallel, N., Jorissen, F. J., Guichard, F., Dennielou, B., Berné, S., Labeyrie, L., & Fontugne, M. (2009). Abrupt climate change, sea surface salinity and paleoproductivity in the western Mediterranean Sea (Gulf of Lion) during the last 28 kyr. *Palaeogeography, Palaeoclimatology, Palaeoecology*, *279*(1–2), 96–113. https://doi.org/10.1016/j.palaeo.2009.05.005

Ménot, G., Pivot, S., Bouloubassi, I., Davtian, N., Hennekam, R., Bosch, D., Ducassou, E., Bard, E., Migeon, S., & Revel, M. (2020). Timing and stepwise transitions of the African Humid Period from geochemical proxies in the Nile deep-sea fan sediments. *Quaternary Science Reviews*, *228*. https://doi.org/10.1016/j.quascirev.2019.106071

Millot, C. (1987). Circulation in the Hydrodynamics General circulation Mediterranean Sea Mesoscale phenomena. *Oceanologica Acta*, *10*(2), 143–149.

Millot, C. (1999). Circulation in the Western Mediterranean Sea. *Journal of Marine Systems*, *20*(1–4), 423–442. https://doi.org/10.1016/S0924-7963(98)00078-5

Millot, C. (2009). Another description of the Mediterranean Sea outflow. *Progress in Oceanography*, *82*(2), 101–124. https://doi.org/10.1016/j.pocean.2009.04.016

Millot, C., Candela, J., Fuda, J. L., & Tber, Y. (2006). Large warming and salinification of the Mediterranean outflow due to changes in its composition. *Deep-Sea Research Part I: Oceanographic Research Papers*, *53*(4), 656–666. https://doi.org/10.1016/j.dsr.2005.12.017

Pérez-Asensio, J. N., Frigola, J., Pena, L. D., Sierro, F. J., Reguera, M. I., Rodríguez-Tovar, F. J., Dorador, J., Asioli, A., Kuhlmann, J., Huhn, K., & Cacho, I. (2020). Changes in western Mediterranean thermohaline circulation in association with a deglacial Organic Rich Layer formation in the Alboran Sea. *Quaternary Science Reviews*, *228*. https://doi.org/10.1016/j.quascirev.2019.106075

Pierre, C. (1999). The oxygen and carbon isotope distribution in the Mediterranean water masses. *Marine Geology*, *153*(1–4), 41–55. https://doi.org/10.1016/S0025-3227(98)00090-5

Pinardi, N., & Masetti, E. (2000). Variability of the large scale general circulation of the Mediterranean Sea from observations and modelling: A review. *Palaeogeography, Palaeoclimatology, Palaeoecology*, *158*(3–4), 153–173. https://doi.org/10.1016/S0031-0182(00)00048-1

Rasmussen, S. O., Andersen, K. K., Svensson, A. M., Steffensen, J. P., Vinther, B. M., Clausen,

H. B., Johnsen, S. J., Larsen, L. B., Bigler, M., Ro, R., & Fischer, H. (2006). *A new Greenland ice core chronology for the last glacial termination*. *111*, 1–16. https://doi.org/10.1029/2005JD006079

Revel, M., Ducassou, E., Skonieczny, C., Colin, C., Bastian, L., Bosch, D., Migeon, S., & Mascle, J. (2015). 20,000 years of Nile River dynamics and environmental changes in the Nile catchment area as inferred from Nile upper continental slope sediments. *Quaternary Science Reviews*, *130*, 200–221. https://doi.org/10.1016/j.quascirev.2015.10.030

Rogerson, M., Cacho, I., Jimenez-Espejo, F., Reguera, M. I., Sierro, F. J., Martinez-Ruiz, F., Frigola, J., & Canals, M. (2008). A dynamic explanation for the origin of the western Mediterranean organic-rich layers. *Geochemistry, Geophysics, Geosystems*, *9*(7). https://doi.org/10.1029/2007GC001936

Rogerson, M., Rohlin, E. J., & Weaver, P. P. E. (2006). Promotion of meridional overturning by Mediterranean-derived salt during the last deglaciation. *Paleoceanography*, *21*(4), 1–8. https://doi.org/10.1029/2006PA001306

Rohling, E. J., & De Rijk, S. (1999). Holocene climate optimum and last glacial maximum in the Mediterranean: The marine oxygen isotope record. *Marine Geology*, *153*(1–4), 57–75. https://doi.org/10.1016/S0025-3227(98)00020-6

Rohling, E. J., Hayes, A., De Rijk, S., Kroon, D., Zachariasse, W. J., & Eisma, D. (1998). Abrupt cold spells in the northwest Mediterranean. *Paleoceanography*, *13*(4), 316–322. https://doi.org/10.1029/98PA00671

Shackleton, N. J. (1974). Attainment of isotopic equilibrium between ocean water and the benthonic foraminifera geuns *Uvigerina*: Isotopic changes in the ocean during the last glacial. *Colloques Internationaux Du C.N.R.S.*, *219*, 203–210.

Skliris, N. (2014). *Past , Present and Future Patterns of the Thermohaline Circulation and Characteristic Water Masses of the Mediterranean Sea*. 29–48. https://doi.org/10.1007/978-94-007-6704-1

Stenni, B., Nichetto, P., Bregant, D., Scarazzato, P., & Longinelli, A. (1995). The δ18O signal of the northward flow of Mediterranean waters in the Adriatic Sea. *Oceanologica Acta*, 18(3), 319–328

Tachikawa, K., Roy-Barman, M., Michard, A., Thouron, D., Yeghicheyan, D., & Jeandel, C. (2004). Neodymium isotopes in the Mediterranean Sea: Comparison between seawater and sediment signals. *Geochimica et Cosmochimica Acta*, 68(14), 3095–3106. https://doi.org/10.1016/j.gca.2004.01.024

Tesi, T., Asioli, A., Minisini, D., Maselli, V., Dalla Valle, G., Gamberi, F., Langone, L., Cattaneo, A., Montagna, P., & Trincardi, F. (2017). Large-scale response of the Eastern Mediterranean thermohaline circulation to African monsoon intensification during sapropel S1 formation. *Quaternary Science Reviews*, *159*, 139–154. https://doi.org/10.1016/j.quascirev.2017.01.020

Toucanne, S., Angue Minto'o, C. M., Fontanier, C., Bassetti, M. A., Jorry, S. J., & Jouet, G. (2015). Tracking rainfall in the northern Mediterranean borderlands during sapropel deposition. *Quaternary Science Reviews*, *129*, 178–195. https://doi.org/10.1016/j.quascirev.2015.10.016

Trias-Navarro, S., Cacho, I., De La Fuente, M., Pena, L. D., Frigola, J., Lirer, F., & Caruso, A. (2021). Surface hydrographic changes at the western flank of the Sicily Channel associated with the last sapropel. *Global and Planetary Change*, *204*, 103582. https://doi.org/10.1016/j.gloplacha.2021.103582

Vance, D., Scrivner, A. E., Beney, P., Staubwasser, M., Henderson, G. M., & Slowey, N. C. (2004). The use of foraminifera as a record of the past neodymium isotope composition of seawater. *Paleoceanography*, 19(2), 1–17. https://doi.org/10.1029/2003PA000957

Vinther, B. M., Clausen, H. B., Johnsen, S. J., Rasmussen, S. O., Andersen, K. K., Buchardt, S. L., Seierstad, I. K., Steffensen, J. P., Svensson, A., Olsen, J., & Heinemeier, J. (2006). *A synchronized dating of three Greenland ice cores throughout the Holocene*. *111*, 1–11.

https://doi.org/10.1029/2005JD006921

Wu, J., Liu, Z., Stuut, J. B. W., Zhao, Y., Schirone, A., & de Lange, G. J. (2017). North-African paleodrainage discharges to the central Mediterranean during the last 18,000 years: A multiproxy characterization. *Quaternary Science Reviews*, *163*(May), 95–113. https://doi.org/10.1016/j.quascirev.2017.03.015

...It appeared that there had even been demonstrations to thank Big Brother

for raising the chocolate ration to twenty grammes a week.

And only yesterday, he reflected, it had been announced

that the ration was to be reduced to twenty grammes a week.

Was it possible that they could swallow that, after only twenty-four hours?

Yes, they swallowed it.

Extracto de “1984” (George Orwell)

6 CONCLUSIONS

The new data here produced from the sediment core NDT-6-2016 located at western flank of Sicily channel at 1066 m (W-Sicily), allow to characterize both surface and deep hydrology during the late deglacial period and the Holocene (last 15 kyr). The new generated ε_{Nd} record provide for the first time quantitative information on the export rates of Eastern Mediterranean Sourced Water (ESMW) towards the western Mediterranean basin (W-Med), during the last deglacial period and the Holocene, indicating significant changes over the cold Younger Dryas (YD, 12.95-11.65 kyr BP) and the last Sapropel (S1, ~ 10.5-7 kyr BP). Furthermore, our new data from planktic foraminifera ecology and stable oxygen isotopes measured in both planktic foraminifera *Globigerina bulloides* and *Globigerinoides ruber* allow the characterization of very distinctive surface hydrographic conditions during the S1 interval (10.5-7 kyr cal. BP), as compared to the pre-S1 and post-S1. In addition, the Mg/Ca records obtained from *G. bulloides* support a seasonality increase during the S1, also evidenced by planktonic foraminifera assemblages. Moreover, Mg/Ca data from benthic foraminifera *Uvigerina* spp. represents the first record of Mediterranean paleotemperatures for the late deglacial period and the Holocene, indicating important variations along the studied period. Finally, the obtained $\delta^{18}O_{sw}$ records of surface and deep hydrology provide new information of the basin evaporation-precipitation balance and the dynamics of deep water exchange between the eastern (E-Med) and the W-Med, respectively.

During the YD, high percentages of EMSW identified at W-Sicily (57 ± 5%) would indicate an enhanced deep water interconnection between the E-Med and the W-Med. In addition, the predominating higher *U. mediterranea* $\delta^{18}O_{sw}$ ($\delta^{18}O_{dsw}$) values detected over the same period at the studied location would also suggest major contribution of the EMSW. We speculate that this situation responded to the combined effect of climate-driven enhanced convection in the Aegean and Levantine basins and a weaker western deep water formation that led to a deeper expansion of the EMSW into the W-Med. We propose that this enhanced western flow of EMSW also correspond with the previous described stronger currents at intermediate depths in the W-Med,

ceasing the stagnation at ~ 900m that had been initiated with the last ORL formation in the westernmost part of the Mediterranean Sea.

Moreover, during the YD both planktic foraminifera ecology and stable isotopic records from W-Sicily were closer to analogous records from the Sicily channel and the Alboran Sea, a situation coherent with the current oceanography at these locations, directly affected by the eastern path of the Modified Atlantic water (MAW). Then, all these indicators suggest that during the YD enhanced surface and deep interconnection between the E- and the W-Med prevailed. From the end of the YD, a general surface freshening all over the Mediterranean Sea occurred, that lasted until the end of the S1. This situation was likely promoted by the combined effect of 1) an increase of the sea level produced by the north Atlantic ice-melting and the consequent increase of the flow of Atlantic waters into the W-Med and 2) enhanced fresh water supply together with less evaporation associated with humid prevailing conditions during the S1.

The S1 is characterized in the new produced ε_{Nd} record by the minimum export rates (16 ± 6%), supporting a substantial weakening of the EMSW outflow through the Strait of Sicily. In addition, the low $\delta^{18}O_{dsw}$ values recorded during the S1a would also suggest an important decrease of the EMSW contribution at current location. This reduced westward flow of EMSW through the Sicily channel over the S1 would be further accompanied by a major reduction in detrital contribution at W-Sicily (Si/Al) and significant decrease in the sedimentation rates. Since detrital particles arrived to W-Sicily mainly transported within the EMSW, a strong reduction in the EMSW contribution would have resulted in a large decrease in the arrival of these detrital particles, which consequently would get reflected in a large reduction of sedimentation rates. Then, all these indicators support that an intermediate/deep water exchange between the two basins would have been significantly reduced during the S1.

Moreover, the described limited exit of EMSW through the Strait of Sicily might have also promoted a reduction in the surface eastward flow of MAW. As a consequence, MAW could mainly have headed northwards reducing its influence in the W-Sicily. A comparison of the obtained $\delta^{18}O$ and planktic foraminifera distribution results, with similar records from the Alboran

Sea, Balearic Sea, Tyrrhenian Sea and Strait of Sicily reveals that the S1 conditions in the studied location contrasted to those developed in the Sicily channel and also in the Alboran Sea, showing higher similarity to those of the Tyrrhenian Sea. This is an opposite situation to that developed during YD, when conditions in W-Sicily were closer to those of the Sicily channel and the Alboran Sea.

The increase in *G. inflata* and *G. ruber* at W-Sicily during the S1 interval suggest a marked seasonality with intense water winter mixing and summer stratification. These conditions of high seasonality turned more extreme during the S1b and changed progressively along the post-S1 toward lower seasonality. Consequently, we propose that during the S1 a reduced surface water interconnection between E-Med and W-Med prevailed likely driven by the E-Med stagnation. This oceanographic condition caused a weakening of the eastward flow of MAW, reducing its entrance through the Strait of Sicily and over the studied W-Sicily site. Consequently, the predominant conditions that prevailed in central-southern Europe during the S1 interval played an essential role, promoting the observed high seasonality in the W-Sicily surface hydrology. This particularly situation would have favored the formation of a higher salinity intermediate-water during the S1b, likely produced in the Tyrrhenian Sea area.

The reactivation of the interconnection between the E-Med and W-Med would have taken place around 1 kyr before the absolute end of the S1 (6.1 kyr cal. BP). Here is proposed that the exit of the EMSW through the Strait of Sicily at 7.5-7 kyr BP agrees with the earlier convection enhancement in the Adriatic and Aegean Seas, that marked the end of the stagnant conditions at intermediate depths of the E-Med, while the re-activation of the deep basin would have taken longer. This hypothesis would also have supported by higher $\delta^{18}O_{dsw}$ values recorded at this time, probably indicating the exit of higher-salinity EMSW through the Strait of Sicily.

...De todos nuestros infiernos, encendimos una hoguera,

Quemaron como el invierno al llegar la primavera

Tembló el firmamento, mientras los mares ardían,

Rugieron los vientos, en tu compañía.

Volamos hacia el infinito, como un cometa errante,

Y nos encontramos, por siempre, un instante…

De un viaje hacia el infinito

7 APPENDIX

7.1 Planktic foraminifera distribution from core NDT-6-2016 in percentage (%).

Depth	Age kyr BP	*G. bulloides*	*Globoturborotalita sp*	*G. siphonifera*	*G.glutinata*
1	-0.14	26.16	4.97	1.66	0.99
6	0.11	35.00	5.33	2.67	3.00
11	0.37	27.12	2.61	2.29	1.63
16	0.62	36.54	1.66	1.66	3.65
21	0.88	43.67	2.67	4.33	1.33
26	1.13	39.00	5.67	3.00	1.67
31	1.39	39.00	3.67	1.33	1.67
36	1.64	36.52	3.41	2.05	3.75
41	1.90	33.22	3.32	3.65	7.64
46	2.15	31.56	5.32	1.99	3.65
51	2.40	31.33	7.67	3.00	5.00
56	2.65	33.67	6.00	2.67	7.33
61	2.91	34.33	7.67	2.67	9.00
71	3.30	21.45	2.97	1.32	7.26
81	3.70	26.03	3.17	0.95	4.76
101	4.71	31.51	6.75	1.61	6.43
111	5.23	24.92	5.85	0.62	8.31
123	5.85	24.60	1.94	1.62	5.18
128	6.11	24.08	2.68	2.68	4.68
133	6.37	22.84	3.70	1.54	4.01
138	6.63	23.97	4.42	1.89	5.68
143	7.02	16.45	3.23	0.65	5.16
148	7.56	18.27	3.99	1.99	3.65
150	7.79	17.54	2.05	3.51	2.63
153	8.25	20.63	4.44	1.90	5.40
155	8.60	25.25	4.32	1.66	9.97
158	9.09	22.59	3.32	1.66	11.63
160	9.41	24.76	2.89	0.64	10.93
163	9.70	26.67	4.00	0.67	15.00
165	9.85	28.00	3.00	0.67	13.00
168	10.00	26.69	2.25	1.29	11.58
173	10.17	22.59	4.32	0.00	22.26
178	10.30	22.92	2.99	0.00	17.94
183	10.39	26.86	3.56	0.32	12.94
188	10.48	26.03	2.54	0.00	12.06
193	10.55	24.31	2.78	0.00	14.93
197	10.62	19.67	1.64	0.98	14.75
203	10.71	15.05	3.76	0.00	27.90
208	10.79	19.48	3.25	0.32	20.78
214	10.88	24.21	2.83	0.31	16.35

218	10.94	28.93	4.09	0.00	17.92
223	11.02	23.36	3.62	0.00	17.43
228	11.10	22.22	3.70	0.00	14.48
233	11.17	21.07	4.35	0.00	15.38
238	11.24	20.44	4.09	0.00	19.50
243	11.31	15.41	5.25	0.00	23.28
248	11.38	17.67	3.33	0.00	19.00
255	11.49	16.94	2.61	0.00	14.01
261	11.60	16.24	1.27	0.00	16.24
271	11.75	21.14	1.89	0.00	17.03
276	11.84	19.24	1.89	0.00	14.51
280	11.91	17.21	2.92	0.00	14.29
281	11.93	18.89	1.95	0.00	18.89
286	12.01	14.71	4.25	0.00	17.65
291	12.08	18.21	1.28	0.00	11.18
296	12.15	26.82	2.98	0.00	15.56
301	12.23	20.25	2.18	0.00	14.64
306	12.32	19.74	2.96	0.00	21.05
311	12.40	18.04	0.63	0.00	22.15
316	12.48	17.11	0.99	0.33	20.72
320	12.55	19.67	2.33	0.00	12.33
321	12.57	14.47	0.96	0.00	23.47
326	12.65	14.43	0.33	0.00	25.57
331	12.73	15.06	2.88	0.00	25.64
341	12.90	15.71	0.00	0.32	16.67
360	13.27	26.28	0.64	0.00	4.17
381	13.88	24.53	2.20	0.00	12.26
401	14.47	17.38	3.93	0.00	5.90
405	14.59	24.61	2.49	0.00	8.10
410	14.73	29.25	0.63	0.00	4.40

Depth	Age kyr BP	*G. elongatus*	*G. ruber* (alba)	*G. ruber* (pink)	*G. sacculifer*	*G. inflata*
1	-0.14	2.98	5.96	1.99	1.32	34.44
6	0.11	3.67	7.00	1.00	3.00	16.33
11	0.37	6.86	8.17	0.98	2.29	29.41
16	0.62	2.99	12.96	0.33	1.00	21.26
21	0.88	2.00	9.67	0.00	0.00	18.33
26	1.13	3.00	16.00	3.00	1.33	9.33
31	1.39	3.67	9.33	1.00	1.67	21.33
36	1.64	0.00	6.48	1.37	1.71	23.89
41	1.90	1.33	6.98	2.99	0.33	25.25
46	2.15	3.32	10.30	0.66	0.33	26.25
51	2.40	3.67	7.67	0.67	1.00	22.67
56	2.65	1.67	10.67	1.33	0.67	18.67
61	2.91	0.67	8.67	0.00	1.33	12.67
71	3.30	3.63	11.88	0.99	4.95	26.07
81	3.70	3.81	11.11	1.90	2.54	26.35
101	4.71	2.57	12.86	0.32	1.29	20.26
111	5.23	3.69	11.38	0.31	0.62	23.38
123	5.85	2.59	13.59	1.29	0.32	23.30
128	6.11	3.01	11.71	1.00	0.00	22.41
133	6.37	1.85	15.12	0.93	0.00	23.15
138	6.63	1.26	15.46	3.47	0.32	20.82
143	7.02	1.61	19.35	0.32	1.29	22.58
148	7.56	1.00	20.93	1.00	0.00	19.93
150	7.79	1.17	24.85	0.29	0.88	26.32
153	8.25	1.59	15.56	1.59	0.00	15.24
155	8.60	1.66	13.62	0.00	0.66	19.60
158	9.09	1.33	14.95	1.99	0.00	22.92
160	9.41	1.93	15.76	0.32	0.00	16.40
163	9.70	0.67	5.33	0.33	0.33	20.33
165	9.85	1.33	9.67	0.00	0.33	14.33
168	10.00	0.96	8.68	0.32	0.00	11.90
173	10.17	1.00	8.97	0.00	0.00	11.30
178	10.30	0.66	10.96	0.00	0.00	11.30
183	10.39	2.27	7.44	0.32	0.00	10.68
188	10.48	0.95	5.08	0.32	0.00	18.10
193	10.55	0.00	7.29	0.00	0.00	10.76
197	10.62	0.33	9.51	0.00	0.00	11.15
203	10.71	0.31	7.84	0.00	0.00	4.70
208	10.79	0.32	4.55	0.00	0.00	4.22
214	10.88	0.94	6.92	0.00	0.00	5.66
218	10.94	0.31	4.09	0.00	0.00	7.55
223	11.02	0.99	4.61	0.00	0.00	7.24
228	11.10	0.34	4.04	0.00	0.00	12.46
233	11.17	1.00	5.69	0.33	0.00	8.70
238	11.24	0.94	2.83	0.00	0.00	10.06

243	11.31	0.00	3.28	0.00	0.00	3.28
248	11.38	0.33	3.67	0.00	0.00	7.00
255	11.49	0.00	2.28	0.00	0.00	3.91
261	11.60	0.32	2.23	0.00	0.32	5.73
271	11.75	0.32	2.21	0.00	0.00	0.95
276	11.84	0.32	2.52	0.00	0.00	2.52
280	11.91	0.65	3.57	0.00	0.00	1.62
281	11.93	0.00	2.28	0.00	0.00	2.93
286	12.01	0.00	2.29	0.00	0.00	2.29
291	12.08	0.00	3.19	0.00	0.00	3.83
296	12.15	0.00	2.32	0.00	0.00	2.98
301	12.23	0.31	2.18	0.00	0.00	1.56
306	12.32	0.33	1.64	0.00	0.00	3.29
311	12.40	0.32	2.53	0.32	0.00	3.16
316	12.48	0.00	1.97	0.00	0.33	3.62
320	12.55	0.00	3.00	0.00	0.00	3.67
321	12.57	0.00	3.22	0.00	0.00	3.54
326	12.65	0.00	1.31	0.00	0.00	1.97
331	12.73	0.32	1.28	0.00	0.00	3.21
341	12.90	0.00	1.60	0.00	0.00	4.49
360	13.27	0.00	5.13	0.00	0.00	4.49
381	13.88	0.00	3.46	0.00	0.00	9.43
401	14.47	0.00	13.11	0.00	0.33	13.44
405	14.59	0.93	5.61	0.00	0.00	10.28
410	14.73	0.00	2.20	0.00	0.31	10.38

Depth	Age kyr BP	G. scitulas dx	G. scitula sx	G. truncatulinoides sx	N. dutertrei
1	-0.14	0.00	0.00	11.59	0.00
6	0.11	0.00	0.00	7.33	0.33
11	0.37	0.00	0.00	8.17	0.33
16	0.62	0.00	0.33	3.65	0.33
21	0.88	0.00	0.00	6.00	1.33
26	1.13	0.00	0.00	4.00	0.00
31	1.39	0.00	0.00	4.67	0.00
36	1.64	0.00	0.00	7.85	0.00
41	1.90	0.00	0.00	7.31	0.00
46	2.15	0.00	0.00	5.65	0.00
51	2.40	0.00	0.00	3.67	0.00
56	2.65	0.00	0.00	4.33	0.00
61	2.91	0.00	0.00	4.00	0.00
71	3.30	0.33	0.00	1.65	0.66
81	3.70	0.32	0.00	0.95	0.32
101	4.71	1.29	0.00	2.57	0.00
111	5.23	0.31	0.00	1.23	1.85
123	5.85	0.00	0.00	0.32	0.32
128	6.11	0.00	0.00	0.00	0.67
133	6.37	0.00	0.31	0.00	1.23
138	6.63	0.00	0.32	0.00	0.63
143	7.02	0.00	0.00	0.00	0.32
148	7.56	1.00	0.00	0.00	0.00
150	7.79	0.29	0.00	0.00	0.00
153	8.25	0.95	0.00	0.00	0.63
155	8.60	0.00	0.00	0.00	0.00
158	9.09	0.00	0.00	0.00	0.00
160	9.41	1.61	0.32	1.61	0.32
163	9.70	0.33	0.00	0.33	0.00
165	9.85	1.67	0.00	1.00	0.00
168	10.00	0.00	0.00	0.00	0.00
173	10.17	0.33	0.00	0.00	0.00
178	10.30	0.33	0.00	0.00	0.33
183	10.39	0.32	0.00	0.00	0.00
188	10.48	3.81	0.00	0.00	0.00
193	10.55	2.08	0.00	0.00	0.00
197	10.62	1.31	0.00	0.33	0.00
203	10.71	2.51	0.00	0.00	0.00
208	10.79	1.62	0.00	0.00	0.00
214	10.88	3.14	0.00	0.00	0.00
218	10.94	2.20	0.00	0.31	0.31
223	11.02	1.64	0.33	0.00	0.00
228	11.10	3.37	0.67	0.34	0.67
233	11.17	5.35	0.00	0.67	0.67
238	11.24	4.09	0.00	0.31	0.00

243	11.31	4.92	0.00	0.33	0.00
248	11.38	5.33	0.00	0.00	0.00
255	11.49	2.93	0.33	0.00	3.26
261	11.60	1.91	0.00	0.00	3.18
271	11.75	2.21	0.00	0.00	7.26
276	11.84	0.32	0.63	0.00	5.99
280	11.91	1.30	0.00	0.00	1.95
281	11.93	0.98	0.00	0.00	4.23
286	12.01	2.29	0.33	0.00	2.29
291	12.08	0.64	0.00	0.00	4.79
296	12.15	0.33	0.00	0.00	4.64
301	12.23	1.87	0.31	0.00	8.41
306	12.32	2.30	0.00	0.00	6.25
311	12.40	1.58	0.00	0.00	5.38
316	12.48	0.33	0.00	0.00	5.59
320	12.55	3.67	0.00	0.00	3.67
321	12.57	1.29	1.93	0.00	6.11
326	12.65	0.33	0.00	0.00	8.85
331	12.73	0.32	0.32	0.00	3.85
341	12.90	4.81	0.32	0.00	2.88
360	13.27	0.96	0.00	0.00	1.92
381	13.88	2.52	0.00	0.00	1.57
401	14.47	3.61	0.00	0.00	1.31
405	14.59	1.87	0.00	0.00	1.87
410	14.73	1.57	0.00	0.00	0.94

Depth	Age kyr BP	*G. truncatulinoides* dx	*N. incompta* dx	*N. pachyderma* sx
1	-0.14	1.32	1.32	0.33
6	0.11	0.33	4.33	1.00
11	0.37	0.00	2.29	0.65
16	0.62	0.00	2.66	1.00
21	0.88	0.00	3.00	0.33
26	1.13	0.00	3.33	0.00
31	1.39	0.33	2.67	0.67
36	1.64	0.00	4.10	0.68
41	1.90	0.00	1.66	0.66
46	2.15	0.33	2.33	0.33
51	2.40	0.00	1.33	0.67
56	2.65	0.00	1.67	0.00
61	2.91	0.00	3.67	1.67
71	3.30	6.93	0.99	0.99
81	3.70	2.86	3.81	0.95
101	4.71	0.00	3.54	0.32
111	5.23	0.00	10.15	0.31
123	5.85	0.00	15.21	0.00
128	6.11	0.00	15.72	0.00
133	6.37	0.00	16.36	0.00
138	6.63	0.00	14.20	0.00
143	7.02	0.00	18.06	0.32
148	7.56	0.66	16.94	0.00
150	7.79	0.00	14.33	0.29
153	8.25	0.32	18.41	0.00
155	8.60	0.00	8.97	0.33
158	9.09	0.33	7.64	0.00
160	9.41	0.00	4.50	0.64
163	9.70	2.33	3.33	1.00
165	9.85	0.00	7.67	0.33
168	10.00	0.64	11.58	1.29
173	10.17	0.66	6.31	1.99
178	10.30	0.33	8.64	1.33
183	10.39	0.65	4.85	0.97
188	10.48	0.63	6.35	1.27
193	10.55	0.00	4.17	1.39
197	10.62	0.33	8.52	0.66
203	10.71	0.00	7.21	1.57
208	10.79	0.32	8.12	0.65
214	10.88	0.94	3.14	0.94
218	10.94	0.00	3.77	0.63
223	11.02	0.33	5.92	0.66
228	11.10	0.34	5.05	0.67
233	11.17	0.67	4.35	0.67
238	11.24	0.00	3.46	0.63

243	11.31	0.00	4.92	0.98
248	11.38	0.00	7.67	2.00
255	11.49	0.00	14.01	0.98
261	11.60	0.00	11.15	0.32
271	11.75	0.00	14.83	2.21
276	11.84	0.00	12.62	2.21
280	11.91	0.00	16.23	4.87
281	11.93	0.00	15.31	1.30
286	12.01	0.00	16.34	1.63
291	12.08	0.00	17.89	0.00
296	12.15	0.00	12.25	1.32
301	12.23	0.00	12.77	1.56
306	12.32	0.00	12.17	0.66
311	12.40	0.00	12.34	0.95
316	12.48	0.00	19.08	0.33
320	12.55	0.00	16.67	2.67
321	12.57	0.00	18.97	1.93
326	12.65	0.00	21.64	0.66
331	12.73	0.00	15.71	1.60
341	12.90	0.00	11.86	1.92
360	13.27	0.00	21.47	0.00
381	13.88	0.00	18.24	0.63
401	14.47	0.00	11.80	0.98
405	14.59	0.31	14.02	0.93
410	14.73	0.63	8.49	0.00

Depth	Age kyr BP	*O. universa*	*T. quinqueloba*	*Tenuitella* spp.	Unknow	*Neoglob* sp
1	-0.14	0.66	3.31	0.66	0.33	0.00
6	0.11	1.00	6.67	0.67	1.33	0.00
11	0.37	0.65	5.23	0.65	0.65	0.00
16	0.62	0.33	7.64	1.33	0.66	0.00
21	0.88	1.00	5.00	0.33	1.00	0.00
26	1.13	1.00	8.00	0.67	1.00	0.00
31	1.39	0.67	7.00	0.00	1.33	0.00
36	1.64	1.02	5.80	0.00	1.37	0.00
41	1.90	1.33	2.66	0.66	1.00	0.00
46	2.15	1.00	4.32	1.33	1.33	0.00
51	2.40	1.00	9.00	0.00	1.67	0.00
56	2.65	0.67	7.00	2.33	1.33	0.00
61	2.91	1.00	9.33	1.67	1.67	0.00
71	3.30	0.99	5.94	0.66	0.33	0.00
81	3.70	4.13	2.86	2.86	0.32	0.00
101	4.71	1.93	5.14	1.29	0.32	0.00
111	5.23	0.62	3.69	1.23	1.54	0.00
123	5.85	1.29	2.91	3.24	2.27	0.00
128	6.11	5.02	3.01	2.34	1.00	0.00
133	6.37	3.40	3.09	0.62	1.85	0.00
138	6.63	2.84	2.52	0.63	1.58	0.00
143	7.02	0.97	7.10	1.61	0.97	0.00
148	7.56	2.66	4.98	1.33	1.66	0.00
150	7.79	2.05	2.63	0.58	0.58	0.00
153	8.25	3.17	6.67	2.22	1.27	0.00
155	8.60	1.00	9.97	1.33	1.66	0.00
158	9.09	0.66	7.64	2.33	1.00	0.00
160	9.41	1.29	12.54	1.93	1.61	0.00
163	9.70	0.67	15.00	2.67	1.00	0.00
165	9.85	1.33	15.00	1.67	1.00	0.00
168	10.00	0.96	17.04	3.54	1.29	0.00
173	10.17	0.33	16.61	2.99	0.33	0.00
178	10.30	0.00	16.94	3.65	1.66	0.00
183	10.39	0.00	20.39	7.44	0.97	0.00
188	10.48	0.95	18.10	3.49	0.32	0.00
193	10.55	0.69	22.22	8.33	1.04	0.00
197	10.62	0.66	20.33	7.21	2.62	0.00
203	10.71	0.94	18.18	8.78	1.25	0.00
208	10.79	0.32	25.00	9.42	1.62	0.00
214	10.88	0.31	22.96	10.69	0.63	0.00
218	10.94	1.26	19.18	7.23	0.63	1.57
223	11.02	0.00	26.32	7.24	0.33	0.00
228	11.10	0.67	22.56	6.40	0.67	1.35
233	11.17	0.00	20.74	7.69	1.00	1.67
238	11.24	0.31	24.53	5.35	1.57	1.89

243	11.31	0.33	25.57	9.84	0.66	1.97
248	11.38	0.00	21.00	10.67	1.33	1.00
255	11.49	0.00	33.88	3.26	1.63	0.00
261	11.60	0.00	38.54	1.59	0.96	0.00
271	11.75	0.00	27.76	0.63	1.58	0.00
276	11.84	0.00	35.02	0.00	2.21	0.00
280	11.91	0.32	31.17	1.95	1.95	0.00
281	11.93	0.00	31.60	0.00	1.63	0.00
286	12.01	0.00	34.64	0.65	0.65	0.00
291	12.08	0.00	37.06	0.32	1.60	0.00
296	12.15	0.00	30.13	0.33	0.33	0.00
301	12.23	0.00	31.78	0.31	1.87	0.00
306	12.32	0.00	27.30	0.33	1.97	0.00
311	12.40	0.00	30.70	0.00	1.90	0.00
316	12.48	0.00	27.96	0.00	1.64	0.00
320	12.55	0.00	30.00	1.67	0.67	0.00
321	12.57	0.00	22.83	0.00	1.29	0.00
326	12.65	0.00	21.64	0.98	2.30	0.00
331	12.73	0.00	28.53	0.00	1.28	0.00
341	12.90	0.00	34.29	3.85	1.28	0.00
360	13.27	0.32	32.69	1.92	0.00	0.00
381	13.88	0.00	19.50	4.09	1.57	0.00
401	14.47	0.00	23.61	3.28	1.31	0.00
405	14.59	0.62	25.86	0.62	1.87	0.00
410	14.73	0.63	37.42	2.52	0.63	0.00

7.2 *G. bulloides* Sea Surface Temperatures (SST) from core NDT-6-2016.

Depth	Age kyr BP	SST *G. bulloides*	std (°C)
21	0.8785	19.15	1.52
31	1.3888	18.87	1.51
41	1.903	18.70	1.50
51	2.4003	18.82	1.50
61	2.9094	18.50	1.49
76	3.5068	18.03	1.47
81	3.7041	18.45	1.48
86	3.9313	17.33	1.43
101	4.7116	18.23	1.48
111	5.2309	18.58	1.49
123	5.8529	18.45	1.48
131	6.2631	17.62	1.45
138	6.6311	17.57	1.44
141	6.798	16.83	1.41
145	7.23	17.05	1.42
146	7.3402	18.49	1.49
148	7.5635	19.09	1.51
149	7.6757	17.52	1.44
151	7.8994	19.36	1.53
153	8.2494	17.38	1.43
154	8.4241	19.04	1.51
155	8.5975	19.04	1.51
156	8.7696	20.00	1.56
158	9.0854	20.55	1.59
160	9.4052	20.35	1.58
161	9.5639	17.18	1.43
164	9.7751	19.21	1.52
166	9.9151	20.18	1.57
170	10.0751	21.16	1.62
177	10.2746	20.45	1.58
183	10.3939	21.58	1.64
193	10.5532	21.77	1.65
199	10.6478	19.67	1.54
208	10.7875	19.38	1.53
213	10.8652	18.22	1.47
214	10.8812	19.72	1.55
223	11.0212	19.75	1.55
233	11.1721	20.51	1.59
238	11.2386	20.21	1.57
248	11.3837	17.54	1.44
253	11.462	21.15	1.62
259	11.5642	19.24	1.52
271	11.7498	17.97	1.46

281	11.9255	18.00	1.46
301	12.2336	16.47	1.39
311	12.3985	16.87	1.41
320	12.55	16.87	1.41
331	12.7321	18.73	1.50
341	12.9001	20.09	1.57
361	13.2846	20.05	1.56
381	13.8794	19.25	1.52
391	14.1776	20.09	1.57
405	14.5855	20.76	1.60
415	14.8779	20.55	1.59
415	14.8779	20.42	1.58

7.3 $\delta^{18}O$ *G. bulloides* from core NDT-6-2016.

Depth	Age kyr BP	$\delta^{18}O$ *G. bulloides*	Depth	Age kyr BP	$\delta^{18}O$ *G. bulloides*
11	0.37	1.15	163	9.70	1.30
20	0.83	1.04	164	9.78	1.20
31	1.39	0.83	166	9.92	1.47
40	1.85	1.25	168	10.00	1.40
51	2.40	1.47	169	10.04	1.42
61	2.91	1.28	171	10.12	1.39
71	3.30	0.98	173	10.17	1.46
76	3.51	1.21	174	10.20	1.45
81	3.70	1.00	176	10.25	1.50
86	3.93	1.01	177	10.27	1.62
91	4.20	1.00	178	10.30	1.87
101	4.71	1.12	179	10.32	1.62
111	5.23	1.13	181	10.36	1.56
121	5.75	0.93	183	10.39	1.88
123	5.85	1.26	184	10.41	1.57
124	5.90	1.45	186	10.44	1.53
126	6.01	1.33	188	10.48	1.68
128	6.11	1.13	189	10.49	1.68
129	6.16	1.13	193	10.55	1.62
131	6.26	1.08	194	10.57	1.51
133	6.37	1.12	196	10.60	1.46
134	6.42	1.13	197	10.62	1.62
136	6.52	1.25	199	10.65	1.82
138	6.63	0.96	201	10.68	1.72
139	6.69	1.59	203	10.71	1.68
141	6.80	1.42	204	10.72	1.76
143	7.02	1.16	206	10.76	1.74
144	7.12	1.31	208	10.79	1.79
145	7.23	1.21	209	10.80	1.91
146	7.34	1.55	211	10.83	1.61
147	7.45	2.00	213	10.87	1.54
148	7.56	2.01	213	10.87	2.24
149	7.68	1.62	218	10.94	1.74
150	7.79	1.42	219	10.96	1.94
151	7.90	1.99	221	10.99	1.92
152	8.07		223	11.02	2.11
153	8.25	1.74	224	11.04	1.98
154	8.42	1.49	226	11.07	2.41
155	8.60	1.11	228	11.10	2.07
156	8.77	1.32	229	11.11	2.09
158	9.09	1.15	231	11.15	1.93
159	9.24	1.23	233	11.17	1.82
160	9.41	1.20	234	11.19	1.68
161	9.56	1.41	236	11.21	1.85

238	11.24	2.08	291	12.08	2.70
239	11.25	1.85	296	12.15	2.70
241	11.28	2.17	301	12.23	2.47
243	11.31	2.00	306	12.32	2.63
244	11.32	2.29	311	12.40	2.51
246	11.35	2.12	316	12.48	2.69
248	11.38	2.48	320	12.55	2.73
249	11.40	2.23	326	12.65	2.69
251	11.43	2.63	331	12.73	2.90
253	11.46	2.48	341	12.90	2.33
255	11.49	2.68	361	13.28	2.55
257	11.53	2.46	381	13.88	2.68
259	11.56	2.74	391	14.18	2.28
261	11.60	2.55	401	14.47	2.32
271	11.75	2.92	404	14.56	2.29
276	11.84	2.52	410	14.73	2.57
281	11.93	2.56	415	14.88	1.84
291	12.08	2.46			

7.4 $\delta^{18}O_{sw}$ *G. bulloides* from core NDT-6-2016.

Depth	Age kyr BP	$\delta^{18}O_{sw}$ *G. bulloides*	Depth	Age kyr BP	$\delta^{18}O_{sw}$ *G. bulloides*
21	0.88	1.68	166	9.92	2.06
31	1.39	1.40	170	10.08	2.21
41	1.85	1.78	177	10.27	2.23
51	2.40	2.03	183	10.39	2.76
61	2.91	1.76	193	10.55	2.54
76	3.51	1.56	199	10.65	2.20
81	3.70	1.46	208	10.79	2.08
86	3.93	1.19	213	10.87	1.51
101	4.71	1.52	214	10.88	1.88
111	5.23	1.61	223	11.02	2.50
123	5.85	1.71	233	11.17	2.39
131	6.26	1.31	238	11.24	2.55
138	6.63	1.17	248	11.38	2.26
141	6.80	1.42	253	11.46	3.15
145	7.23	1.23	259	11.56	2.95
146	7.34	1.92	271	11.75	2.89
148	7.56	2.51	281	11.93	2.33
149	7.68	1.72	301	12.23	1.96
151	7.90	2.56	311	12.40	2.08
153	8.25	1.81	320	12.55	2.30
154	8.42	1.95	331	12.73	2.94
155	8.60	1.53	341	12.90	2.70
156	8.77	1.98	361	13.28	2.86
158	9.09	1.95	381	13.88	2.72
160	9.41	1.94	391	14.18	2.48
161	9.56	1.30	405	14.59	2.62
164	9.78	1.59	415	14.88	2.10

7.5 $\delta^{18}O$ *G. ruber* from core NDT-6-2016.

Depth	Age kyr BP	$\delta^{18}O$ *G. ruber*
31	1.39	-0.05
61	2.91	-0.02
71	3.30	0.32
81	3.70	0.90
91	4.20	0.43
101	4.71	0.36
111	5.23	0.07
121	5.75	0.25
131	6.26	0.02
136	6.52	-0.45
141	6.80	-0.43
146	7.34	0.46
151	7.90	0.27
156	8.77	0.10
161	9.56	0.39
166	9.92	0.33
171	10.12	0.04
176	10.25	0.56
181	10.36	0.75
196	10.60	0.27
201	10.68	0.10
206	10.76	0.39
211	10.83	0.76
221	10.99	1.13
226	11.07	1.27
231	11.15	1.61
236	11.21	1.41
241	11.28	1.40
246	11.35	1.32
251	11.43	1.87
261	11.60	1.47
271	11.75	1.51
280	11.91	1.26
301	12.23	1.74
331	12.73	1.05
341	12.90	0.92
361	13.28	1.58
381	13.88	1.62
401	14.47	1.49
415	14.88	2.04

7.6 *U. mediterranea* Deep Water Temperature (DWT) from core NDT-6-2016.

Depth	Age kyr BP	DWT (*Uvigerina* ssp)	std (°C)
1	-0.14	13.92	0.36
5	0.06	12.27	0.20
7	0.16	16.01	0.17
9	0.27	13.97	0.27
11	0.37	13.55	0.15
13	0.47	12.75	0.35
15	0.57	13.80	0.15
17	0.67	13.88	0.30
19	0.77	12.80	0.14
21	0.88	14.34	0.20
23	0.98	12.92	0.22
25	1.08	13.83	0.12
27	1.18	13.72	0.20
29	1.29	14.25	0.34
31	1.39	14.47	0.18
33	1.49	12.86	0.25
35	1.59	12.29	
37	1.69	13.22	0.22
39	1.80	13.42	0.35
41	1.90	14.65	0.23
43	2.00	12.62	0.14
45	2.10	15.17	0.19
47	2.20	14.37	0.25
49	2.30	13.76	0.21
51	2.40	12.76	0.17
53	2.50	13.21	0.20
55	2.60	15.13	0.24
57	2.70	13.71	0.19
59	2.81	14.88	0.28
81	3.70	13.21	0.25
91	4.20	14.08	0.43
101	4.71	15.14	0.58
111	5.23	13.45	0.16
121	5.75	15.64	0.15
123	5.85	14.16	2.60
124	5.90	12.40	2.43
126	6.01	11.81	0.22
128	6.11	14.93	1.74
129	6.16	12.24	2.36
131	6.26	15.01	0.23
133	6.37	18.07	2.53
134	6.42	17.92	2.25
136	6.52	15.68	1.41
139	6.69	14.02	2.07

141	6.80	18.00	0.29
142	6.91	12.74	0.28
143	7.02	14.09	2.07
144	7.12	14.21	1.42
145	7.23	15.75	0.26
146	7.34	14.20	0.25
147	7.45	13.04	0.32
148	7.56	13.41	2.98
149	7.68	14.67	2.15
150	7.79	13.50	0.41
151	7.90	15.11	0.24
152	8.07	12.35	0.53
153	8.25	13.19	2.63
154	8.42	14.94	2.44
155	8.60	14.44	0.65
156	8.77	12.79	0.22
157	8.93	12.96	0.84
158	9.09	12.95	2.35
159	9.24	15.08	2.21
160	9.41	13.66	0.78
161	9.56	13.22	0.11
162	9.63	12.53	0.34
163	9.70	12.90	2.11
164	9.78	13.33	2.47
166	9.92	11.18	0.19
168	10.00	14.78	2.05
171	10.12	13.30	0.17
173	10.17	14.77	1.65
174	10.20	14.63	1.60
178	10.30	13.51	1.52
179	10.32	12.04	1.88
183	10.39	13.66	1.69
184	10.41	13.67	2.04
186	10.44	11.66	0.18
188	10.48	12.55	2.81
189	10.49	10.68	2.59
193	10.55	12.95	2.29
194	10.57	11.72	2.00
196	10.60	14.31	0.24
197	10.62	11.53	2.59
201	10.68	16.34	0.36
203	10.71	13.81	2.15
204	10.72	11.55	3.14
206	10.76	14.15	0.16
208	10.79	12.31	1.31
209	10.80	14.95	1.61
211	10.83	13.01	0.22
213	10.87	12.48	2.08

214	10.88	13.13	2.33
216	10.91	12.56	0.19
218	10.94	13.33	2.37
219	10.96	14.67	2.12
221	10.99	14.89	0.14
223	11.02	13.30	1.99
224	11.04	17.57	2.40
226	11.07	13.98	0.39
228	11.10	13.24	1.66
229	11.11	10.67	1.82
231	11.15	13.16	0.32
233	11.17	13.69	2.89
234	11.19	13.20	3.27
236	11.21	11.41	2.43
239	11.25	12.68	2.23
243	11.31	11.13	2.47
244	11.32	17.68	2.03
246	11.35	10.77	0.27
248	11.38	11.68	2.16
249	11.40	11.43	2.13
251	11.43	14.45	0.15
253	11.46	12.60	0.50
255	11.49	11.55	0.09
257	11.53	13.61	0.12
261	11.60	15.55	0.34
280	11.91	15.30	0.08
286	12.01	11.89	3.53
291	12.08	10.39	0.91
301	12.23	12.58	0.57
306	12.32	11.72	2.30
311	12.40	11.70	3.00
316	12.48	10.17	0.84
331	12.73	11.37	0.81
341	12.90	11.32	0.76
349	13.05	11.49	0.41
361	13.28	13.79	0.10
381	13.88	10.44	0.12
401	14.47	13.27	0.12
415	14.88	11.83	0.15

7.7 $\delta^{18}O$ *U. mediterrana* from core NDT-6-2016.

Depth	Age kyr BP	$\delta^{18}O$ (PDB) *U. mediterranea*	Depth	Age kyr BP	$\delta^{18}O$ (PDB) *U. mediterranea*
1	-0.14	2.19	133	6.37	2.31
3	-0.04	2.14	134	6.42	2.23
5	0.06	2.17	136	6.52	2.11
7	0.16	2.15	138	6.63	2.11
9	0.27	2.17	139	6.69	2.07
11	0.37	2.10	141	6.80	2.41
13	0.47	2.23	142	6.91	2.24
15	0.57	2.18	143	7.02	2.21
17	0.67	2.20	144	7.12	2.34
19	0.77	2.13	145	7.23	2.03
21	0.88	2.04	146	7.34	2.40
23	0.98	2.22	147	7.45	2.45
25	1.08	2.13	148	7.56	2.98
27	1.18	2.17	149	7.68	2.93
29	1.29	2.02	150	7.79	2.62
31	1.39	2.16	151	7.90	2.76
33	1.49	2.16	152	8.07	2.14
35	1.59	2.16	153	8.25	3.03
37	1.69	2.15	154	8.42	2.16
39	1.80	2.17	155	8.60	2.40
41	1.90	2.15	156	8.77	2.43
43	2.00	2.16	157	8.93	2.24
45	2.10	2.17	158	9.09	2.34
47	2.20	2.18	159	9.24	2.24
49	2.30	2.10	160	9.41	2.46
51	2.40	2.21	161	9.56	2.29
53	2.50	2.20	162	9.63	2.30
55	2.60	2.17	163	9.70	2.43
57	2.70	2.26	164	9.78	2.51
59	2.81	2.19	166	9.92	2.48
61	2.91	2.08	168	10.00	2.61
71	3.30	2.11	169	10.04	2.71
81	3.70	2.03	171	10.12	2.48
91	4.20	2.09	173	10.17	2.56
101	4.71	1.97	174	10.20	2.62
111	5.23	1.93	176	10.25	2.59
121	5.75	2.07	178	10.30	2.55
123	5.85	2.05	179	10.32	2.62
124	5.90	2.10	183	10.39	2.73
126	6.01	2.20	184	10.41	2.71
128	6.11	2.10	186	10.44	2.72
129	6.16	2.12	188	10.48	2.82
131	6.26	2.14	189	10.49	2.74

191	10.52	2.75	239	11.25	3.01
193	10.55	2.74	243	11.31	3.08
194	10.57	2.76	244	11.32	3.03
196	10.60	2.31	246	11.35	3.10
197	10.62	2.66	248	11.38	2.93
199	10.65	2.69	249	11.40	3.03
201	10.68	2.80	251	11.43	3.59
203	10.71	2.43	253	11.46	3.33
204	10.72	2.70	255	11.49	3.33
206	10.76	2.92	257	11.53	3.31
208	10.79	2.65	259	11.56	3.24
209	10.80	2.92	261	11.60	3.28
213	10.87	2.86	281	11.93	3.32
214	10.88	2.90	291	12.08	3.66
216	10.91	2.83	296	12.15	3.59
218	10.94	2.89	301	12.23	3.54
219	10.96	2.92	306	12.32	3.45
221	10.99	2.99	311	12.40	3.56
223	11.02	3.09	316	12.48	3.61
224	11.04	2.91	320	12.55	3.43
226	11.07	2.91	331	12.73	3.63
228	11.10	2.99	341	12.90	3.43
229	11.11	2.99	349	13.05	3.55
231	11.15	2.94	361	13.28	3.54
233	11.17	2.91	381	13.88	3.48
234	11.19	2.92	391	14.18	3.55
236	11.21	3.11	401	14.47	3.36
238	11.24	3.05	415	14.88	3.48

7.8 $\delta^{18}O_{sw}$ *U. mediterrana* from core NDT-6-2016.

Depth	Age kyr BP	$\delta^{18}O_{sw}$ *U. mediterranea*	Error
1	-0.14	1.52	0.12
5	0.06	1.09	0.09
7	0.16	2.01	0.09
9	0.27	1.52	0.11
11	0.37	1.34	0.09
13	0.47	1.27	0.12
15	0.57	1.48	0.09
17	0.67	1.52	0.11
19	0.77	1.19	0.09
21	0.88	1.48	0.09
23	0.98	1.30	0.10
25	1.08	1.44	0.09
27	1.18	1.45	0.09
29	1.29	1.44	0.12
31	1.39	1.63	0.09
33	1.49	1.23	0.10
35	1.59	1.09	
37	1.69	1.31	0.10
39	1.80	1.38	0.12
41	1.90	1.66	0.10
43	2.00	1.17	0.09
45	2.10	1.82	0.09
47	2.20	1.62	0.10
49	2.30	1.39	0.10
51	2.40	1.25	0.09
53	2.50	1.35	0.09
55	2.60	1.81	0.10
57	2.70	1.54	0.09
59	2.81	1.76	0.11
81	3.70	1.18	0.10
91	4.20	1.45	0.13
101	4.71	1.60	0.17
111	5.23	1.13	0.09
121	5.75	1.82	0.09
123	5.85	1.42	0.66
124	5.90	1.04	0.61
126	6.01	0.98	0.10
128	6.11	1.66	0.44
129	6.16	1.01	0.60
131	6.26	1.72	0.10
133	6.37	2.64	0.64
134	6.42	2.53	0.57
136	6.52	1.85	0.36
139	6.69	1.38	0.52

141	6.80	2.71	0.11
142	6.91	1.21	0.11
143	7.02	1.51	0.52
144	7.12	1.66	0.36
145	7.23	1.72	0.10
146	7.34	1.70	0.10
147	7.45	1.44	0.11
148	7.56	2.06	0.75
149	7.68	2.31	0.54
150	7.79	1.72	0.13
151	7.90	2.27	0.10
152	8.07	0.97	0.15
153	8.25	2.05	0.66
154	8.42	1.60	0.62
155	8.60	1.67	0.18
156	8.77	1.30	0.10
157	8.93	1.13	0.22
158	9.09	1.24	0.59
159	9.24	1.66	0.56
160	9.41	1.50	0.21
161	9.56	1.19	0.08
162	9.63	1.02	0.12
163	9.70	1.24	0.53
164	9.78	1.41	0.62
166	9.92	0.82	0.09
168	10.00	1.85	0.52
171	10.12	1.33	0.09
173	10.17	1.77	0.42
174	10.20	1.79	0.41
178	10.30	1.43	0.39
179	10.32	1.12	0.48
183	10.39	1.64	0.43
184	10.41	1.62	0.52
186	10.44	1.12	0.09
188	10.48	1.44	0.71
189	10.49	0.90	0.65
193	10.55	1.45	0.58
194	10.57	1.16	0.51
196	10.60	1.36	0.10
197	10.62	1.01	0.65
201	10.68	2.35	0.12
203	10.71	1.34	0.54
204	10.72	1.04	0.79
206	10.76	1.90	0.09
208	10.79	1.17	0.34
209	10.80	2.10	0.41
213	10.87	1.40	0.53
214	10.88	1.60	0.59

216	10.91	1.39	0.09
218	10.94	1.65	0.60
219	10.96	2.03	0.54
221	10.99	2.16	0.09
223	11.02	1.87	0.50
224	11.04	2.75	0.61
226	11.07	1.86	0.13
228	11.10	1.75	0.42
229	11.11	1.10	0.46
231	11.15	1.68	0.11
233	11.17	1.77	0.73
234	11.19	1.66	0.82
236	11.21	1.39	0.61
239	11.25	1.60	0.56
243	11.31	1.27	0.62
244	11.32	2.86	0.51
246	11.35	1.19	0.10
248	11.38	1.24	0.55
249	11.40	1.29	0.54
251	11.43	2.59	0.09
253	11.46	1.87	0.15
255	11.49	1.61	0.08
257	11.53	2.10	0.09
261	11.60	2.57	0.12
281	11.93	2.52	0.08
291	12.08	1.63	0.24
301	12.23	2.06	0.16
306	12.32	1.74	0.58
311	12.40	1.83	0.76
316	12.48	1.50	0.23
331	12.73	1.83	0.22
341	12.90	1.60	0.21
349	13.05	1.71	0.13
361	13.28	2.29	0.08
381	13.88	1.33	0.09
401	14.47	1.80	0.09
415	14.88	1.56	0.09

7.9 Grain-size measurements (silt/clay) from core NDT-6-2016.

Depth	Age kyrs BP	Silt/clay
1	-0.14	0.34
2	-0.09	0.26
3	-0.04	0.27
4	0.01	0.25
5	0.06	0.37
6	0.11	0.66
7	0.16	0.28
8	0.22	0.30
9	0.27	0.30
10	0.32	0.32
11	0.37	0.22
12	0.42	0.22
13	0.47	0.35
14	0.52	0.22
15	0.57	0.22
16	0.62	0.27
17	0.67	0.18
18	0.72	0.46
19	0.77	0.18
21	0.88	0.36
22	0.93	0.36
23	0.98	0.30
24	1.03	0.23
25	1.08	0.38
26	1.13	0.23
27	1.18	0.35
28	1.24	0.21
29	1.29	0.21
31	1.39	0.62
32	1.44	0.23
33	1.49	0.20
34	1.54	0.24
35	1.59	0.36
36	1.64	0.34
37	1.69	0.36
38	1.75	0.37
39	1.80	0.28
41	1.90	0.13
42	1.95	0.17
43	2.00	0.14
44	2.05	0.35
45	2.10	0.17
46	2.15	0.19
47	2.20	0.30

Depth	Age kyrs BP	Silt/clay
48	2.25	0.25
49	2.30	0.25
51	2.40	0.25
52	2.45	0.26
53	2.50	0.32
54	2.55	0.30
55	2.60	0.34
56	2.65	0.25
57	2.70	0.21
58	2.75	0.45
59	2.81	0.35
61	2.91	0.23
62	2.95	0.23
63	2.99	0.28
64	3.03	0.34
65	3.07	0.30
66	3.11	0.22
67	3.15	0.37
68	3.18	0.28
69	3.22	0.28
71	3.30	0.40
72	3.34	0.32
73	3.39	0.31
74	3.43	0.20
75	3.47	0.24
76	3.51	0.60
77	3.55	0.44
78	3.58	0.42
79	3.63	0.30
81	3.70	0.35
82	3.75	0.29
83	3.80	0.32
84	3.84	0.38
85	3.89	0.39
86	3.93	0.48
87	3.98	0.27
88	4.04	0.41
89	4.09	0.47
90	4.14	0.18
91	4.20	0.51
92	4.25	0.42
93	4.30	0.45
94	4.35	0.58
95	4.40	0.72

96	4.45	0.50	144	7.12	0.96
97	4.50	0.63	145	7.23	1.01
98	4.55	0.61	146	7.34	0.56
99	4.61	0.46	147	7.45	0.99
100	4.66	0.40	148	7.56	0.69
101	4.71	0.64	149	7.68	0.81
102	4.76	0.61	150	7.79	0.53
103	4.81	0.52	151	7.90	0.72
104	4.87	0.44	152	8.07	0.62
105	4.92	0.57	153	8.25	0.70
106	4.97	0.48	154	8.42	0.50
107	5.02	0.58	155	8.60	0.80
108	5.07	0.66	156	8.77	0.67
109	5.13	0.69	157	8.93	0.34
110	5.18	0.89	158	9.09	0.38
111	5.23	0.54	159	9.24	0.54
112	5.28	0.57	160	9.41	0.42
113	5.34	0.64	161	9.56	0.68
114	5.39	0.62	162	9.63	0.97
115	5.44	0.74	163	9.70	0.58
116	5.49	0.62	164	9.78	0.44
117	5.54	0.61	165	9.85	0.68
118	5.60	0.83	166	9.92	0.62
119	5.65	0.68	167	9.96	0.85
120	5.70	0.84	168	10.00	0.58
121	5.75	0.79	169	10.04	0.31
122	5.80	0.71	171	10.12	0.20
123	5.85	0.61	172	10.14	0.30
124	5.90	0.66	173	10.17	0.31
125	5.96	0.82	174	10.20	0.37
126	6.01	0.62	175	10.23	0.23
127	6.06	0.56	176	10.25	0.32
128	6.11	0.54	177	10.27	0.37
129	6.16	0.83	178	10.30	0.19
130	6.21	0.58	179	10.32	0.27
131	6.26	0.83	181	10.36	0.36
132	6.31	0.82	182	10.38	0.23
133	6.37	0.84	183	10.39	0.34
134	6.42	0.67	184	10.41	0.56
135	6.47	0.88	185	10.43	0.42
136	6.52	0.85	186	10.44	0.25
137	6.58	0.83	187	10.46	0.38
138	6.63	0.85	188	10.48	0.70
139	6.69	0.64	189	10.49	0.69
140	6.74	0.47	191	10.52	0.31
141	6.80	0.87	192	10.54	1.29
142	6.91	0.84	193	10.55	0.41
143	7.02	0.82	194	10.57	0.43

195	10.58	0.54	248	11.38	0.33
196	10.60	0.41	249	11.40	0.72
197	10.62	0.40	251	11.43	0.63
198	10.63	0.20	252	11.45	1.02
199	10.65	0.26	253	11.46	0.72
201	10.68	0.34	254	11.48	0.66
202	10.69	0.35	255	11.49	0.76
203	10.71	0.29	256	11.51	0.80
204	10.72	0.34	257	11.53	0.79
205	10.74	0.64	258	11.55	0.85
206	10.76	0.46	259	11.56	0.52
207	10.77	0.54	261	11.60	0.70
208	10.79	0.58	262	11.62	1.01
209	10.80	0.91	263	11.63	1.06
211	10.83	0.52	264	11.65	0.91
212	10.85	0.56	265	11.66	1.06
213	10.87	0.44	266	11.67	0.63
214	10.88	0.39	267	11.69	0.71
215	10.90	0.97	268	11.70	0.68
216	10.91	0.69	269	11.72	0.95
217	10.93	0.81	271	11.75	1.04
218	10.94	0.52	272	11.77	0.97
219	10.96	0.92	273	11.79	0.60
221	10.99	0.68	274	11.80	0.90
222	11.01	0.74	275	11.82	0.70
223	11.02	0.60	276	11.84	0.62
224	11.04	0.81	277	11.85	0.70
225	11.05	0.86	278	11.87	0.65
226	11.07	0.67	279	11.89	1.59
227	11.08	0.52	281	11.93	1.98
228	11.10	1.07	282	11.94	0.49
229	11.11	0.82	283	11.96	0.65
231	11.15	0.43	284	11.98	0.64
232	11.16	0.61	285	12.00	0.62
233	11.17	0.57	286	12.01	0.89
234	11.19	0.59	287	12.03	0.60
235	11.20	0.41	288	12.04	0.77
236	11.21	1.06	289	12.06	0.55
237	11.23	0.98	291	12.08	0.52
238	11.24	0.82	292	12.10	0.55
239	11.25	1.08	293	12.11	0.65
241	11.28	0.88	294	12.13	0.59
242	11.29	0.86	295	12.14	0.49
243	11.31	0.87	296	12.15	0.60
244	11.32	1.30	297	12.17	0.51
245	11.34	0.40	298	12.19	0.56
246	11.35	0.68	299	12.20	0.47
247	11.37	0.52	301	12.23	0.53

302	12.25	0.49	355	13.17	0.39
303	12.27	1.16	356	13.19	0.80
304	12.28	0.65	357	13.21	0.93
305	12.30	0.50	358	13.23	0.47
306	12.32	0.46	359	13.25	0.92
307	12.33	0.74	361	13.28	0.66
308	12.35	0.81	362	13.31	0.30
309	12.37	0.55	363	13.34	0.71
311	12.40	0.56	364	13.37	0.61
312	12.42	0.66	365	13.40	0.76
313	12.43	0.57	366	13.43	1.29
314	12.45	0.60	367	13.46	1.02
315	12.47	0.42	368	13.49	0.60
316	12.48	0.63	369	13.52	0.85
317	12.50	0.50	371	13.58	0.87
318	12.52	1.16	372	13.61	1.24
319	12.53	1.06	373	13.64	0.89
321	12.57	0.39	374	13.67	1.21
322	12.58	0.47	375	13.70	1.09
323	12.60	0.82	376	13.73	0.90
324	12.62	0.62	377	13.76	1.23
325	12.63	0.62	378	13.79	0.85
326	12.65	0.76	379	13.82	0.75
327	12.67	0.14	381	13.88	0.99
328	12.68	0.56	382	13.91	1.42
329	12.70	1.09	383	13.94	0.61
331	12.73	0.39	384	13.97	0.44
332	12.75	0.35	385	14.00	0.56
333	12.77	0.51	386	14.03	0.86
334	12.78	1.13	387	14.06	0.80
335	12.80	0.71	388	14.09	0.47
336	12.82	0.97	389	14.12	0.85
337	12.83	0.33	391	14.18	1.03
338	12.85	0.61	392	14.21	0.47
339	12.87	1.18	393	14.24	0.81
341	12.90	0.75	394	14.27	0.38
342	12.92	0.68	395	14.30	0.95
343	12.94	0.42	396	14.33	0.79
344	12.96	0.80	397	14.35	1.24
345	12.97	0.95	398	14.38	0.67
346	12.99	1.04	399	14.41	1.05
347	13.01	1.48	401	14.47	0.75
348	13.03	1.38	402	14.50	0.89
349	13.05	0.77	403	14.53	0.97
351	13.09	1.06	404	14.56	0.99
352	13.11	0.57	405	14.59	0.50
353	13.13	0.68	406	14.61	0.88
354	13.15	0.63	407	14.64	1.01

408	14.67	0.42	413	14.82	0.52
409	14.70	0.88	414	14.85	0.51
411	14.76	0.52	415	14.88	1.08
412	14.79	0.53			

7.10 Bulk sediement geochemistry analyses from core NDT-6-2016.

Depth	Age Kyr BP	K/Al	Ti/Al	Ba/Ti	Si/Al
1	-0.14	7.07	3.38	0.19	10.83
2	-0.09	6.34	2.86	0.23	10.12
3	-0.04	5.91	2.81	0.20	9.69
4	0.01	6.44	2.80	0.20	10.06
5	0.06	6.47	2.94	0.23	10.68
6	0.11	6.24	2.73	0.20	9.89
7	0.16	5.50	2.49	0.23	9.45
8	0.22	6.02	2.68	0.26	10.14
9	0.27	5.68	2.48	0.25	9.54
10	0.32	6.28	2.75	0.24	10.18
11	0.37	5.63	2.47	0.21	9.47
12	0.42	5.41	2.37	0.18	9.46
13	0.47	5.28	2.27	0.19	9.30
14	0.52	5.54	2.35	0.19	9.50
15	0.57	5.62	2.38	0.22	9.59
17	0.67	5.09	2.12	0.22	9.28
18	0.72	5.13	2.20	0.16	9.03
19	0.77	5.45	2.36	0.17	9.20
20	0.83	5.68	2.35	0.19	9.46
21	0.88	5.46	2.30	0.17	9.43
22	0.93	5.97	2.58	0.20	10.10
23	0.98	5.47	2.40	0.20	9.28
24	1.03	5.29	2.16	0.20	9.08
25	1.08	5.52	2.31	0.21	9.49
26	1.13	5.61	2.40	0.20	9.52
27	1.18	5.28	2.23	0.17	9.47
28	1.24	5.33	2.26	0.18	9.24
29	1.29	5.31	2.22	0.17	9.41
30	1.34	4.99	2.00	0.21	8.82
31	1.39	5.25	2.19	0.17	9.32
32	1.44	5.06	2.09	0.18	9.17
33	1.49	5.03	2.14	0.15	9.01
34	1.54	4.91	2.12	0.19	8.84
35	1.59	4.93	2.07	0.22	8.92
36	1.64	5.01	2.17	0.20	9.08
37	1.69	5.17	2.30	0.16	8.93
38	1.75	4.95	2.21	0.19	8.79
39	1.80	4.99	2.14	0.21	8.82
40	1.85	5.23	2.27	0.17	9.03
41	1.90	5.32	2.29	0.22	9.26
42	1.95	5.12	2.24	0.19	8.97
43	2.00	5.02	2.13	0.21	8.83
44	2.05	5.04	2.17	0.21	8.83
45	2.10	5.01	2.11	0.17	8.89

46	2.15	5.78	2.31	0.26	9.67
47	2.20	5.43	2.24	0.18	9.39
48	2.25	5.89	2.32	0.22	9.69
49	2.30	5.88	2.31	0.20	9.69
50	2.35	5.44	2.18	0.23	9.26
51	2.40	5.87	2.46	0.19	9.77
52	2.45	5.38	2.21	0.26	9.44
53	2.50	5.29	2.08	0.20	9.26
54	2.55	5.61	2.19	0.19	9.77
55	2.60	5.16	2.03	0.26	9.16
56	2.65	5.50	2.08	0.24	9.71
56	2.65	5.08	2.01	0.21	9.11
56	2.65	5.09	1.98	0.20	9.17
57	2.70	5.24	2.07	0.23	9.46
58	2.75	5.25	2.09	0.22	9.37
59	2.81	5.22	2.05	0.21	9.29
60	2.86	5.23	2.03	0.22	9.33
61	2.91	5.63	2.33	0.24	9.65
62	2.95	6.09	2.48	0.21	9.91
63	2.99	5.38	2.13	0.28	9.25
64	3.03	5.59	2.18	0.22	9.70
65	3.07	5.62	2.23	0.24	9.69
66	3.11	5.67	2.38	0.19	9.65
67	3.15	5.74	2.26	0.24	9.97
68	3.18	5.25	2.06	0.22	9.21
69	3.22	5.91	2.33	0.16	9.89
70	3.26	5.73	2.35	0.21	9.89
71	3.30	5.50	2.23	0.26	9.38
72	3.34	5.60	2.18	0.21	9.86
73	3.39	5.34	2.14	0.20	9.40
74	3.43	5.68	2.28	0.23	9.78
75	3.47	6.19	2.47	0.24	9.80
76	3.51	5.50	2.15	0.23	9.57
77	3.55	5.95	2.33	0.24	9.91
78	3.58	5.81	2.30	0.23	10.05
79	3.63	5.65	2.20	0.21	9.81
80	3.66	5.45	2.11	0.24	9.43
81	3.70	5.40	2.12	0.23	9.47
82	3.75	6.12	2.45	0.23	10.09
83	3.80	5.73	2.25	0.23	9.86
84	3.84	5.66	2.23	0.25	9.53
85	3.89	5.71	2.28	0.19	9.92
86	3.93	5.57	2.14	0.22	9.44
87	3.98	5.73	2.28	0.28	9.94
88	4.04	6.33	2.53	0.25	10.14
89	4.09	5.99	2.29	0.28	9.96
90	4.14	6.03	2.32	0.26	10.18
91	4.20	6.56	2.51	0.23	10.60

92	4.25	6.17	2.35	0.29	10.45
93	4.30	6.52	2.44	0.29	10.48
94	4.35	5.82	2.12	0.25	9.51
95	4.40	5.76	2.20	0.27	9.97
96	4.45	5.52	2.04	0.28	9.91
96	4.45	5.45	1.98	0.28	9.80
96	4.45	5.69	2.09	0.30	10.04
97	4.50	5.82	2.22	0.25	10.12
98	4.55	5.74	2.06	0.27	10.33
99	4.61	6.10	2.22	0.24	10.33
100	4.66	6.37	2.39	0.24	10.45
101	4.71	5.82	2.16	0.27	10.13
102	4.76	6.10	2.22	0.25	10.48
103	4.81	5.95	2.04	0.29	10.21
104	4.87	5.78	2.03	0.30	10.04
105	4.92	5.76	2.14	0.28	9.96
106	4.97	6.25	2.35	0.30	10.34
107	5.02	6.66	2.57	0.26	10.91
108	5.07	6.71	2.43	0.27	10.84
109	5.13	6.43	2.37	0.31	10.68
110	5.18	6.32	2.29	0.27	10.63
111	5.23	6.22	2.23	0.28	10.37
112	5.28	6.18	2.28	0.28	10.24
113	5.34	6.33	2.28	0.28	10.44
114	5.39	5.62	2.00	0.26	10.15
115	5.44	7.12	2.19	0.25	10.44
117.15	5.55	7.53	2.78	0.30	11.40
118.15	5.60	6.35	2.31	0.28	10.62
119.15	5.65	6.22	2.23	0.28	10.55
120.15	5.71	6.23	2.21	0.26	10.37
121.15	5.76	6.13	2.07	0.29	10.29
122.15	5.81	6.61	2.30	0.24	10.57
123.15	5.86	6.33	2.26	0.29	10.36
124.15	5.91	6.34	2.26	0.31	10.37
125.15	5.96	6.25	2.17	0.28	10.28
126.15	6.02	5.75	2.01	0.23	9.97
127.15	6.07	6.10	2.08	0.22	10.37
128.15	6.12	6.40	2.30	0.32	10.69
129.15	6.17	5.88	2.08	0.29	10.08
130.15	6.22	6.02	2.14	0.23	10.33
131.15	6.27	6.09	2.23	0.28	10.28
132.15	6.32	5.74	2.03	0.32	9.94
133.15	6.37	6.27	2.19	0.22	10.51
134.15	6.43	5.92	2.08	0.32	10.26
135.15	6.48	5.82	2.06	0.27	10.19
136.15	6.53	5.64	1.91	0.30	10.08
137.15	6.58	5.99	2.15	0.33	10.27
138.15	6.64	6.18	2.30	0.30	10.36

139.15	6.70	6.03	2.05	0.32	10.43
140.15	6.75	6.32	2.18	0.29	11.03
141.15	6.81	6.20	2.08	0.32	10.71
142.15	6.92	5.77	1.87	0.25	10.20
143.15	7.03	6.04	2.08	0.29	10.36
144.15	7.14	6.18	2.08	0.25	10.84
145.15	7.25	5.99	1.95	0.31	10.38
146.15	7.36	6.21	2.15	0.23	10.52
147.15	7.47	6.24	2.11	0.29	10.83
148.15	7.58	6.20	2.04	0.24	10.71
149.15	7.69	6.05	2.03	0.23	10.33
150.15	7.80	5.55	1.83	0.28	10.03
151.15	7.93	6.27	2.04	0.24	10.79
152.15	8.10	5.68	1.94	0.28	10.04
153.15	8.28	5.76	1.82	0.31	10.08
154.15	8.45	5.73	1.91	0.27	9.97
155.15	8.62	5.78	1.86	0.33	10.13
156.15	8.79	5.65	1.90	0.32	9.81
156.15	8.79	5.64	1.92	0.32	9.92
156.15	8.79	6.03	2.06	0.27	10.32
157.15	8.95	6.34	2.18	0.32	10.69
158.15	9.11	5.94	1.93	0.29	9.96
159.15	9.27	5.81	1.92	0.35	10.31
160.15	9.43	5.65	1.90	0.39	10.02
161.15	9.57	5.93	2.04	0.28	10.23
162.15	9.65	6.07	2.03	0.34	10.21
163.15	9.72	6.13	2.01	0.29	10.25
164.15	9.79	6.04	2.06	0.30	10.24
165.15	9.86	6.16	2.16	0.31	10.58
166.15	9.92	6.16	2.10	0.30	10.33
167.15	9.96	6.47	2.23	0.33	11.01
168.15	10.00	5.90	2.04	0.30	10.26
169.15	10.04	6.39	2.24	0.30	10.67
170.15	10.08	6.02	2.05	0.30	10.18
171.15	10.12	5.93	2.07	0.35	10.15
172.15	10.15	6.41	2.32	0.29	11.10
173.15	10.18	5.64	2.03	0.25	9.98
174.15	10.20	5.67	1.99	0.28	9.84
175.15	10.23	6.01	2.23	0.27	10.60
176.15	10.26	6.37	2.20	0.30	10.66
177.15	10.28	6.35	2.46	0.27	11.08
178.15	10.30	6.52	2.33	0.34	10.67
179.15	10.32	6.06	2.22	0.30	10.25
180.15	10.34	7.38	2.31	0.24	10.88
181.15	10.36	6.05	2.32	0.28	10.45
182.15	10.38	6.29	2.27	0.28	10.77
183.15	10.40	6.05	2.17	0.28	10.44
184.15	10.41	5.64	2.00	0.35	9.97

185.15	10.43	6.75	2.46	0.29	11.00
186.15	10.45	6.64	2.48	0.29	11.10
187.15	10.46	6.17	2.35	0.30	10.65
188.15	10.48	6.26	2.33	0.27	10.55
189.15	10.49	6.49	2.41	0.30	11.08
190.15	10.51	6.55	2.55	0.33	11.51
191.15	10.52	6.61	2.53	0.34	11.33
192.15	10.54	6.04	2.25	0.31	10.45
193.15	10.56	6.25	2.29	0.29	10.96
194.15	10.57	6.12	2.40	0.27	10.59
195.15	10.59	6.35	2.17	0.30	10.72
196.15	10.60	7.03	2.59	0.33	11.62
196.15	10.60	7.16	2.60	0.35	11.63
196.15	10.60	6.22	2.27	0.36	10.37
197.15	10.62	6.77	2.57	0.28	10.99
198.15	10.63	6.55	2.43	0.27	10.90
199.15	10.65	6.79	2.42	0.31	10.91
200.15	10.67	6.43	2.33	0.28	10.65
201.15	10.68	6.39	2.28	0.27	10.74
202.15	10.70	6.93	2.42	0.32	11.56
203.15	10.71	6.83	2.48	0.32	10.94
204.15	10.73	6.83	2.44	0.30	10.87
205.15	10.74	7.58	2.71	0.29	11.52
206.15	10.76	6.92	2.60	0.31	10.93
207.15	10.77	7.19	2.84	0.30	11.28
208.15	10.79	7.56	2.80	0.36	11.44
209.15	10.80	7.46	2.79	0.36	11.65
210.15	10.82	7.35	2.62	0.36	11.56
211.15	10.84	6.89	2.53	0.33	10.96
212.15	10.85	7.51	2.72	0.34	11.81
213.15	10.87	7.10	2.45	0.34	11.43
214.15	10.88	7.02	2.39	0.33	11.57
215.15	10.90	6.56	2.19	0.41	10.83
216.15	10.92	6.72	2.40	0.41	10.77
217.7	10.94	6.38	2.19	0.36	10.94
218.7	10.96	6.79	2.47	0.32	11.77
219.7	10.97	6.54	2.40	0.34	11.44
220.7	10.99	6.80	2.53	0.29	12.01
221.7	11.00	6.63	2.42	0.34	11.58
222.7	11.02	6.55	2.39	0.37	11.82
223.7	11.03	6.62	2.34	0.36	11.69
224.7	11.05	6.36	2.38	0.34	11.35
225.7	11.06	6.95	2.47	0.37	11.92
226.7	11.08	6.81	2.55	0.37	11.64
227.7	11.09	6.70	2.41	0.39	11.45
228.7	11.11	6.82	2.34	0.34	11.80
229.7	11.13	7.09	2.51	0.33	11.64
230.7	11.14	7.33	2.52	0.37	11.95

231.7	11.15	7.03	2.51	0.33	11.37
232.7	11.17	7.72	2.71	0.35	12.88
233.7	11.18	7.56	2.77	0.40	12.97
234.7	11.20	6.77	2.38	0.38	11.07
235.7	11.21	6.82	2.31	0.36	11.60
236.7	11.22	7.81	2.76	0.30	12.75
237.7	11.23	6.39	2.26	0.36	11.19
238.7	11.25	7.10	2.50	0.35	12.31
239.7	11.26	7.05	2.39	0.37	11.90
240.7	11.27	7.11	2.61	0.41	12.43
241.7	11.29	6.54	2.24	0.37	11.87
242.7	11.30	6.40	2.19	0.37	11.33
243.7	11.32	6.70	2.40	0.36	12.03
244.7	11.33	6.11	2.17	0.35	11.67
245.7	11.35	6.19	2.12	0.40	11.48
246.7	11.36	6.96	2.31	0.38	12.24
247.7	11.38	6.83	2.53	0.38	12.03
248.7	11.39	7.00	2.39	0.34	12.28
249.7	11.41	6.46	2.40	0.36	11.62
250.7	11.43	8.23	3.15	0.34	13.79
251.7	11.44	7.03	2.64	0.35	11.73
252.7	11.46	6.87	2.39	0.35	11.75
253.7	11.47	7.66	2.76	0.38	12.84
254.7	11.49	7.66	2.82	0.38	12.37
254.7	11.49	6.81	2.41	0.35	11.52
254.7	11.49	7.10	2.55	0.40	12.30
255.7	11.50	6.80	2.34	0.37	11.47
256.7	11.52	6.84	2.43	0.32	11.53
257.7	11.54	6.65	2.38	0.34	11.43
258.7	11.56	7.54	2.69	0.38	12.71
259.7	11.58	7.35	2.61	0.31	12.20
260.7	11.60	7.44	2.59	0.34	11.92
261.7	11.61	7.76	2.62	0.29	12.09
262.7	11.63	6.58	2.31	0.32	11.70
263.7	11.64	6.08	2.11	0.32	10.72
264.7	11.66	6.42	2.25	0.32	11.44
265.7	11.67	6.23	2.16	0.36	11.10
266.7	11.69	6.51	2.32	0.35	11.46
267.7	11.70	6.10	2.13	0.45	10.86
268.7	11.72	6.43	2.27	0.33	11.39
269.7	11.73	5.71	2.05	0.34	10.69
270.7	11.75	5.92	2.08	0.36	10.84
271.7	11.76	6.45	2.25	0.39	11.32
272.7	11.78	6.56	2.26	0.34	11.70
273.7	11.80	6.50	2.22	0.38	11.91
274.7	11.81	5.91	2.08	0.40	10.90
275.7	11.83	6.11	2.20	0.36	11.32
276.7	11.85	6.06	2.07	0.31	11.11

277.7	11.87	5.92	2.10	0.38	10.85
278.7	11.89	5.98	2.21	0.34	10.87
279.7	11.90	5.87	2.09	0.30	10.79
280.7	11.92	6.17	2.23	0.34	11.27
281.7	11.94	7.22	2.63	0.36	12.41
282.7	11.96	6.84	2.43	0.33	12.38
283.7	11.97	6.25	2.18	0.33	11.00
284.7	11.99	5.89	2.17	0.34	10.68
285.7	12.01	6.20	2.18	0.34	11.17
286.7	12.02	6.63	2.35	0.35	11.51
287.7	12.04	6.08	2.18	0.30	10.76
288.7	12.05	7.41	2.37	0.28	11.18
289.7	12.07	6.07	2.11	0.30	10.72
290.7	12.08	5.70	2.01	0.31	10.42
291.7	12.09	5.84	2.01	0.30	10.61
292.7	12.11	6.04	2.03	0.34	11.01
293.7	12.12	5.82	2.00	0.29	10.32
294.7	12.14	5.86	2.04	0.37	10.41
294.7	12.14	5.82	2.09	0.29	10.40
294.7	12.14	5.74	2.00	0.31	10.39
295.7	12.15	5.82	1.94	0.29	10.28
296.7	12.16	5.91	2.07	0.33	10.33
297.7	12.18	6.19	2.12	0.25	10.80
298.7	12.20	6.11	2.12	0.29	10.86
299.7	12.21	5.63	1.96	0.31	10.11
300.7	12.23	5.73	2.06	0.30	10.44
301.7	12.24	5.48	1.91	0.29	9.98
302.7	12.26	6.02	2.07	0.31	10.58
303.7	12.28	5.64	1.95	0.28	10.22
304.7	12.29	5.74	2.00	0.30	10.44
305.7	12.31	5.97	1.94	0.27	10.63
306.7	12.33	5.91	2.12	0.27	10.50
307.7	12.34	5.88	1.92	0.29	10.56
308.7	12.36	5.96	1.99	0.28	10.25
309.7	12.38	5.99	2.08	0.28	10.56
310.7	12.39	6.32	2.07	0.33	11.10
311.7	12.41	5.73	1.94	0.29	10.31
312.7	12.43	5.86	1.99	0.29	10.43
313.7	12.44	5.54	1.82	0.30	10.20
314.7	12.46	5.80	1.92	0.26	10.20
315.7	12.48	5.96	2.15	0.27	10.21
317.1	12.50	5.79	1.91	0.32	10.68
318.1	12.52	6.98	2.38	0.38	12.08
319.1	12.53	6.67	2.29	0.34	11.10
320.1	12.55	6.25	2.13	0.34	10.93
321.1	12.57	6.59	2.14	0.33	11.46
322.1	12.58	6.88	2.26	0.35	11.58
323.1	12.60	6.83	2.36	0.37	11.61

324.1	12.62	7.12	2.36	0.29	11.56
325.1	12.63	6.98	2.46	0.34	11.84
326.1	12.65	6.79	2.23	0.36	11.38
327.1	12.67	7.48	2.51	0.39	12.36
328.1	12.68	7.00	2.46	0.32	11.60
329.1	12.70	6.58	2.26	0.30	10.78
330.1	12.72	6.62	2.32	0.31	10.82
331.1	12.73	6.24	2.20	0.34	11.06
332.1	12.75	6.63	2.43	0.39	11.31
333.1	12.77	6.74	2.39	0.39	11.57
334.1	12.78	6.90	2.40	0.32	12.01
335.1	12.80	6.93	2.41	0.41	11.50
336.1	12.82	6.91	2.43	0.33	11.71
337.1	12.83	6.55	2.32	0.40	11.31
338.1	12.85	7.27	2.53	0.45	12.12
339.1	12.87	6.83	2.34	0.36	11.38
340.1	12.88	6.65	2.38	0.35	11.57
341.1	12.90	6.66	2.25	0.37	11.82
342.1	12.92	8.27	2.32	0.41	11.70
343.1	12.94	7.27	2.44	0.38	12.46
344.1	12.96	7.43	2.60	0.35	12.23
345.1	12.98	8.13	2.82	0.39	12.99
346.1	12.99	7.43	2.69	0.37	12.25
347.1	13.01	6.85	2.55	0.40	11.48
348.1	13.03	6.96	2.51	0.36	12.03
349.1	13.05	6.85	2.41	0.37	11.94
350.1	13.07	6.92	2.49	0.36	12.13
351.1	13.09	6.86	2.40	0.38	11.92
352.1	13.11	7.00	2.50	0.37	12.13
353.1	13.13	8.40	2.62	0.39	11.99
354.1	13.15	8.18	2.78	0.44	13.02
355.1	13.17	7.61	2.76	0.41	12.59
356.1	13.19	7.57	2.75	0.38	11.89
356.1	13.19	7.11	2.49	0.37	11.88
356.1	13.19	7.20	2.54	0.36	12.15
357.1	13.21	7.50	2.70	0.38	12.05
358.1	13.23	7.10	2.45	0.34	11.91
359.1	13.25	7.03	2.47	0.40	11.47
360.1	13.27	6.84	2.38	0.33	11.23
361.1	13.29	7.36	2.42	0.41	12.40
362.1	13.32	6.74	2.46	0.34	11.41
363.1	13.35	7.96	2.69	0.39	12.96
364.1	13.38	7.19	2.47	0.35	12.16
365.1	13.41	7.08	2.38	0.37	11.97
366.1	13.43	6.99	2.35	0.39	11.79
367.1	13.46	6.49	2.24	0.38	11.34
368.1	13.49	7.78	2.87	0.39	12.93
369.1	13.53	7.36	2.66	0.34	12.29

370.1	13.56	7.21	2.47	0.41	11.90
371.1	13.59	7.63	2.65	0.34	12.48
372.1	13.62	6.91	2.38	0.41	11.92
373.1	13.65	7.47	2.65	0.37	12.06
374.1	13.67	6.69	2.48	0.30	11.62
375.1	13.70	7.01	2.50	0.34	11.72
376.1	13.73	6.33	2.03	0.33	10.96
377.1	13.76	6.50	2.21	0.32	11.77
378.1	13.79	6.64	2.28	0.29	11.40
379.1	13.82	7.04	2.45	0.31	11.02
380.1	13.85	7.12	2.44	0.31	11.74
381.1	13.88	7.49	2.69	0.31	12.52
382.1	13.91	6.05	2.10	0.28	10.83
383.1	13.94	7.15	2.32	0.31	12.19
384.1	13.97	6.26	2.11	0.29	10.92
385.1	14.00	6.21	2.14	0.31	10.98
386.1	14.03	6.56	2.36	0.27	10.72
387.1	14.06	6.94	2.43	0.37	11.68
388.1	14.09	6.70	2.29	0.35	11.13
389.1	14.12	7.01	2.45	0.34	11.50
390.1	14.15	7.02	2.46	0.37	11.62
391.1	14.18	6.46	2.28	0.32	10.83
392.1	14.21	6.85	2.41	0.31	11.81
393.1	14.24	6.55	2.32	0.32	10.59
394.1	14.27	6.23	2.12	0.36	10.82
395.1	14.30	7.25	2.51	0.38	12.17
396.1	14.33	7.58	2.61	0.28	11.72
396.1	14.33	6.70	2.32	0.30	11.17
396.1	14.33	7.46	2.63	0.35	11.99
397.1	14.36	6.85	2.44	0.36	11.40
398.1	14.39	7.26	2.60	0.34	11.96
399.1	14.42	6.45	2.21	0.31	11.21
400.1	14.45	6.03	2.10	0.27	11.18
401.1	14.47	7.06	2.57	0.31	12.17
402.1	14.50	6.87	2.45	0.34	12.08
403.1	14.53	6.47	2.18	0.30	11.00
404.1	14.56	5.86	2.06	0.27	10.53
405.1	14.59	6.28	2.20	0.31	10.74
406.1	14.62	6.42	2.25	0.33	11.11
407.1	14.65	6.41	2.28	0.33	11.52
408.1	14.68	6.68	2.31	0.29	11.30
409.1	14.71	6.63	2.32	0.33	11.54
410.1	14.74	5.88	2.03	0.32	10.91
411.1	14.76	6.61	2.33	0.33	11.39
412.1	14.79	6.37	2.37	0.38	10.89
413.1	14.82	7.03	2.61	0.31	11.68
414.1	14.85	7.53	2.88	0.29	12.26
415.1	14.88	8.33	3.17	0.36	13.17

416.1	14.91	7.07	2.80	0.26	12.22

7.11 Neodymium isotopes measurements (ε_{Nd}) from core NDT-6-2016.

Depth	Age kyr BP	ε_{Nd}	Error (2sd)
11	0.37	-7.91	0.28
31	1.39	-8.13	0.28
51	2.40	-8.13	0.28
71	3.30	-7.67	0.29
81	3.70	-7.61	0.29
91	4.20	-7.62	0.29
101	4.71	-8.24	0.25
111	5.23	-7.80	0.25
121	5.75	-7.63	0.28
123	5.85	-8.01	0.26
129	6.16	-7.52	0.26
138	6.63	-7.27	0.26
144	7.12	-7.47	0.26
147	7.45	-7.84	0.30
148	7.56	-8.44	0.26
151	7.90	-7.87	0.28
153	8.25	-8.08	0.26
154	8.42	-8.24	0.26
158	9.09	-8.38	0.26
159	9.24	-7.77	0.27
161	9.56	-7.77	0.26
163	9.70	-8.26	0.36
179	10.32	-7.92	0.55
197	10.62	-7.96	0.43
211	10.83	-7.41	0.58
223	11.02	-7.16	0.41
243	11.31	-7.09	0.41
247	11.37	-7.25	0.37
261	11.60	-7.03	0.36
280	11.91	-6.26	0.34
301	12.23	-5.80	0.47
321	12.57	-5.62	0.43
349	13.05	-7.71	0.43
361	13.28	-8.11	0.41
381	13.88	-7.54	0.44

8 APPENDIX 2

8.1 Acronyms

AHP African Humid Period

AMOC Atlantic Meridional Overturning Circulation

AW Atlantic Water

DCM Deep Chlorophyll Maximum

DWT Deep Water Temperature

EMDW Eastern Mediterranean Deep Water

E-Med Eastern Mediterranean

EMSW Eastern Mediterranean Sourced Water

ES1 Expression of Sapropel 1

LIW Levantine Intermediate Water

MAW Modified Atlantic Water

Med-THC Mediterranea Thermohaline Circulation

MOW Mediterranean Outflow Water

ORL Organic Rich Layer

S1 Sapropel 1

SST Sea Surface Temperature

VPDB Vienna Pee Dee Belemnite

WMDW Western Mediterranean Deep Water

W-Med Western Mediterranean

W-Sicily Western Sicily

YD Younger Dryas

... "La utopía está en el horizonte. Y por mucho que yo camine nunca la voy a alcanzar.

Si camino diez pasos, ella se aleja diez pasos y el horizonte se corre diez pasos más allá.

¿Entonces para qué sirve la utopía? Para eso, sirve para caminar".

Fernando Birri

UNIVERSITÀ DEGLI STUDI DI PALERMO

erc

tirred

UNIVERSITAT DE BARCELONA